# Thermal Imagery in Plant Phenotyping: Assessing Stomatal Conductance through Energy Balance Modelling

A Thesis Submitted to the
College of Graduate and Postdoctoral Studies
in Partial Fulfillment of the Requirements
for the degree of Master of Science
in the Department of Chemical and Biological Engineering
University of Saskatchewan
Saskatoon

By
Keith Halcro

# Permission to Use

In presenting this thesis in partial fulfilment of the requirements for a Postgraduate degree from the University of Saskatchewan, I agree that the Libraries of this University may make it freely available for inspection. I further agree that permission for copying of this thesis in any manner, in whole or in part, for scholarly purposes may be granted by the professor or professors who supervised my thesis work or, in their absence, by the Head of the Department or the Dean of the College in which my thesis work was done. It is understood that any copying or publication or use of this thesis or parts thereof for financial gain shall not be allowed without my written permission. It is also understood that due recognition shall be given to me and to the University of Saskatchewan in any scholarly use which may be made of any material in my thesis.

Requests for permission to copy or to make other use of material in this thesis in whole or part should be addressed to:

Head of the Department of Chemical and Biological Engineering
University of Saskatchewan
3B48 Engineering Building, 57 Campus Drive
Saskatoon, Saskatchewan S7N 5A9 Canada

OR

Dean
College of Graduate and Postdoctoral Studies
University of Saskatchewan
116 Thorvaldson Building, 110 Science Place
Saskatoon, Saskatchewan S7N 5A9 Canada

# Abstract

In phenotyping, plants are assessed to determine characteristics arising as a consequence of plant genetics interacting with the local environment. Phenotypic data are of interest to plant breeders working to create cultivars suited for efficient food production. Practical use of field data will uncover the influence of the genotype on growth to select the best cultivars in breeding programs. Field data would include plant temperature, which can be considered the result of energy handling processes that directly influence growth and water usage by balancing energy uptake and rejection.

Confidence in the value of temperature extracted from thermal images requires a good handle on the behaviour of radiation outward from a surface. This study investigated emitted and reflected thermal radiation from leaf surfaces. All of the field crop leaves tested had very high emissivity at all view angles above the surface. The majority of outward radiation from leaves was due to emitted radiation, and radiometric corrections showed apparent and surface temperatures were within half a degree due to high emissivity when measured near 35 degrees Celsius.

Leaf temperatures of outdoor crops continuously shift as energy is taken in and stored while waste heat is discarded. Heat loss is primarily through passive channels which are based on leaf temperature. Part of the resistance to latent energy loss is actively governed by plants, and an ideal theoretical energy balance calculates the plant response necessary to result in the temperature observed at measured environmental conditions. Stomatal opening governs the rate of water loss and the stomatal conductance is calculated to satisfy the energy balance. Theoretical models require all energy interactions between the leaf and environment to be quantified. The response of the theoretical method to standard weather and climate conditions was investigated and plotted to show the behaviour of the model. Empirical methods of calculating stomatal conductance included the temperature of reference surfaces that represent fringe cases of maximum and minimum leaf temperature. Theoretical and empirical methods were implemented in an outdoor study, and both methods isolated the active plant response of stomatal conductance.

An investigation into stomatal conductance response under drought stress showed that

empirical and theoretical modelling approaches distinguished water deficit wheat from unstressed wheat when grown under otherwise similar conditions. Stomatal conductance differed between cultivars, suggesting that stomatal conductance response is tied strongly to genetics. Daily trends in stomatal conductance reported for each variety evolved as lowered water potential increasingly affected the plant behaviour. Stomatal conductance in drought stressed wheat was lower than unstressed crops of the same variety for short periods of time near noon which expanded into a consistent difference in the morning which widened across the entire day as drought stress intensified. The theoretical model of stomatal conductance consistently reported values higher than expected as it made an explicit assumption that all energy absorbed is lost as heat. The assumption can be revisted when expanding the model to include plant parameters related to energy usage such as reflectance or photosynthetic rate. Further work can introduce more data to minimize assumptions of heat transfer between the environment and the leaf.

# Acknowledgements

The author would like to formally acknowledge the following:

Funding support from the Canada First Research Excellence Fund via the Plant Phenotyping and Imaging Research Centre,

Dr. Scott Noble for supervising the project,

Dave Pastl and Tyrone Keep for their assistance in gathering in-field data,

Committee members Dr. David Torvi and Dr. Trever Crowe,

Dr. Steve Shirtliffe, Dr. Rosalind Bueckert, Dr. Karen Tanino, and Ellen Misfeldt from the College of Agriculture and Bioresources for allowing use of their laboratory and/or materials, and

Pierre-Luc Pradier, Dr. Dave Schneider, and Pankaj Banik at the Global Institute for Food Security and Mary Bertoncini of the National Research Council of Canada for their aid in accessing and using greenhouse facilities.

# Contents

# List of Tables

# List of Figures

# Nomenclature

| | | |
|---|---|---|
| $c$ | Specific Heat | $[\mathrm{J{\cdot}kg^{-1}{\cdot}K^{-1}}]$ |
| $CWSI$ | Crop Water Stress Index | [-] |
| $d$ | Characteristic Dimension | [m] |
| $E$ | Radiative Energy Flux | $[\mathrm{W{\cdot}m^{-2}}]$ |
| $e$ | Saturation Pressure | [Pa] |
| $G$ | Net Incident Radiation | $[\mathrm{W{\cdot}m^{-2}}]$ |
| $g$ | Stomatal Conductance | $[\mathrm{m{\cdot}s^{-1}}]$ |
| $I_g$ | Stomatal Conductance Index | [-] |
| $R$ | Coefficient of Reflectance | [-] |
| $r$ | Heat/Water Loss Resistance | $[\mathrm{s{\cdot}m^{-1}}]$ |
| $RH$ | Relative Humidity | [-] |
| $s$ | Rate of Change of Saturation Pressure | $[\mathrm{Pa{\cdot}K^{-1}}]$ |
| $T$ | Temperature | [K] |
| $t$ | Time | [s] |
| $u$ | Wind Speed | $[\mathrm{m{\cdot}s^{-1}}]$ |
| $VPD$ | Vapour Pressure Deficit | [Pa] |
| $\alpha$ | Coefficient of Absorption | [-] |
| $\epsilon$ | Emissivity | [-] |
| $\gamma$ | Psychrometric Constant | $[\mathrm{Pa{\cdot}K^{-1}}]$ |
| $\ell^*$ | Leaf Thickness | [m] |
| $\rho$ | Density | $[\mathrm{kg{\cdot}m^{-3}}]$ |
| $\sigma$ | Stefan-Boltzmann Constant | $[\mathrm{W{\cdot}m^{-2}{\cdot}K^{-4}}]$ |
| $\tau$ | Transmittance | [-] |

# Chapter 1

# Introduction

## 1.1 Phenotyping and Cultivar Development

Plant breeding is the procedure of crossing genetic material of plants to create progeny and selecting the best among them as new cultivars. Plant breeding efforts are responsible for the continued development of commercial crops which increase the output of farmland and provide significant contributions to food security. New cultivars within crop species are often developed to increase yield in target environments that already produce that particular crop, while other cultivars are poised to expand into new areas where that species does not typically thrive. The field of plant science employs a wide array of research themes to support efforts to refine cultivars to best match their growing conditions and ultimately produce a large yield of high-quality material. Research efforts in the field of genomics statistically link traits to strings of genetics in the sequenced genome (Hirayama and Shinozaki, 2010). A closely related avenue of research is phenomics, which deals with measurements of phenotypic plant traits (Fiorani and Schurr, 2013). The phenotype is the outward expression of a plant arising as a combination of cultivar genotype, growing environment, as well as interactions between genotype and environment. Any quantitative or qualitative measurement of a plant through this definition is always a phenotypic measurement. Linking genome sequences to phenotype is not a direct one-to-one relation as the variation brought in by the environment gives rise to many phenotypes from genetically identical samples. The phenotypic plasticity is the ability of a genotype to produce divergent phenotypes in response to different environmental conditions (Tardieu et al., 2017). Useful phenotypic traits requires consistent, repeatable, and reproducible data collection that take the local environment into account.

Plant phenotyping efforts measure properties of plants to chart plant development and

ultimately the production of useful materials: food, fuel, feed or fibre. In traditional methods, crews are sent out to subsample a field of plants and gather measurements of general properties related to biomass or yield potential such as plant height, canopy coverage, a count of seed pods or estimated disease progression. Obvious drawbacks to manual methods include a great capacity for human error which is compounded as acquisition takes a significant amount of time despite subsampling, increasing susceptibility to temporal and spatial variance. Correct identification of genetic influence on the phenotype is accomplished by subjecting cultivars to varied environments and using semi-randomized testing layouts in repeated studies (Leinonen et al., 2006, Esmaeili et al., 2016). Fieldwork is an expensive process requiring an immense amount of work, which includes significant advance preparation. Disparate methods and the requirement of extensive documentation severely hamper widespread sharing of phenotypic data gathered by field crews (Ćwiek-Kupczyńska et al., 2016).

Automated plant phenotyping is a very appealing tool for plant breeders as it would work to solve issues outlined that are due in part to the extensive use of field crews. Automated collection and processing of phenotypic traits would make enormous amounts of data available that up to this point have been inaccessible (Fiorani and Schurr, 2013, Tardieu et al., 2017). Ideally, an automated method would be completely independent of operator judgment and measure selected traits while recording any pertinent information such as environmental conditions or parameters of acquisition. Input costs to developing phenotyping platforms are high as novel technologies introduce an unusual problem in plant breeding, the problem of excessive data (Fiorani and Schurr, 2013). In sharp contrast to conventional methods, automated phenotyping on a large scale could quickly produce repeated measurements of individual plants in a typical field setting or breeding trial. The incredible throughput potential requires diligence in selecting instruments to gather data and meticulous attention paid to the processing pipeline that will convert raw measurements to a more compact form easily implemented in existing plant breeding workflows (Fahlgren et al., 2015, Tardieu et al., 2017). Repeatability is paramount in plant studies and must be applied to any new addition to the toolkit. Stringent data collection and standardized methods of analysis are necessary to make practical use the data harvested by automated phenotyping.

Automated data collection will require extensive development to integrate the expertise of plant scientists with new tools to ensure the applicability of the undertaking (Fiorani and Schurr, 2013). The development of automated phenotyping requires exploration of the measurement tools and their underlying principles to provide a stable footing for the rest of the project to proceed (Fahlgren et al., 2015). New acquisition technologies will take time to develop as the validity of the measurement in conventional plant breeding programs has to be investigated thoroughly (Fiorani and Schurr, 2013, Tardieu et al., 2017). Members of disparate disciplines brought onto the project need to be in close communication with plant scientists and technicians who would be involved with the operation of automated phenotyping platforms. It is imperative that all of the contributors to the project be aware of the requirements and end users understand the limitations of an automated phenotyping system.

## 1.2 Thermal Imaging for Phenotyping

The greater research community has identified leaf and plant temperature as extremely useful in many phenotyping applications, including controlled studies and outdoor field studies (Costa et al., 2013, Khanal et al., 2017, Maes and Steppe, 2012, Jones et al., 2009, Jackson, 1986, Esmaeili et al., 2016). Measuring leaf temperature is a difficult thing to achieve with contact thermometry as leaves are delicate enough that the measurement of temperature can introduce significant loading error. Contact methods upset natural processes in addition to being labour intensive and were discarded in favour of non-contact infrared thermometry to determine the apparent temperature in an area observed by optical radiation sensors (Jackson et al., 1981). Infrared thermometers measure radiation and report a single temperature value, integrated over the volume of space in front of the sensor. Thermal cameras use the same measurement principles but with many sensors packed into an array, creating an image of discrete pixels. Non-contact thermometry principles apply to both devices, but the thermal camera has the advantage of spatial resolution which allows for image processing.

### 1.2.1 Thermography and Energy

Long-wave thermal cameras and infrared thermometers use detectors sensitive to electromagnetic wavelengths of around 8-13 µm depending on the choice of detector and lens. The long-infrared waveband, often referred to as the thermal infrared radiation (TIR) band in remote sensing and thermography, encompasses most of the radiation emitted by objects at temperatures where earth-based natural processes occur. From the principles of blackbody radiation, all objects emit radiation with increasing power and decreasing peak wavelength as the body becomes more energetic and temperature increases. The Stefan-Boltzmann Law describes the relationship between emitted radiative power and temperature in the form:

$$E_e = \epsilon \sigma T_{surface}^4, \tag{1.1}$$

where:

$E_e$ is the radiant power emitted over all wavelengths [W·m$^{-2}$],

$\epsilon$ is the emissivity of the surface,

$\sigma$ is the Stefan-Boltzmann constant [W·m$^{-2}$·K$^{-4}$], and

$T_{surface}$ is the surface temperature [K].

Thermal images contain spatial and energetic information as each pixel has an associated value of temperature intensity. These intensities are reported based on a calibration from the energy measured in the wavebands incident to the sensor. Wavelengths present in direct sunlight are too short to be detected by TIR responsive sensors, whereas diffuse sunlight contains emitted long wavelengths in the TIR band radiated from atmospheric particles heated by direct sunlight (Jones, 2013). Direct and diffuse sunlight in the visible range is absorbed with high efficiency by most plant matter, increasing plant energy (Gates et al., 1965, Jones, 2013). Plants actively regulate their internal energy, and non-contact thermometry uncovers the result of the energy balance as plant temperature (Sirault et al., 2009).

### 1.2.2 Image Processing

Thermal cameras introduce spatial information to non-contact temperature measurement. Unfortunately, many thermal cameras have relatively low pixel count and lower resolution than common RGB image sensors. Low resolution obfuscates detail and can introduce pixels which represent a combination of physically distinct objects smaller than the area covered by a pixel. Leveraging the available spatial information requires image processing to extract only pertinent information from images. Established image segmentation methods are quite varied as the field is very well developed and extensively used in research, manufacturing, and automation (van der Walt et al., 2014). Any image processing function developed to work with greyscale images that have one value of intensity per pixel will work with thermal images. Thermal images have one value at each pixel to represent temperature, compared to colour images which often have three values per pixel to represent red, green and blue intensity in a typical RGB colour space.

In the case of radiometric thermal cameras which report a temperature, radiometric corrections can be implemented in the image processing stage of the analysis pipeline. Correcting raw image data is always a concern in image analysis, but the process of correcting radiometric thermal images is different to RGB images. RGB cameras primarily observe light reflected from a surface except in the case of luminescent materials which do emit visible light. Thermal cameras capture outbound radiation within their sensitivity range from a surface, and it is possible to decompose a reading of the total radiation into the portion emitted by the source and the portion of the reflected radiation. Assuming of no transmission of TIR wavelengths through the body and applying Kirchoff's law of thermal radiation, energy measured is broken down to temperatures in the form:

$$E = \sigma T_{apparent}^4 = \epsilon \sigma T_{surface}^4 + (1 - \epsilon)\sigma T_{reflected}^4 \tag{1.2}$$

where:

$E$ is the radiant power incident to the detector [W·m$^{-2}$],

$T_{apparent}$ is the temperature reading at an emissivity of one [K], and

$T_{reflected}$ represents external energy reflected from the opaque surface originally emitted from surrounding objects [K].

## 1.3 Goals

Devices to measure thermal infrared radiation from crops are currently being used in plant phenotyping to study the temperature of plants in the field. However, the use of temperature data collected in great amounts from non-contact methods in plant studies is not utilized to its full potential for phenotyping and field studies (Khanal et al., 2017). The major confounding effect is environmental variability that greatly influences the temperature and must be considered when attempting to use thermal data (Costa et al., 2013, Munns et al., 2010). The surrounding area will shape the development of a plant in the long-term while short-term variation in the environment will affect any measurement taken (Fahlgren et al., 2015). The use of a thermal camera introduces practical considerations such as what physical objects should be in a thermal image and what the influence sensor-target geometry has on thermal images. The management of field level influences on thermography is currently inadequate (Costa et al., 2013). The use of infrared thermometers is not discussed here, despite using the same sensing principles, as analysis is fundamentally very different without spatial information.

Therefore, the goal of this work was firstly to address the practical concerns of sensor-target distance and sensor-target angle on thermal imaging in field phenotyping. The value of higher spatial resolution in interpreting temperature information from a thermal image was studied. Higher image resolution makes objects more distinct, allowing for individual leaves to be isolated but their shape will be dependent on camera view angle. The second goal of this work was to explore the potential of energy balance modelling to estimate the dynamic behaviour of a plant in a field. An energy balance considers the environment and its immediate effect on shaping plant temperature. With accurate energy balance models, the influence of the environment and the plant behaviour in determining plant temperature response can be separated. Thirdly, unique approaches to characterizing the environmental influence on plants in the field were investigated to select a method best suited for automated

phenotyping. Standardized analysis will allow for plant status to be isolated in a consistent manner to ensure repeated analyses can be compared.

## 1.4 Hypotheses

Phenotyping groups working with measurements of phenotypic elements that react to the environment are very aware that local conditions influence field data. With precise and repeatable analyses of field data, concrete links between plant phenotype and genetics can be generated. Stronger linkage of breeding programs to real-world results will drastically improve cultivar development speeds, allowing breeders to introduce better cultivars to the marketplace. The six hypotheses outlined here are required to move from thermal image acquisition to the development of plant behaviour models:

1. The emissivity of leaves is high at all view angles, and thus radiometric corrections do not rely on view angle.

2. Thermal images of crops in the field obtained at any time of day can be automatically processed to extract leaf temperature.

3. Continually shifting environmental conditions make leaf temperature exceptionally variable over short time frames in a field.

4. Energy balance models can uncover the active response required of the plant to result in a particular temperature at given conditions.

5. Results of energy-based phenotype models change in response to stress events quickly and definitively.

6. Phenotyping operations that gather temperature information with thermal cameras must combine temperature with quantified weather data from other sensors to enable an energy balance model to reliably and repeatably assess stress state.

### 1.4.1 Directional Emissivity, Reflection and Transmission

A change in emissivity or significant reflections arising in the leaf tissue would complicate the implementation of radiometric corrections. It was hypothesized that leaf tissue would have an emissivity greater than 0.96 at all view angles, with no significant long-wave thermal reflection occurring at any view. When emissivity is high, the reflected radiation contributes very little to the net outward radiance. This hypothesis was addressed first to verify the capability of thermal imagery by addressing error and corrections available at the data acquisition stage.

### 1.4.2 Isolation of Leaf Temperature

Once the radiation exiting leaves is understood, it is prudent to focus the examination of temperatures to the leaves, the active sites where most of the energy exchange between plant and environment occurs. Image segmentation in thermography is troubled by low resolution which is more problematic when the sensor-to-target distance is high. Thermal images acquired from aerial systems show a bird's-eye view in which it would be difficult to isolate leaf temperature. These images instead report a canopy temperature - which is influenced significantly by canopy type and closure as pixels may contain temperature information from non-leaf objects. At close scales with enough resolution to distinctly view individual leaves, there is hypothesized to be a method of automated, and thus repeatable, segmentation of leaf tissue. Such a method could be carried forward as the standardized approach to extracting leaf temperatures from thermography.

### 1.4.3 Environment-Driven Leaf Temperature Variation

As plants are living organisms that respond actively to their environment, it stands to reason that they respond relatively quickly to take advantage of every opportunity given them. Plant behaviour related to growth and energy handling in response to the environment would be made manifest in the temperature - a representation of the energy of the plant. The hypothesis was that exceptional oscillation of leaf temperature was a consequence of thin leaves with low thermal mass receiving a significant amount of energy from the sun with a lagged dynamic response to dissipate that energy.

### 1.4.4 Environmental Models

Plant behaviour is inexorably linked to the environment. Many phenotypes can emerge from identical genotypes because of the influence of the environment. It is important to note that the phenotype is not a static culmination of select previous interactions that have given rise to the current state; the phenotype is continuously evolving in response to many events. Long-term and short-term environmental effects give rise to the phenotype, and as such point measurements require environmental data to set the phenotype measurement in context. Environmental conditions can be recorded with explicit measurements or ignored by comparing measurements captured at the same time, with objects under the same environmental influence. It was hypothesized that energy balance analysis of leaves of plants in the field would isolate and uncover the plant behaviour that results in the phenotypic temperature response.

### 1.4.5 Phenotypic Stress Response

Automated phenotyping catalogues the parameters of a plant as it grows, and stress inhibits growth in the long-term. Any consideration of growth impairment and thus stress must be done with due consideration of the environment and its effect on the plant. The active plant response estimated from the energy balance is expected to be stable and insensitive to short-term environmental factors across daytime hours. The hypothesis was stress in a plant would affect the plant response as a consistent offset from baseline unstressed behaviour at any point in daytime hours. Differences would exist between stressed and unstressed plants at all daytime hours, enabling stress sensing at any point in the day.

### 1.4.6 Phenotypic Models

There are two major approaches to characterizing the environment when converting measurements of plant temperature to the active plant response via modelling. Empirical methods have been used to estimate plant status at a single time point based entirely on temperature comparisons between plants or reference surfaces with faith that all objects experience the same conditions. A theoretical model would require data brought in from other instruments to describe the environment explicitly. The hypothesis was an accurate and repeatable anal-

ysis of energy handling in plants will require quantifiable data from several sensors to build a many-faceted model to set the context of environmental conditions.

## 1.5 Structure of the Thesis

The thesis is arranged around the hypotheses described in the previous section. A general literature review in chapter 2 covers thermal radiation, measurement of plant temperature and its relation to stress and phenotyping approaches. An exploration of fundamental questions related to leaf emissivity and directional effects to address hypothesis one follows in chapter 3. The first outdoor study contained in chapter 4 fulfills hypotheses two, three, and four by investigating field data. The second outdoor study in chapter 5 is an expanded investigation into the response of parameters modelled from field data collection, similar to the first outdoor study, and addresses hypotheses five and six. A portion of chapter 5 was submitted to the 2018 ASABE Annual International Meeting as a paper with an accompanying presentation at the event (Halcro and Noble, 2018). The studies are appended by a conclusion in chapter 6 that focuses on the application of this work into the phenotyping sphere by addressing the status of the goals outlined here.

# Chapter 2

# Literature Review

## 2.1 Radiation

All objects with internal energy passively convert that energy to electromagnetic energy which enables radiative energy transfer with their surroundings. Planck's Law describes the spectral distribution of radiation emitted by a black body object as a function of temperature. A black body is the theoretically most efficient body for radiative heat transfer, absorbing and emitting more radiation at every frequency of the electromagnetic spectrum than any other object at the same temperature. The radiance emitted by an object can be converted into a measure of temperature using the Stefan-Boltzmann Law which states that the total energy emitted by an object across all wavelengths is proportional to the fourth power of the object's absolute temperature. The equation can be modified by including the emissivity, the ratio of a real body's emissive power to that of the theoretical black body. The reported emissivity is waveband-specific and is usually constrained to long-wave infrared radiation, where thermal radiation is actively emitted by objects.

Radiation incident to a body can be absorbed into, transmitted through, or reflected off of the surface. The relation between the three is intuitive as each incident ray of radiation has to go through one of the processes as described by $\alpha + \tau + R = 1$ where $\alpha$ is the absorptance, $\tau$ is the transmittance and $R$ is the reflectance. Radiation exiting a surface can only be due to transmission through the body, reflection of other sources nearby or emission from the body. A waxy leaf surface transmits thermal infrared wavelengths allowing radiation to enter and exit the cellular structures of the leaf, but a leaf body as a whole is opaque to thermal radiation (Gates and Tantraporn, 1952). Kirchoff's law of thermal radiation states that any body emitting and absorbing thermal radiation in thermodynamic equilibrium with

its surroundings has an emissivity equal to the absorptivity. The conclusion that Kirchoff's law holds in outdoor field conditions opens the door for more confident analysis of radiation (Zhang, 2005, Korb et al., 1999, Salisbury et al., 1994). With the application of Kirchoff's Law and the assumption of zero transmission, the outward radiation from a surface consists entirely of emitted radiation and incident radiation that is not absorbed into the body but is instead reflected outwards. The total outward radiation is sometimes referred to as the radiosity or radiant flux intensity but will be explicitly referred to as total outward radiation.

The radiation captured by a sensor is the net amount of emitted and reflected radiation, minus any losses in the path between target and sensor. Determining the fraction of captured radiation that is emitted by a surface requires an excellent description of the local illumination (McCarthy et al., 2010). The Bidirectional Reflectance Distribution Function (BRDF) describes the reflective behaviour of radiation incident to a surface (Schaepman-Strub et al., 2006, Wang et al., 2014). BRDF is often used in visual or near-infrared remote sensing applications with sensors that range from very coarse to very fine resolution (Coburn et al., 2010). Attempts to extend BRDF to the thermal domain found that canopies with ideal leaf surfaces can still display significant emissivity directionality at long distances due to the canopy structure (Snyder and Wan, 1998). Greenhouse gases in the atmosphere, including water vapour, can absorb and emit thermal energy influencing the measurement of incident radiation. Humidity between a sensor and target 25m apart contributes a maximum of one degree of error on non-contact temperature measurements with an air temperature of 30 degrees Celsius and relative humidity varying between zero and 100% (Aubrecht et al., 2016). The atmospheric effect of greenhouse gas absorption and emission can be compensated for with hyperspectral thermal infrared imaging to isolate absorption bands (Gerhards et al., 2016).

## 2.2 Temperature of Plants

Any plant in a field must dissipate absorbed energy before cell damage occurs, and much of the energy lost is in the form of radiation (Gates et al., 1965). The amount of heat required to change the temperature of a leaf is dependent on the heat capacity. Studies have shown

that plant tissue heat capacity is dominated by water content, and water makes up half the weight of grass leaves at full saturation (Hedlund and Johansson, 2000). At full saturation, the specific heat capacity of a leaf is only slightly below the value of specific heat capacity of water (Jayalakshmy and Philip, 2010). Leaf temperature change in response to shading modelled as a first order system had a measured time constant of roughly twenty seconds for large leaf surfaces (Leigh et al., 2006). Studies that investigated the radiative portion of heat loss isolated emitted and assumed reflected radiation was entirely diffuse. Diffuse scattering of thermal radiation within the leaf body is a safe assumption as the cellular structures under the leaf wax are roughly two to five times as large as thermal infrared wavelengths which promotes entirely diffuse Mie scattering (Gates and Tantraporn, 1952, Gates, 1970). Lab (López et al., 2012) and field studies (da Luz and Crowley, 2007) using distinct techniques have reported high emissivity values for vegetation.

### 2.2.1 Canopy Architecture in Images

Early studies discovered that contact thermometry was very difficult to perform with plants as the leaves are very delicate and thermally bonding objects to a leaf would influence the leaf greatly. In addition to loading errors, sunlight would also heat the contact thermometers which were quite large compared to current day thermocouples (Gale et al., 1970). Contact methods of temperature measurement were replaced with non-contact methods that capture radiation to estimate temperature (Mahan and Yeater, 2008). Of those non-contact measurement devices, thermal cameras have spatial information that can be capitalized on to isolate distinct regions in the plants under study.

Operating a thermal camera allows studies to examine specific targets in images that were difficult to investigate with infrared thermometers and contact measurements. High resolution images avoid excessive pixelation of the plant canopy, and image segmentation methods can be employed to split the image into distinct regions with unique information (Leinonen and Jones, 2004). Thermal images taken from greater distances will have details lost by aggregation (Faye et al., 2016) and mixed pixels consisting of several distinct sources of thermal radiation of sub-pixel size have to be discarded (Jones and Sirault, 2014). Mixed pixels containing soil and vegetation in thermal images of plant canopies are more apparent

and more disruptive as canopy coverage decreases (Hackl et al., 2012). Manual selection to avoid mixed pixel effects isolates pixels at the crown of the canopy (Prashar et al., 2013).

The selection of pixels representative of vegetative matter depends on the type of canopy formed by the plants, an issue as field crops have many different canopy architectures. A canola plant does not have a full canopy at the top of the plant as most of the broad leaves are in the rosette near the bottom of the main stem. Cereals such as wheat or rice do not form a fully closed canopy and have long thin leaves that require high resolution to distinguish. A balance has to be struck between acquiring many high-resolution images or acquiring images that represent a larger area, reducing time to acquire data for an entire field. Quickly collecting field data reduces the changes introduced by the environment, but a high-resolution image is crucial to enable adequate segmentation of canopy or leaf tissue (Jones and Sirault, 2014).

### 2.2.2 Environment and Sunlight

Plants are living organisms and respond to the environment to better their chance of survival so they can reproduce. It is essential to keep in mind that measurements of leaf temperature are only a small window into internal processes stimulated by local conditions such as soil status, environmental pressures from local weather, and other organisms. Standard quantifiable local weather around a plant would include radiant flux of incident sunlight, wind speed and direction, ambient temperature, and ambient humidity. These quantities feature prominently in models that describe energy transfer between plants and their surroundings (Jackson, 1986, Leinonen et al., 2006, Kim et al., 2016, Jones, 2013). A shifting environment incites a plant to action; either capitalizing on abundant resources or conserving when faced with adverse pressures and resource deficits.

Direct sunlight consists of short, energetic wavelengths and has very little power in the thermal waveband (Reda et al., 2015). Photochemical processes in plants are discussed very briefly here but they are tremendously important components of plant development. Photosynthesis, potentially the most important process on earth, captures sunlight energy in visible wavelengths to be used in biochemical processes while lower energy radiation is re-emitted through fluorescence when photosynthetic demand is exceeded (Rossini et al.,

2013). The process of respiration releases stored energy to provide the plant with the energy necessary for growth and maintenance. Photosynthesis, fluorescence and respiration are processes that have been extensively studied in biochemistry and plant physiology and the finer details are out of scope here. In addition to providing energy, the spectral characteristics of light are also important for plant response and function, however these responses have been considered out of scope in the present study. For the remainder of this document, sunlight is considered naively as a source of energy only.

### 2.2.3 Stomata and Energy Balance

Stomata are structures on plant leaves that allow for transfer of gases between the plant and the environment as required by biochemical processes. Carbon dioxide and oxygen transfer are involved in respiration and photosynthesis while water transfer from the plant to the leaf surface is part of the transpiration process that results in evaporative cooling. Plants actively regulate stomatal opening and conductance in response to the environment and particularly strongly with respect to vapour pressure deficit (VPD), the difference in current partial pressure of water in the atmosphere from the saturation pressure at that ambient temperature (McAdam and Brodribb, 2015, Urban et al., 2017). Stomatal regulation is also strongly tied to soil water deficit and leaf water content as stomata may close to preserve water within the plant (Struthers et al., 2015). Stomata on the same leaf are coupled together with the whole leaf responding similarly to a shifting irradiance (Prytz et al., 2003). Stomata are tremendously important in the regulation of energy by governing the rate of processes related to energy use.

Energy flux into the plant is entirely based on radiative transfer, in which direct and diffuse sunlight are the most significant sources of energy. Radiation incident to a leaf is affected by sky conditions as clear skies emit very little thermal radiation and as such have a lower effective sky temperature than a cloudy day which has a lot of molecular components that capture and emit heat (Li et al., 2017). There are three pathways for collected energy that has been converted to thermal energy to be dispersed into the environment from the plant: radiative heat transfer, convective heat transfer and latent heat transfer. The plant loses most of the energy to the environment through sensible heat transfer; convective and

radiative transfer account for roughly 75% of the total heat loss (Ortega-Farías et al., 2016). The sensible heat losses increase as the leaf temperature relative to surroundings increases. Ambient air temperature is used in indexes to chart the growth of plants (Jackson, 1986) and influences the VPD as the upper limit of water content is higher in warmer air. The remainder of the energy lost is through latent heat loss as energy is removed from the leaf to evaporate water moved to the leaf surface via transpiration. Local air currents influence the transpiration rate as fresh unsaturated air increases the driving potential for water to evaporate.

## 2.3 Stress and the Connection to Temperature

In this document, anything that disrupts the growth of plants and results in less biomass or yield production is considered stress. Stress is induced through several different influences, broadly grouped into biotic and abiotic sources. Biotic stress is damage done to the crop by any living organism such as bacterial or fungal pathogens, insects, or other non-crop plants. Abiotic stresses are brought upon by non-living sources, often related to resource availability and include salt stress or drought stress that restrict water uptake of the plant. Abiotic stress can include temperature stress when plants are subjected to high temperatures and drought stress when water availibility is low and the growth medium is dried out. Stressed plants have reduced growth potential because they shift to conserve resources or repair damage instead of producing more biomass before maturing (Jackson, 1986). Stress is a complex topic and many phenotypic properties are influenced by the stress state and are connected to a reduced yield, but physical measurements evaluated to confirm lowered potential often occur after the stress period has elapsed (Reynolds et al., 1998). Stress-tolerant plants would not significantly adjust their operation and continue with little to no growth reduction whereas stress-susceptible plants would have their growth halted significantly as the plant reacts strongly to the conditions (Munns et al., 2010). The absolute quantification of stress is usually a comparison of the average yield of crops under stress to the average yield of a control of the same genotype. Some studies look at the total biomass harvested only a few weeks after planting, which is sufficient to quantify stress when plants of the same cultivar are

grown in tightly controlled environments with the same conditions across all plants (Sirault et al., 2009).

The onset of drought stress caused by soil water deficit has been correlated with increased canopy temperatures of a plant through the impairment of transpiration because of stomatal closure limiting water loss (Vadez et al., 2014, Chaves et al., 2002). Recommendations have been made for field studies to measure temperature values around solar noon on a day without clouds to acquire temperature at the time of stress plateau to obtain consistent results (Jackson, 1986, Alchanatis et al., 2009). The push for repeatable and verifiable results has resulted in a myriad of temperature indices to provide a measurement considering the environmental state. Stress indices include the Crop Water Stress Index (CWSI) (Jackson et al., 1981, Maes and Steppe, 2012), Stomatal Conductance Index (Maes et al., 2016, Guilioni et al., 2008) and the Three-Temperature Method (Qiu et al., 2009). Each of the three previous indices relates leaf temperature to temperatures of reference surfaces contained within the same scene to establish expected boundaries of the leaf temperature. The easiest method of utilizing reference surfaces is to capture thermal images containing the any targets and appropriate reference surfaces so that all measurements are taken at once (Munns et al., 2010).

Thermal images can be associated with other image data to increase the stress prediction assessment as noted in a mini-review covering RGB, fluorescence and hyperspectral imaging (Humplík et al., 2015). Fluorescence imaging investigates photochemical reactions related to photosynthetic demand to predict stress before visible manifestations (Ellenson and Amundson, 1982), which is a similar goal to thermal imagery. In some specific cases where the genotype is well known, more direct techniques to evaluate fluorescence such as narrow band reflectance in visible wavelengths have shown comparable potential for stress detection compared to thermal imagery (Carter et al., 1996, Zarco-Tejada et al., 2012). A hyperspectral analysis in the TIR waveband can investigate the influence of biochemical compounds or stress events on spectral emissivity (Gerhards et al., 2016). Integration of thermal imaging into a larger stress-sensing platform that also includes fluorescence and spectral sensing would increase the sensitivity of stress detection in phenotyping operations (Prashar and Jones, 2014). More stress-sensing approaches would increase the sensitivity and specificity

of stress detection by providing a precise description of water status in plants (Ihuoma and Madramootoo, 2017).

### 2.3.1 Abiotic Drought Stress

Changes in plant behaviour due to abiotic stress are often spread across the entire plant, particularly in the case of annual plants which rely on fast responses to adapt and survive (Chaves et al., 2002). Comparisons of mean plant temperature measured under growth chamber conditions show the presence and the magnitude of growth impairment due to applied stresses (Sirault et al., 2009, Hatfield et al., 1984, Esmaeili et al., 2016). Assessing abiotic stress based on the whole-plant response is possible with fairly low resolution images taken from aerial platforms that can cover vast areas in a short time (Zarco-Tejada et al., 2012, Gómez-Candón et al., 2016). The mean plant temperature of separable dense canopies is easy to capture and compare within a single thermal image, independent of time of day or physiological state when the image is captured (Prashar et al., 2013).

The temperature of a canopy is influenced by the transpiration rate which is limited by the amount of water in a leaf. The behaviour of plant tissue when dehydrated determines the assessment of drought tolerance or drought avoidance in the genotype. Tolerant varieties experience the least reduction in plant growth and transpiration when dehydrated, while varieties with a strong response to drought stress retain water in plant tissue under water deficit (Blum et al., 1982, Tardieu and Simonneau, 1998). In the case of anisohydric plants such as wheat, leaf water content lowers under water deficit resulting in dehydration of leaf tissue as transpiration continues. Stomatal conductance in the anisohydric case remains high until water potential becomes critically low (Munns et al., 2010).

Sequences of genes that correlate with the expected stress handling behaviour have been isolated and genetic markers identified to track if those traits are likely to manifest in new cultivars based on genotypic analysis (Hirayama and Shinozaki, 2010). Charting these sequences in breeding programs can determine how stress handling is carried through to new generations by using marker-assisted breeding. Unfortunately, the bottleneck is quick and dependable field level phenotypic evaluations of stress tolerance that account for the full variability of the environment (White et al., 2012).

## 2.4 Phenotyping Models

A driving factor behind the push for phenotyping is to gather more data of plant development, and another tremendous step forward would be to model the behaviour that results in the observed response. These models could be used to assess the severity of stresses and their potential impact on the overall yield, the bottom line in crop production. Establishing concrete links between plant response to stress firmly rooted in plant physiology avoids the use of potentially misleading general indices such as the normalized difference vegetation index (NDVI) or crop water stress index (CWSI). Phenotypic responses are primed to be adapted into models as they are physical parameters that have resulted from the interactions between the environment and the plant.

### 2.4.1 Connecting Lab and Field

Phenotypic observation connects lab and field experiments as phenotypic responses observed in the field are matched to expected behaviour as determined from a lab study. Studies early in the breeding cycle of cultivar development seek to influence the growing environment and chart mechanisms activated by the plant to survive in the face of stress (Esmaeili et al., 2016). Studies of crops in producer fields or yield trials late in the development cycle assess if yield would be adversely impacted through observing responses connected to stress in earlier studies. Yield is the end goal of producers and as such breeders aim to find cultivars that can produce consistently large yields with the conditions present in a field. Plant breeders have already begun to develop cultivars for the conditions expected in the years or decades to come (Chapman et al., 2012). Precision agriculture systems will close the loop by providing more information to producers to facilitate immediate reactions to plant stress, securing increased yield (Khanal et al., 2017).

Continuous monitoring with tools such as thermal cameras can provide useful information related to plant development, such as photosynthetic ability or general productivity. Photosynthetic parameters such as stomatal conductance are valuable means for crop screening and cultivar development (Munns et al., 2010). Some groups have broken biomass generation into mechanistic models that relate instantaneous photosynthesis or total productivity

to another parameter such as radiation intercepted or water transpired over the same time period (Prashar et al., 2013, Furbank et al., 2015). These modelling methods are to be "based on sound crop physiology, not single pot experiments with model species" (Furbank et al., 2015). Relating energy and water use to biomass generation is a step towards approaching crop monitoring from a very analytical perspective. Mechanistic models are currently limited to lab-scale studies or phenotyping facilities as they are primarily used for crop screening.

### 2.4.2 Model of Phenotypic Thermal Response

Recent reviews of thermal imagery highlight models to transform temperature data extracted from thermal images into a form much more attractive to phenotyping research (Costa et al., 2013). The temperature of reference surfaces included in a thermal image provide implicit quantification of the local environment to normalize leaf temperature and remove the effect of the local environment to isolate plant behaviour (Jones, 1999). Leaf-representative reference surfaces mimic leaves at two levels of transpiration - a completely dry leaf with zero transpiration and a leaf that is continually transpiring at the absolute maximum rate allowed by the environment (Maes et al., 2016). The Crop Water Stress Index (CWSI) is calculated as a function of leaf temperature relative to reference temperatures. References can include air temperature or maximum and minimum observed crop temperature depending on which approach is used (Maes and Steppe, 2012). Calculation of the empirical form of CWSI from artificial leaf reference surfaces results in:

$$CWSI = (T_{leaf} - T_{wet})/(T_{dry} - T_{wet}) \tag{2.1}$$

where:

$T_{leaf}$ is the leaf temperature [K],

$T_{wet}$ is the temperature of the wet reference [K],

$T_{dry}$ is the temperature of the dry reference [K].

CWSI is correlated with water deficit as expected in orchard trees, which assists with irrigation scheduling (Gonzalez-Dugo et al., 2013). CWSI fails to distinguish stress under cool

or cloudy conditions with low evaporative demand and minimal incident sunlight (Maes and Steppe, 2012, Gonzalez-Dugo et al., 2013, Jones, 2013). CWSI has been employed to monitor and maintain a slight level of stress to create ideal wine grapes, an excellent application of the quantifiable index (Möller et al., 2006). Observation of CWSI is not the perfect solution to stress sensing as measured stomatal conductance obtained near midday changed significantly in response to stress events more quickly than CWSI obtained from thermal images (Gerhards et al., 2016). Similarly, stomatal conductance measured near midday has been noted to respond faster to stress events compared to canopy temperature difference from ambient temperature (Struthers et al., 2015).

CWSI and the related Stomatal Conductance Index are linked to stomatal conductance (Berni et al., 2009a, Maes et al., 2014), and the full relationship has been approached in several fashions. Continuing to use indices empirically led to modelling stomatal conductance based on Stomatal Conductance Index and the ambient temperature in a polynomial expression fit to measured stomatal conductance (Maes et al., 2016). Calculating stomatal conductance requires energy balance models that incorporate weather data to calculate in field energy fluxes (Jones, 2013). After sufficient assumptions of the radiation behaviour and wind-driven heat transfer, stomatal conductance can be calculated to satisfy the energy balance equation. Accurate leaf representative reference surface temperatures can be substituted into the energy balance equation to simplify the expression. Several forms of the simplified energy balance equation have been derived, and the correct choice depends on the wetting of the reference and the distribution of stomata on the leaf surfaces (Guilioni et al., 2008). Most field crops, including grains, are monocots which can be assumed to have similar distributions of stomata on upper and lower leaf surfaces.

# Chapter 3

# Directionality of Emissivity and Reflectivity

## 3.1 Introduction

Non-contact measurements of plant temperature are desirable as the sensor does not induce a loading error and can capture a temperature quickly and easily. Non-contact thermal sensors include thermal cameras with a small pixel count and infrared thermometers which could be viewed as a single pixel measurement as it produces a single measurement integrated over an area. Low-resolution sensors often are plagued by the issue of mixed pixels, elements which contain information about several disparate objects, such as soil and leaves in the case of canopy imaging (Jones and Sirault, 2014). With advancements in thermal imagery and the introduction of instruments with more sensing elements, more studies can gather high resolution and accurate data from non-contact means.

In order to confidently assess the temperature of vegetation, including leaves, obtained from non-contact radiation sensors, it is necessary to examine the underlying physics that define thermal radiation. Kirchoff's law of thermal radiation states that an object in thermodynamic equilibrium will absorb radiation in the same proportion that it emits radiation to satisfy the energy balance. Kirchoff's law still holds for nonisothermal bodies, but care has to be taken to separate emitted radiation from total outbound radiation (Zhang, 2005). The Stefan-Boltzmann law directly relates the absolute temperature and radiative power emitted by the object, augmented by the surface emissivity as required. The complete set of relations between the incident and outgoing radiation is established with the assumption of zero transmission of thermal wavelengths through an object and applying Kirchoff's Law. Obtaining a value of surface temperature requires isolation of the power emitted from the surface by accounting for reflected radiation that is picked up by the detector. Separating a

radiative power measurement into two components of emitted and reflected radiation based on the Stefan-Boltzmann law and the emissivity of the surface results in:

$$E = \sigma T_{apparent}^4 = \epsilon \sigma T_{surface}^4 + (1 - \epsilon)\sigma T_{reflected}^4, \tag{3.1}$$

where:

$E$ is the radiative power from an observed surface[W·m$^{-2}$],

$\sigma$ is the Stefan-Boltzmann constant [W·m$^{-2}$·K$^{-4}$],

$T_{apparent}$ is the temperature representation of all outgoing thermal radiation from the surface [K],

$\epsilon$ is the surface emissivity,

$T_{surface}$ is the true surface temperature [K], and

$T_{reflected}$ represents external energy originally emitted from an external surface and reflected off of the observed surface [K].

The transmission through and absorption of thermal radiation into the atmosphere is dependent on the amount of greenhouse gas molecules in the path between the sensor and the target. Transmission of thermal radiation through the atmosphere is commonly assumed to be unity at close range (Aubrecht et al., 2016).

The reflection of radiation has two components: a specular reflection which emanates from the surface at the same angle to the surface normal as the incident radiation comes in, and diffuse reflection which scatters incident radiation in all outward directions. If the specular component of reflection is significant, then the outward radiation of the observed surface could be influenced heavily by the presence of a hot object provided the detector-target-source geometry allowed for specular reflection to be viewed. Reflections of thermal wavelengths from bare leaf tissue are expected to be diffuse as the leaf surface is rough due to large cellular structures relative to the light wavelength (Gates et al., 1965). Understanding the nature of the radiation reflected by leaves will help in avoiding incorrect observations when looking at thermal image data. An assumption of diffuse behaviour is prevalent (da Luz

and Crowley, 2007), as is adjusting the reflected temperature to calibrate thermal camera temperatures to the measurement of a reference surface (Gómez-Candón et al., 2016).

Two tests were implemented to determine the emissivity and reflectivity present when observing leaves in a field setting with a thermal camera. The first test to assess the emissivity of leaves used a water bath to set the leaf temperature while thermal images of the leaf were acquired from many different angles. Variation in emissivity of leaves across view angles could be due to physical surface characteristics such as leaf hairs and wax. If leaf emissivity can vary, it would be appropriate to measure the angular variance and state the error introduced by acquiring thermal images of leaves with the assumption of hemispherical average emissivity. Leaves are biologically inclined to be excellent surfaces for radiative heat transfer in order to discard waste heat, and high emissivity at all angles would result in less change of the radiative transfer when the leaf moves.

The second test undertaken addressed the effect of local hot objects on outward surface radiation and investigated different characterizations of incident reflected radiation and the value of applied radiometric corrections based on each characterization. From equation (3.1) it is possible that a local increase in apparent temperature on the surface under observation could be due to the presence of some hotter object nearby reflecting off of the surface. It was expected that specular behaviour would not influence temperature measurements of leaves as reflections would be slight due to high emissivity and entirely diffuse due to cellular structure promoting Mie scattering (Gates and Tantraporn, 1952, Gates, 1970).

## 3.2 Methods

### 3.2.1 Emissivity

Leaf emissivity was calculated using temperatures extracted from thermal images of a leaf set into a water bath with a characterizing surface nearby. An open water bath was heated, and a recently picked leaf was placed carefully to float at the centre of the water surface. The leaf was assumed to have the same temperature as the surface of the water, under the implicit restrictions that emissivity of the water and leaf are similar and convective heat

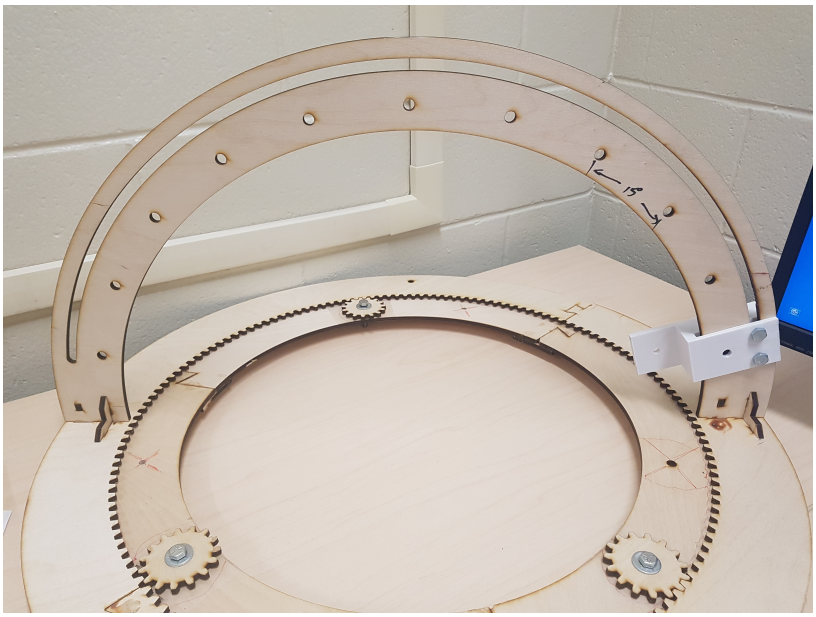

**Figure 3.1:** A picture of the goniometer showing the white plastic camera mount which can slide to pinning points on the zenith arc. A ring gear system allows for travel through azimuth values. The azimuth values are located by pinning the ring gear to the base below it.

transfer from these surfaces were roughly equal. Aluminum foil was crumpled and flattened and set on the water around the floating leaf to aid in characterizing the surroundings. A FLIR Vue Pro R thermal camera (FLIR Systems, Nachua, NH) was rigidly mounted to a goniometer capable of bringing the camera to 61 unique points on a hemispherical shell above the target. The goniometer can be viewed in figure 3.1 with 11 evenly spaced points on the zenith arc every 15° from $-75°$ to 75° and stops every 30° along the azimuth from 0° to 150°. The radiometric camera reports temperature values with a quoted accuracy of $\pm 5$℃ and measurement precision of 0.04℃. The camera is $250 \pm 5$ mm away from the leaf sample at all points on the arc. Thermal images containing the leaf and foil were captured from every point on the goniometer with emissivity set to one and saved as TIFF files with each pixel value corresponding to the apparent temperature at that location.

The emissivity of aluminum foil is very low about 0.07 (Brewster, 1992), which results in very little difference in the values of apparent and reflected temperature. $T_{reflected}$ was assigned to be the mean apparent temperature of the foil following in the example set by other studies that investigated leaf emissivity in a water bath (López et al., 2012). This

assumption should only produce a small amount of error but does result in an overestimation of the reflected temperature incident to the scene if the foil surface temperature is higher than reflected. The aluminum foil was expected to have a surface temperature near the water surface temperature which would be hotter than the surroundings. The apparent water surface temperature was measured from the thermal image, and the water surface temperature was calculated with emissivity set to 0.96 (Brewster, 1992) and apparent foil temperature equal to $T_{reflected}$ in equation (3.1). Water surface temperature was expected to be lower than the bulk volume water temperature due to convective and radiative cooling at the surface. The equation to determine leaf emissivity was based on the Stefan-Boltzmann law decomposition of apparent temperature into the surface and reflected temperatures. Equating the surface temperatures of two instances of equation (3.1), one for water and another for the leaf, results in:

$$\epsilon_\ell = \epsilon_W * (T^4_{\ell,apparent} - T^4_{foil})/(T^4_{W,apparent} - T^4_{foil}), \tag{3.2}$$

where:

$\epsilon_\ell$ is the emissivity of the leaf,

$\epsilon_W$ is the emissivity of water,

$T_{\ell,apparent}$ is the apparent temperature of the leaf [K],

$T_{foil}$ is the temperature of the foil [K], and

$T_{W,apparent}$ is the apparent temperature of the water [K].

The leaf emissivity was calculated by matching the mean temperature value for the entire leaf area to the expected temperature of the leaf, which in this case was set as the mean water surface temperature. This calculation was done for each view angle separately, there was no calculation of emissivity using temperatures from different images.

### 3.2.2 Reflection

The leaf specific nature of thermal reflection was isolated by examining the apparent temperature of a leaf in response to an external source. A leaf was set on a water bath, floating

**Figure 3.2:** The reflection setup with the water bath and two sheets of aluminum foil representing two distinct reflection patterns. The thermal camera is on the platform at the back.

between two sheets of aluminum foil draped over the water. One foil sheet was smooth, and the other crumpled and flattened. These two surfaces showed the distinct difference between specular and diffuse reflection as the smooth foil microstructure does not reflect thermal radiation diffusely. The diffuse reflection viewed from the crumpled foil is instead an average of many specularly behaving facets arranged at random. The thermal camera was set on a stationary platform approximately 30° above horizontal and 250mm away from the centre of the bath. On the opposite side of the bath from the camera, approximately 400mm away from the water bath, was a movable shield that blocked a hotplate acting as a stable heat source. A picture of the setup taken from the location of the hotplate can be viewed in figure 3.2.

The hot plate was set at 50℃ while hidden from the water bath and thermal camera setup. After five minutes to allow the leaf to acclimate, the camera was set to record in video mode to capture raw stacked TIFF files at a rate of five frames per second. The reflective shield that isolated the hot plate was removed a few seconds after recording started. The leaf was allowed to heat for ten seconds, and then the shield was replaced for the last ten seconds in the video. Leaf and water surface temperature were expected to increase instantaneously

due to an increase in reflected radiation and over time due to radiative heat transfer. The magnitude of instantaneous change was used to indicate how specular the reflections from the surfaces were. Surface temperatures were calculated using emissivities determined in the previous study with two characterizations of reflective behaviour to determine if specular behaviour exists in the leaves.

## 3.3 Samples

Data collection occurred December 1st and 4th, 2017 with the aid of faculty in the College of Agriculture and Bioresources at the University of Saskatchewan. The plants investigated were all field crops, and the selected leaves were sourced from a single plant of the variety grown in an environmental chamber. The green bean (*Phaseolus vulgaris* L.) and canola (*Brassica napus* L.) plants were near the end of their life cycle but still possessed healthy leaves. Soybean (*Glycine max* L.), oat (*Avena sativa* L.) and faba bean (*Vicia faba* L.) plants were all seeded on November 2nd and were still in the vegetative stage of growth.

Three leaves in total were picked the upper third of the canopy from one green bean, canola, soybean and faba bean plant, one at a time. Each leaf was laid into the water bath heated to 42℃ with the upper side of the leaf visible for image acquisition. Each leaf was imaged at the 61 unique points on the hemispherical arc with six images at the nadir as an image was acquired for every stop on the zenith arc before the goniometer then rotated along the azimuth. Issues with power delivery to the camera led to some images not saving correctly, and image total per trial did not add up to 66 in all cases. A sample thermal image of a green bean leaf can be viewed in figure 3.3.

Qualitative surface characteristics were assessed visually to log the leaf trichome density and wax load. The green bean leaves were large, covered with very fine trichomes and possessed a moderate wax load. The canola leaves collected had no trichomes and a very waxy upper surface with thick leaves and easily visible veins. Soybean leaves possessed a tremendous amount of trichomes that formed a barrier above the leaf surface, which itself was not particularly waxy. Faba beans were free of trichomes and had a slightly waxy surface.

On the second day of image acquisition the water bath heater broke and was replaced

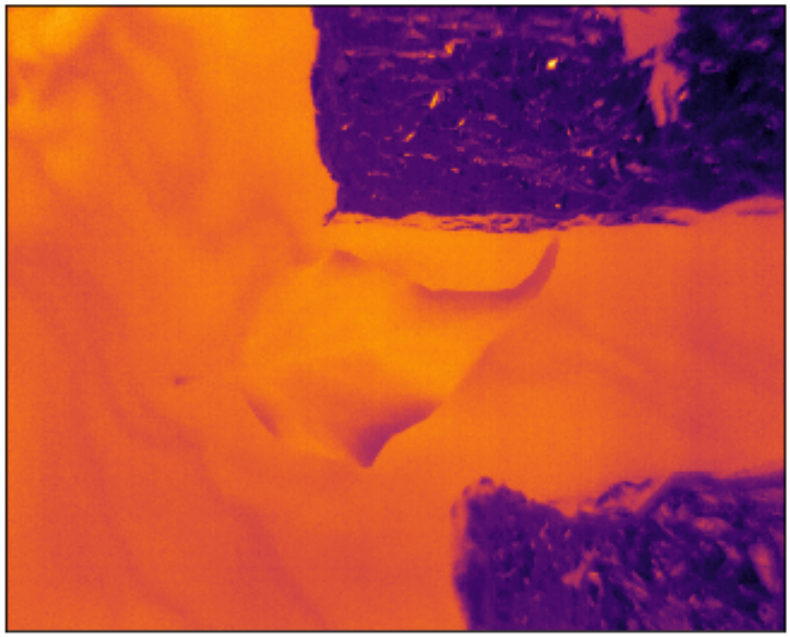

**Figure 3.3:** Sample thermal image of a green bean leaf in the emissivity study, showing foil surfaces and the leaf in the centre.

with a smaller unit. With less heat delivery, the setpoint of the bath was lowered to 35℃. For the last emissivity test, three selected oat leaf segments were placed into the water bath one at a time. Oat leaves had significant striations along the leaf, with no trichomes and a slight wax load. The second day of measurements included the specular experiment. A single leaf was sourced from the upper canopy from each of the same plants as the emissivity experiment. Each leaf was set on the water surface in the centre of the water bath with the tip of the leaf pointed toward the camera with the foil sheets on either side as can be viewed in figure 3.4 for a green bean, with smooth foil on the right and crumpled foil on the left. There were no issues with image capture in this experiment and one video of roughly twenty-five seconds was captured for each leaf.

## 3.4 Analysis

Masking and segmentation of the thermal images was accomplished in MATLAB 2016 (The Mathworks, Natick, MA) using the image segmentation app. Difficulties in automatically

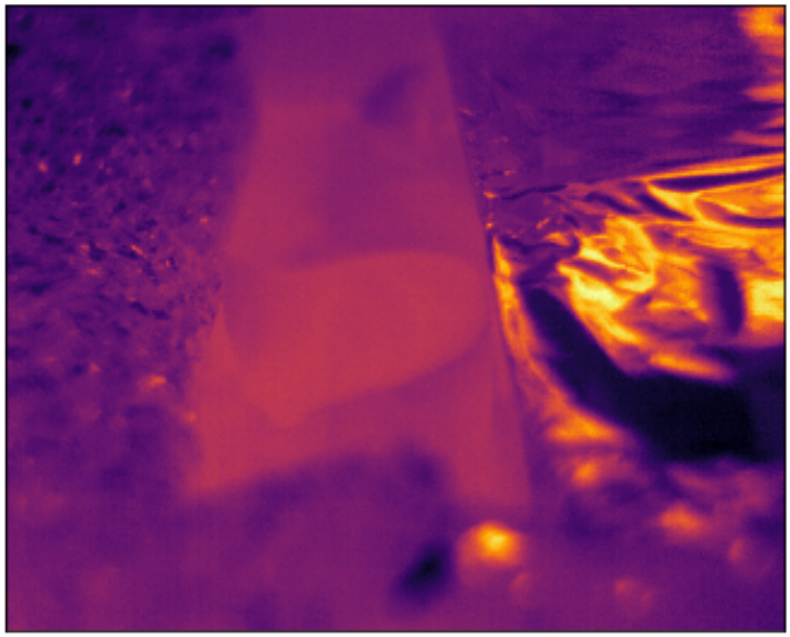

**Figure 3.4:** One frame of the thermal video of a green bean leaf in the reflectivity study, showing crumpled foil on the left and smooth foil on the right with the leaf in the centre.

segmenting the images led to using the freehand tool to select three areas in each image of the emissivity study: the foil surface floating on the water, a section of open water near the leaf, and the leaf. The image mask for the aluminum foil included a portion near the centre of the foil that would reflect a significant amount of the room above the bath due to the many facets on the surface. Pixels selected for the water region were as close as possible to the leaf and away from the heater in the water bath. The mask created for the leaf nominally included the centre of the leaf, avoiding edges and any portion of the leaf lifting away from or dipping under the water surface. Video files acquired in the second experiment only required one mask each because the constituent regions did not move. The masks for the video files had four regions: water, leaf, smooth foil and crumpled foil.

Thermal images and associated masks for experiment one were loaded into an analysis pipeline built in python 3.6. Leaf emissivity is calculated for each view available on each leaf in the first experiment using the mean temperature of each region in equation (3.1). Calculated emissivity values for each leaf were averaged together to create a hemispherical mean emissivity. The standard deviation of the set of calculated emissivity for each leaf was

calculated to determine the variance between angular views.

Apparent mean temperatures extracted from each frame of the videos obtained in the second experiment are plotted against each other to demonstrate the influence of the introduction of the hot object to the scene. Leaf surface temperatures are calculated in four different arrangements, using sample emissivity values of 0.96 and 0.98 with the value of reflected temperature, representing radiant energy from the surroundings, set equal to the measured apparent temperature of either the smooth foil or the rough foil. These leaf surface temperatures were plotted relative to the apparent temperature to uncover the magnitude of radiometric corrections with emissivity values expected for vegetation (López et al., 2012) and two different behaviours of radiation reflection.

## 3.5 Results

The mean and standard deviation of emissivity for each leaf as determined from all views available are presented in table 3.1. Every calculated mean hemispherical value of emissivity was greater than one, which is a physical impossibility. Considerable standard deviation across the view angles was also observed and speculation of the root cause of these issues is contained in section §3.6. The emissivity distribution along the leaf surfaces can be viewed in figure 3.5. Interestingly, the leaves with waxy surfaces (green bean and canola) have higher deviation and the polar plots show these leaves have large patches of high emissivity. The emissivity bias may be an error common to all replicates and is not necessarily an indication of the influence of leaf wax. Oat leaves were not exceptionally waxy but do show patches of high emissivity but they all have high average and standard deviation, and leaf three had exceptionally high emissivity outliers.

A sample of the apparent temperature of each region in images of a soybean leaf taken from all points on the goniometer can be viewed in figure 3.6. Temperatures shown were extracted from manually segmented areas on sequential images acquired at different locations on the goniometer. Water and leaf temperatures follow a similar trend, but the foil temperature does not, highlighting the different behaviour expected of high and low emissivity surfaces. As expected, the foil region has the coldest apparent temperature as the majority of total outward

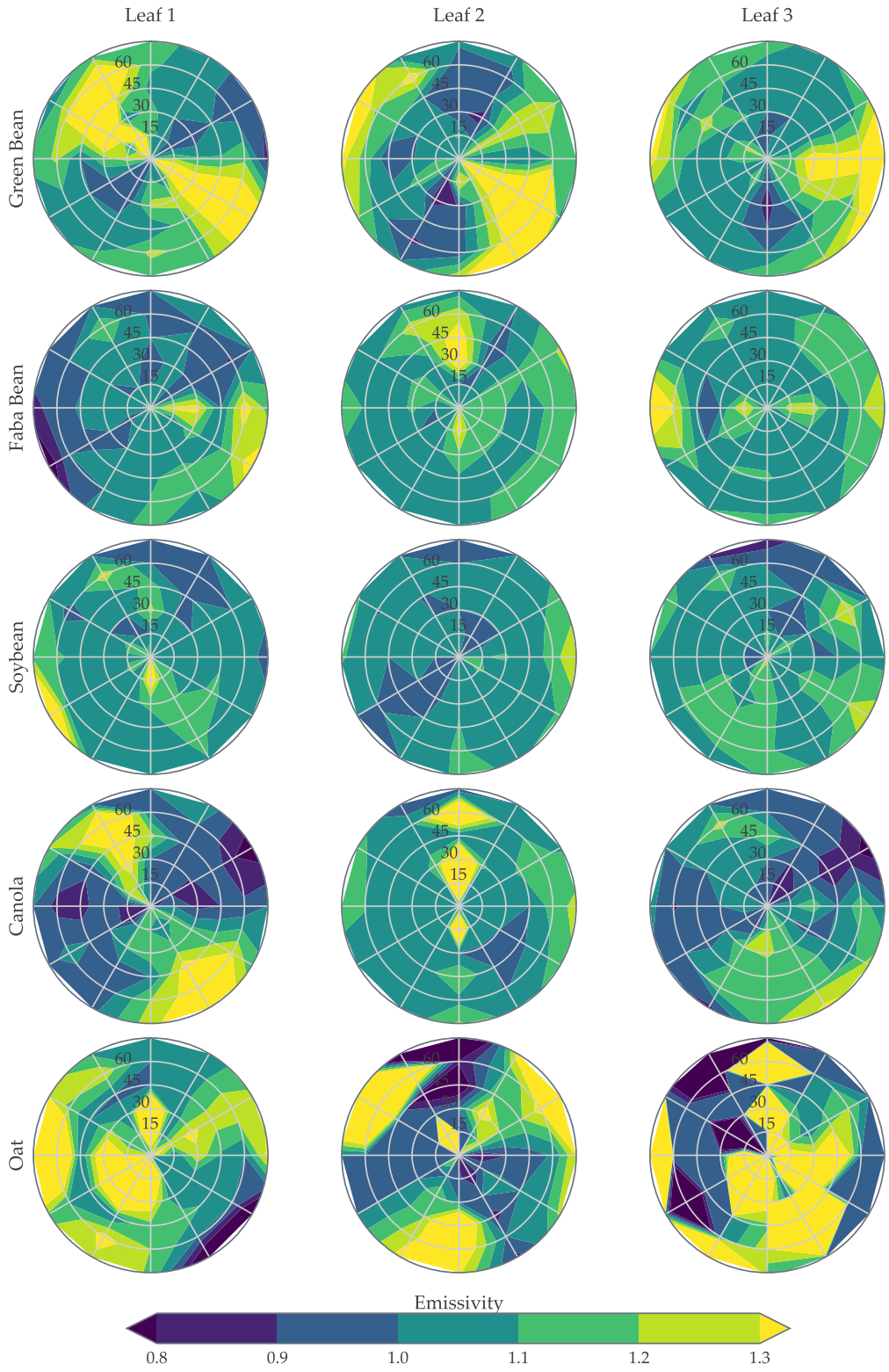


**Figure 3.5:** Polar contour plots of calculated leaf emissivity. The top of each plot is aligned with the leaf tip. The scale for emissivity for each plot is bound between 0.8 and 1.3 and contour lines are drawn at intervals of 0.1. Intersection of lines denotes a measured point.

**Table 3.1:** Hemispherical mean leaf emissivity and standard deviation of emissivity calculated across all views of five leaf species.

| | Leaf 1 | Leaf 2 | Leaf 3 |
|---|---|---|---|
| Green Bean | 1.17 ($SD$=0.20) | 1.16 ($SD$=0.23) | 1.14 ($SD$=0.15) |
| Faba Bean | 1.06 ($SD$=0.13) | 1.13 ($SD$=0.10) | 1.12 ($SD$=0.10) |
| Soybean | 1.10 ($SD$=0.11) | 1.05 ($SD$=0.07) | 1.10 ($SD$=0.08) |
| Argentine Canola | 1.08 ($SD$=0.21) | 1.13 ($SD$=0.25) | 1.04 ($SD$=0.14) |
| Oat | 1.33 ($SD$=0.43) | 1.24 ($SD$=0.69) | 3.00 ($SD$=3.56) |

radiation from the foil surface is the reflection of the cooler surrounding room surfaces. The apparent temperature of the leaf is the highest, which is consistent with the assumption that the emissivity of the leaf is very high. Water temperature appears low compared to leaf temperature - a concern as the calculation of leaf emissivity is based on the difference between temperatures. When water and leaf temperatures diverge significantly, there is a significant jump in calculated leaf emissivity. As shown in figure 3.7, a difference between leaf and water temperature of fewer than 0.3 degrees Celsius will result in a leaf emissivity of less than one.

The influence of the hot plate introduced in experiment two on the leaf and foil temperatures over time can be viewed in figure 3.8. The apparent temperatures are much more stable in this setup as the camera was stationary, and a single mask was applied to continuously captured images. Both foil surfaces had a lower apparent temperature at the start and end as reflections dominate the outward radiation. The foil surfaces registered slightly different temperatures when the hot plate was hidden. Upon uncovering the hot plate, an initial step in the apparent temperature of all items was expected due to the presence of more radiation to reflect. As expected, the smooth foil apparent temperature increased more than the crumpled foil apparent temperature as the reflection in the smooth foil was more specular and reflected more of the hot plate than the random facets of the crumpled foil. The apparent temperature of the smooth foil dipped slightly near the end of the heating period. This was due to slight movement in the support for the hot plate changing the location of the greatest specular reflection and the mask was not updated to reflect the movement. The rough foil

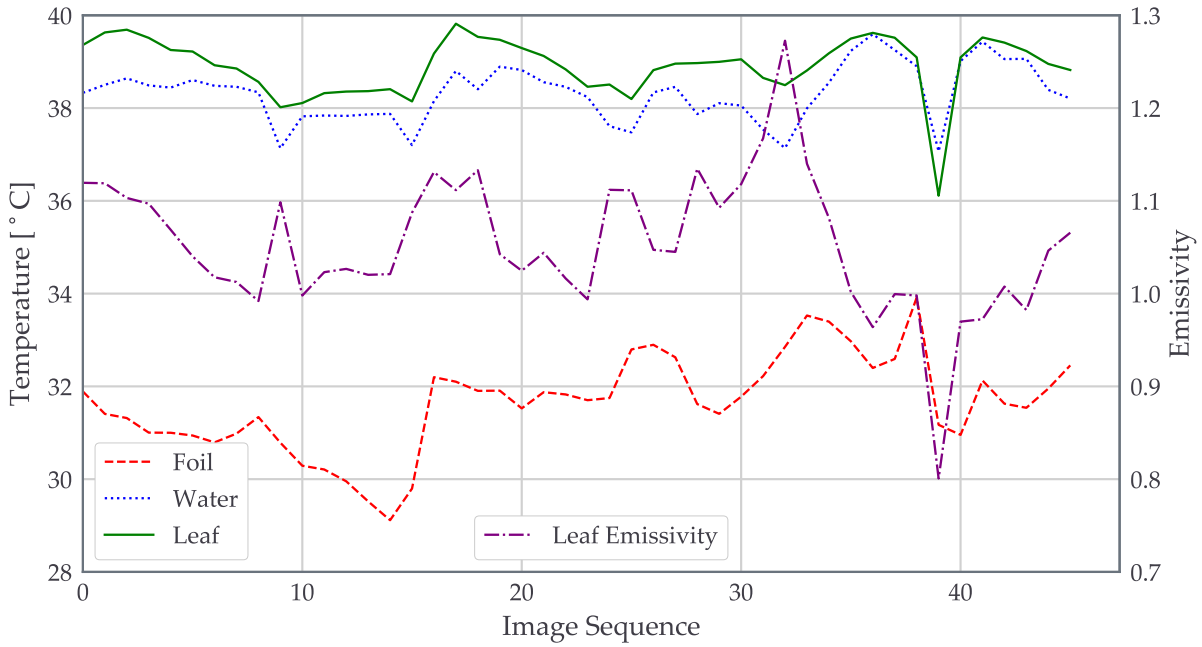


**Figure 3.6:** Mean apparent temperatures of a soybean leaf, foil, and water in manually-collected images in experiment one. The calculated leaf emissivity for each sample is displayed with the scale on the right.

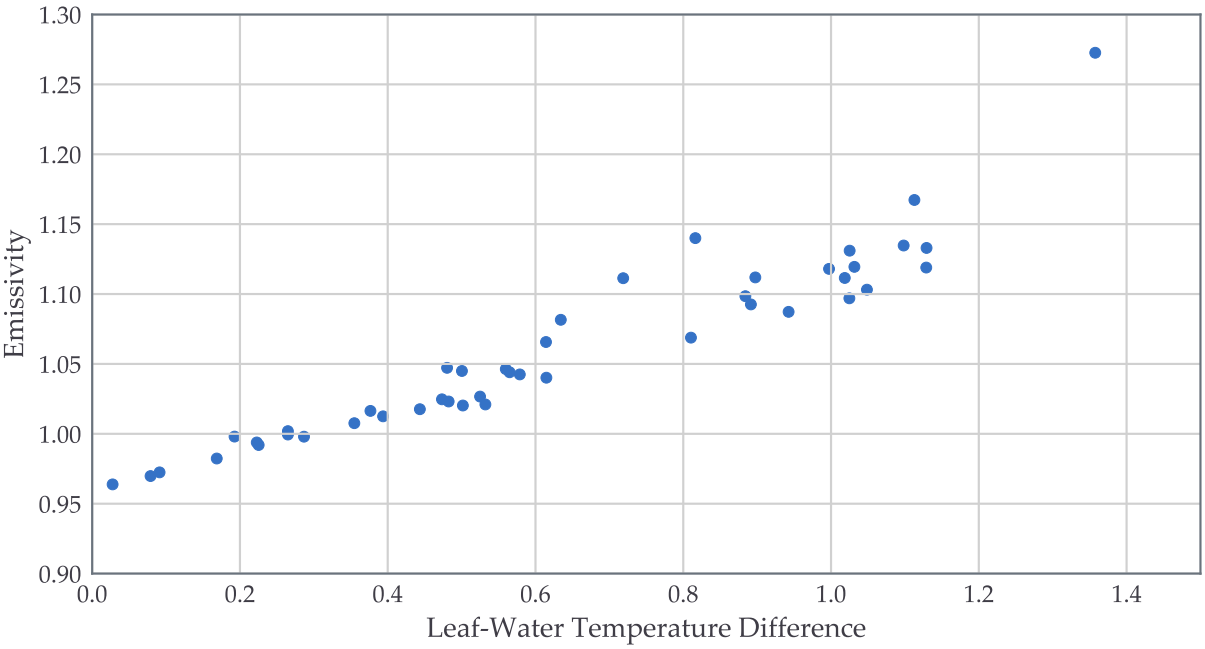


**Figure 3.7:** Calculated leaf emissivity as a function of the difference of the apparent water and leaf temperatures for all views of a soybean leaf collected on a goniometer.

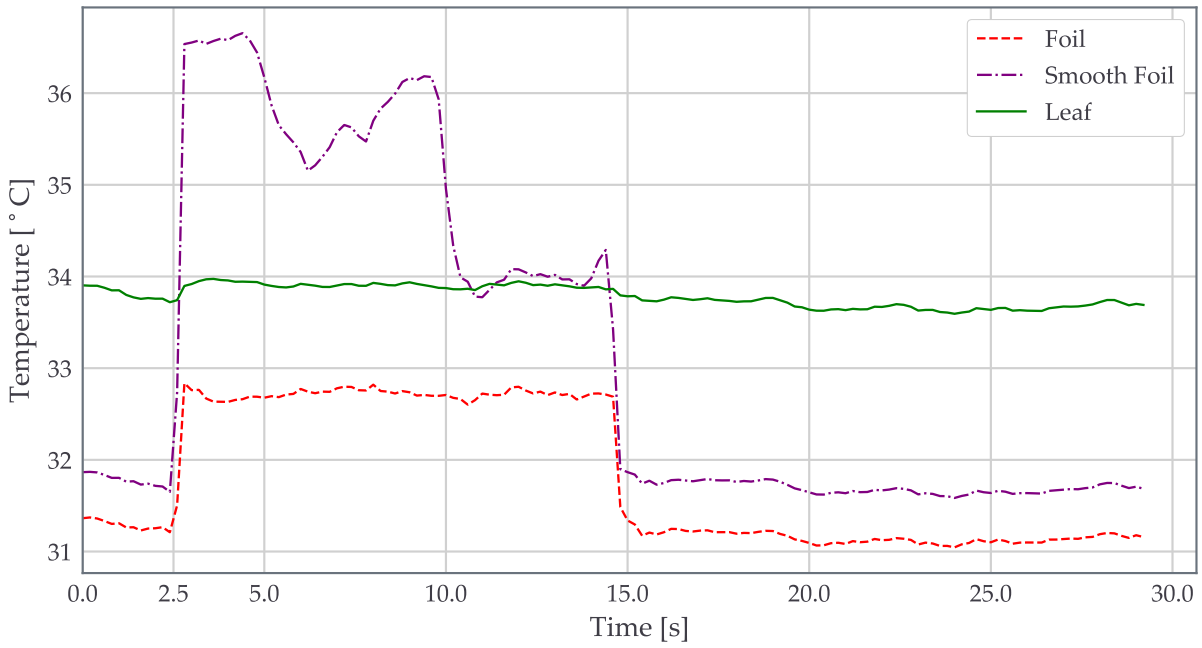


**Figure 3.8:** Apparent temperature of soybean leaf and foil surfaces in response to changing environment in experiment two. A hot source was introduced at roughly two and a half seconds and removed at 15 seconds.

surface was not affected by the slight movement of the hot plate as the surfaces continued to reflect the incoming radiation diffusely.

The difference of leaf surface temperature calculated using these two characterizations of the scene at specified emissivity from the apparent temperature is detailed in figure 3.9. The smooth foil apparent temperature was higher than the leaf apparent temperature when the hot plate was active, and as such the calculated leaf surface temperature was lower than the apparent leaf temperature. With the assumption of specular reflection behaviour, the leaf surface temperature was higher than the apparent initially, then switched when the hot plate was active. Specular radiometric corrections result in leaf surface temperature changing very slightly with the presence of the hot plate as the reflections are assumed to comprise more of the increased apparent temperature. Diffuse behaviour would keep leaf surface temperatures higher than apparent at all points investigated here.

With assumed emissivity values of 0.98 or 0.96, the apparent temperature is so close to the surface temperature that improving the accuracy of the reflected energy characterization will not greatly improve the accuracy of surface temperature measurements. There is a 0.15℃

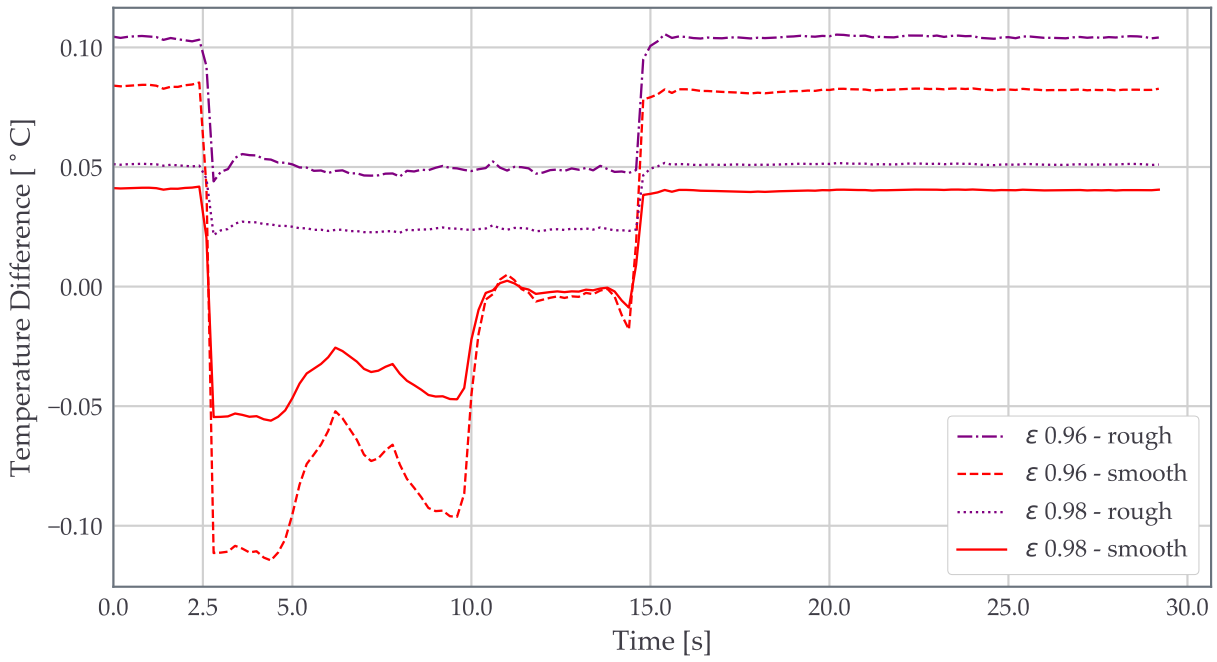


**Figure 3.9:** Difference of calculated leaf surface temperature from apparent temperature in soybean with two characterizations of changing environment in experiment two. At negative values, the leaf surface is cooler than apparent temperature.

difference between the surface temperature calculated with specular and diffuse behaviour at an emissivity of 0.96 with the hot plate active. The difference between surface temperatures from apparent temperature is 0.05℃ for a diffuse thermal reflection and 0.10℃ for specular thermal reflection.

## 3.6 Discussion

Leaf, water and foil regions were manually segmented by drawing the mask on top of the image. In views at high angles from nadir only small areas of water often far away from the leaf were visible. Nadir and near-nadir views also suffered as the sizable non-obstructed area of water had a wide range of temperatures through the bath. Warm currents emanating from the heater were evident and hot areas were deliberately avoided leading to intentionally low water temperature. The temperature variation along the surface of the water bath visible in figure 3.3 was significant enough that the choice of manual segmentation for each image in experiment one introduced operator error.

The differences between leaf and water temperatures were slight as they should have very similar values of emissivity. The apparent temperature of foil used to represent reflected radiant energy in the soybean test viewed in figure 3.6 is roughly eight degrees lower than the leaf and water temperatures. While none of the values of hemispherical emissivity listed are suitable for use, the value of emissivity for oat is much higher as the water and leaf temperature dropped closer to the foil temperature when the heater stopped working. Leaf emissivity calculations are susceptible to slight differences between water and leaf temperatures and the equation requires a substantial difference from the foil temperature to minimize the effect of small changes in the leaf-water temperature relation (López et al., 2012). The findings of López et al. of high emissivity and high variance over the 180 samples when water temperature was close to ambient conditions mirror what was observed here. Calculating a leaf emissivity of less than one holding to the assumption of shared water and leaf temperature with the results displayed in figure 3.6 would require a lower value of water emissivity to explain the difference between leaf and water temperatures. Another potential for error in thermal camera data is biased recordings due to the inaccuracy of the sensor. Many cameras self-calibrate to reduce bias, but leading manufacturers quote accuracy ranges of $\pm 2$℃ for high end actively cooled models and $\pm 5$℃ for uncooled microbolometer elements. The thermal camera sensor does seem to have great precision as noted in the second experiment in which the temperature of diffuse surfaces did not vary more than roughly 0.2℃ in periods with the source active or inactive. The calibration of the sensor appears to be stable, but the bias was not assessed in this study. Including a reference material with known temperature into the scene of each image would help to identify bias. The emissivity calculation relies on the differences of a fourth power of the absolute temperature, and a consistent bias across all image pixels will lead to uncertainty in the emissivity calculation where a linear comparison of temperature would be unaffected.

If a study similar to this is to be attempted again, there are a significant amount of elements that should be improved upon. It is suggested to acquire many images at each point on the goniometer and apply the same mask to each image per point on the goniometer so that each view can have an emissivity with a calculated statistical distribution. The water bath was quite warm when set to 42℃ but the extremely high reflected temperatures

introduced uncertainty. Any similar study should be performed with either a hotter water bath or a much cooler room with surrounding temperatures that are closer to 22-24℃.

## 3.7 Conclusion

This study was positioned to explore the operation of an infrared detector to verify the radiant exitance from a leaf is well understood so it can be converted into accurate temperature measurements. There may be slight directional effects, but overall leaf emissivity is very high. The difficulties in emissivity determination aside, it is concluded from the second study that any radiometric correction of non-contact sensor data would be minimally influenced by surface effects. Reflected thermal radiation from leaves contributes very little to the overall signal registered by a detector. Non-contact apparent leaf temperature and any significant variation in a time series signal can be attributed to the actual surface temperature and not merely a reflection of energy from surrounding bodies. Studies can then focus on image composition and scale without having to consider adjusting emissivity and implementing different radiometric correction protocol based on the leaf angle or leaf type. Radiometric calibration may still be necessary to secure absolute accuracy when working with thermal imagery.

# Chapter 4
# Developing A Model of Plant Temperature Response

## 4.1 Introduction

Plant growth and development is complex - genetics, environment, and interactions between the two create an observable phenotype (Araus and Cairns, 2014, Fahlgren et al., 2015). Crop development groups cross genetic stock to create new and unique cultivars (Tardieu et al., 2017). Plant breeding efforts evaluate the phenotype of cultivars subjected to the lab or field growing environment to select those with the best potential for producers to generate food, fuel, feed or fibre efficiently with the resources available (Fahlgren et al., 2015). Observation of the phenotype is also important to producers as it serves as an indicator of growth and progress toward the advertised potential yield.

A simplified definition of plant stress states that it is responsible for diminished yields and arises in plants when the ability of the plant to grow is reduced in any manner (Jackson, 1986, Jones, 2013). Stresses are induced by non-ideal growing conditions stemming from biotic and abiotic factors. Biotic stresses are induced by other organisms and common stressors include disease, unwanted pest plants, and insects. Biotic damage is difficult to attribute to a particular stressor without significant information on the local environment which includes the history of disease factors accumulated in a field (Jackson, 1986). Abiotic stresses are due to non-living sources and are brought on by field conditions and resource availability. Classic examples of abiotic stress are shortages of nutrients or the presence of heavy metals in the soil (Maes and Steppe, 2012). Other abiotic stresses include extreme temperatures, and the water availability or salinity concentration in the root zone of plants (Jones, 2013, Esmaeili et al.,

2016, Sirault et al., 2009, Munns et al., 2010). Successful crop production must minimize the impact of stresses to maximize yield. The contribution of plant breeders in raising crop yields is to develop cultivars that can handle expected conditions effectively with tolerances that allow the crop to maximize growth through adverse conditions (Chapman et al., 2012, Tardieu et al., 2017).

In a lab or field growing environment, one of the most critical considerations is water availability and drought stress (Chaves et al., 2002, Maes and Steppe, 2012, Munns et al., 2010). A lack of water available to a plant results in impaired transpiration, the process by which a plant manages internal energy. The transpiration process moves water to the leaves where it is released from stomata, resulting in evaporative cooling as the water converts from liquid to gaseous phase and transfers into the local environment. The physiological mechanisms that control this process have variable sensitivity in different crop cultivars, making cultivars tolerant or sensitive to drought (Tardieu and Simonneau, 1998). Tolerance to drought stress will result in normal function at low water potential while sensitive varieties will pause growth and conserve water by closing stomata slightly to restrict the transpiration process. As the transpiration rate affects the energy balance of the plant, the temperature of the plant is an ideal property to measure to assess the severity of drought stress (Leinonen and Jones, 2004, Sirault et al., 2009). Increasing levels of stress can be inferred as transpiration is impaired further and temperature rises. The temperature of a plant is highly variable as it is a function of the shifting local environmental conditions that contribute to the energy balance (Maes and Steppe, 2012, Leinonen et al., 2006). The strength of sunlight changes across the day and is dependent on cloud cover while wind speed affects the rate of heat and water transfer from the leaves by inducing forced convection. Crop canopy temperatures under the same environmental conditions can be compared to assess stress, assuming the weather influence is equal on both crops and only stress would increase temperature (Gómez-Candón et al., 2016).

The analysis developed within this study attempted to link apparent vegetation temperature with local weather to enable more robust comparisons of plant leaf temperatures measured at different times by including consideration of the local environment. An attempt to catalogue environmental influence leads naturally to phenotypic modelling. Modelling

uncovers the plant behaviour required to satisfy the temperature response given the environmental conditions (Leinonen et al., 2006, Maes and Steppe, 2012, Jones, 2013). If the modelled value of the plant property is accurate and more stable across field conditions than raw leaf temperature or a simple leaf-air temperature difference, it would be prudent to measure and report this property to assess plant behaviour. The plant's amenability to water loss, stomatal conductance, can be calculated from an energy balance applied at the leaf level. The feasibility of implementing automated retrieval of temperature from thermal images of outdoor fields at close range and introducing local climate data to model stomatal conductance is explored here to prove a method of stress analysis that is completely automated and reproducible.

## 4.2 Methods

This study investigated leaf temperature from wheat (*Triticum aestivum* L.) in an outdoor field at the University of Saskatchewan Kernen Research Farm. The plot was sown with an air drill, similar to a producer field, with nominal seeding rate and twelve inch row spacing. Twelve 34-gauge T-type thermocouples were attached to flag leaves of twelve different wheat plants to acquire contact measurements of temperature. The thermocouples were secured with a light wire clip to avoid mechanically stressing the leaf; contact between the thermocouple and leaf was very light and excess thermocouple wire hung down the plant to a junction box. A thermal camera was positioned approximately 1.5m above the canopy with all twelve tagged wheat plants in view to capture non-contact measurements of plant temperature. The thermal camera used in this study was a FLIR Vue Pro R (FLIR Systems, Nashua, NH) with the 19mm lens option. The camera has a spatial resolution of 640x512 pixels and the sensor measures radiation in the $7.5 - 13.5\mu m$ band with a measurement accuracy of $\pm 5$℃ and a resolution of 0.04℃.

Weather station sensors were added to the frame that held the thermal camera, allowing for weather data to be acquired in the immediate vicinity to the plot. Ambient temperature and relative humidity were measured with a Campbell Scientific HC2S3-L probe (Campbell Scientific, Logan, UT) with standard error of $\pm 0.1$℃ for temperature and $\pm 0.8\%$ for relative

humidity. Wind speed was measured with a R.M. Young 05103-10 mechanical wind sensor (R.M. Young, Traverse City, MI) with a standard error of $\pm 0.3 m \cdot s^{-1}$. Incident solar radiation power was measured with two Kipp and Zonen SP Lite2 pyranometers (Kipp and Zonen, The Netherlands) installed horizontally with the sensors facing straight up. Both sensors measured radiant power, but one reported the SI unit value while the other reported photosynthetically active radiation, which is a specific fraction of incident radiation. The error of the pyranometer is $\pm 5\%$ of the incident power at an angle of incidence of 80°, and lower angles have less error with minimal error when the sun is above the horizon. The weather station setup in the field can be viewed in figure 4.1. The pyranometers, ambient temperature sensor and wind speed sensor were installed on the crossbar approximately 2m above the ground. The thermal camera was contained within a white bucket to avoid solar heating of the sensor array within the camera. All sensors connected to the cabinet which contained power supplies and a Campbell Scientific CR1000 datalogger (Campbell Scientific).

## 4.3 Model Development

Temperature data from the field were integrated with weather station data to link the vegetation temperature with local weather. A modelling approach was identified and the use of temperature data fit into describing an energy balance. An energy balance model applied at the leaf level requires explicit description of environmental interactions to isolate the plant response. Calculation of the radiation energy flux into a leaf separated shortwave and thermal radiation to examine interactions of each with the leaf. Shortwave radiation comprised of wavelengths from $0.3\mu m$ to $3.0\mu m$ is considered to emanate from the solar disc and hits leaves directly and is reflected from the ground, clouds, and sky. Reflections were assumed to add 20% of the value of downward sunlight power back to the leaf as a sparse canopy allows significant penetration of sunlight, which reflected upwards to the underside of the canopy (Jones, 2013). The leaf was assumed to absorb 54% of the shortwave radiation from the sun and rays reflected by the background, slightly higher than the suggested mean value for a grass leaf to account for the canopy reflecting into itself (Jones, 2013). Thermal radiation of wavelengths between $8\mu m$ and $13\mu m$ emanated from the leaf, all nearby objects, and the sky


**Figure 4.1:** The weather station in field. A: pyranometers, B: ambient temperature and humidity sensor, C: thermal camera within a radiation shield, D: weatherproof cabinet with power supplies and the datalogger. Not shown: the wind speed sensor.

unoccupied by the solar disc. Values of reflectance and absorbance of shortwave radiation for the ground and leaves were assumed to be constant. The emissivity and absorbance of thermal radiation for all surfaces were assumed to be unity. Outgoing thermal radiation from all objects was calculated with the Stefan-Boltzmann law unaugmented by emissivity. The ground temperature was assumed to be a constant 2℃ hotter than leaf temperature. Sky temperature was calculated based on air temperature and humidity (Li et al., 2017). With values assigned to each source, the radiation interactions are illustrated in figure 4.2,
where:

$\epsilon$ is the emissivity,

$\sigma$ is the Stefan-Boltzmann constant [$W \cdot m^{-2} \cdot K^{-4}$],

$T_{leaf}$ is the leaf temperature [K],

$T_{sky}$ is the sky temperature [K],

$T_{bg}$ is the background temperature [K],

$G_s$ is the global sunlight irradiance [$W \cdot m^{-2}$],

$R$ is the coefficient of sunlight reflected by the background, and

$\alpha$ is the coefficient of sunlight absorbed into the leaf.

The net radiation is simply the summation of all of the shortwave and thermal radiation interactions with the leaf. Net radiation for the leaf was converted to net isothermal radiation through the inclusion of radiation transfer that would occur between the leaf surface and a surface with the same properties at ambient air temperature. The net isothermal radiation is the net radiation acting on a surface with identical characteristics to the leaf, but with a temperature equal to the ambient conditions. The difference between net radiation and net isothermal radiation can be considered the amount of heat transferred from the leaf to similar surfaces at the temperature of ambient air through radiation, though that heat transfer pathway does not exist. Using net isothermal radiation allows the artificial radiative and real convective heat losses from the leaf to ambient air to be assessed in parallel to

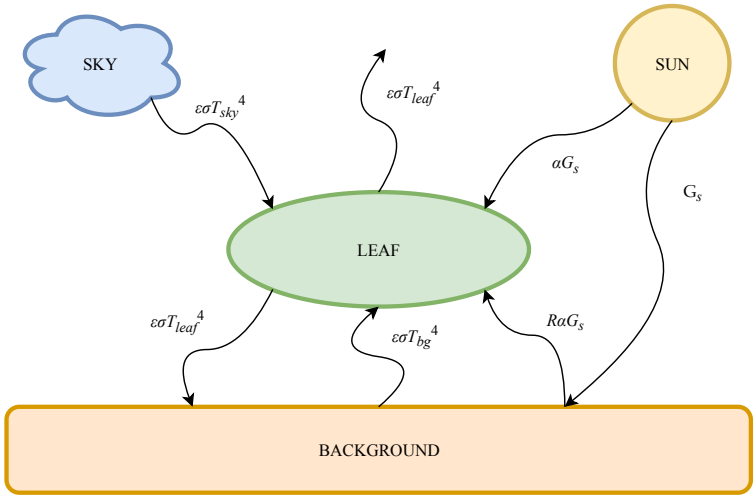


**Figure 4.2:** Diagram of the net radiation acting on a leaf in field including global sunlight irradiance ($G_s$), shortwave background reflectance ($R$), shortwave leaf absorbance ($\alpha$), emissivity ($\epsilon$), and temperatures of the sky ($T_{sky}$), leaf ($T_{leaf}$) and background ($T_{bg}$) converted to emitted power with the Stefan-Boltzmann constant ($\sigma$).

determine the strength of each on creating a leaf-air temperature difference. The leaf-air temperature difference was proposed as a simple method of crop observation for water stress and model development kept this term to more easily relate to early studies or studies using the crop water stress index, which is linearly related to leaf-air temperature difference (Jones, 2013). The heat transfer pathways can be viewed in figure 4.3,
where:

$G_{ni}$ is the net isothermal radiation [W·m$^{-2}$],

$r_R$ is the radiative transfer resistance [s·m$^{-1}$],

$r_{aH}$ is the boundary layer resistance to convective heat loss [s·m$^{-1}$],

$r_{aW}$ is the isolated boundary layer resistance to water vapour transfer [s·m$^{-1}$], and

$r_{\ell W}$ is the leaf (stomatal) resistance to water transfer [s·m$^{-1}$].

Quantification of the resistances starts with convective heat loss that acts through the boundary layer. Assuming the leaf acts as a horizontal flat surface, the empirical flat plate assumption of resistance to forced convective heat loss through a laminar boundary layer is

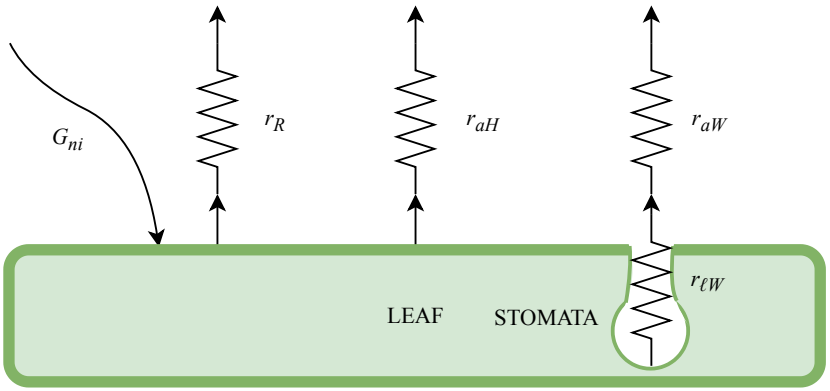


**Figure 4.3:** Diagram of the source and dispersion of energy on a leaf surface including net isothermal radiation ($G_{ni}$), radiative resistance ($r_R$), boundary layer convective resistance ($r_{aH}$), boundary layer water loss resistance ($r_{aW}$), and stomatal resistance to water loss ($r_{\ell W}$).

(Jones, 2013)

$$r_{aH}^{-1} = 6.62(u/d)^{0.5} * 10^{-3}, \tag{4.1}$$

where:

$u$ is the wind speed [m·s$^{-1}$], and

$d$ is distance across the leaf surface in the direction of the wind [m].

Heat and water vapour transfer were assumed to be completed through diffusion. Fick's first law applies to water vapour transfer and Fourier's law that describes heat transfer was adjusted to be analogous to the diffusion equation (Jones, 2013). The conversion factor from heat transfer resistance to water vapour loss resistance was to divide by 1.12 if air was still, 1.08 if the boundary layer was laminar, and 1.00 if the boundary layer was turbulent. It is noteworthy that assumptions of diffusion through laminar boundary layers may overestimate the resistances by a factor of two or more in the case of turbulence (Jones, 2013). Surface roughness and non-uniform temperatures of a leaf favourably influence the development of turbulence. The boundary layer of air above the leaf was assumed turbulent at Reynolds numbers greater than 2000 due to expected turbulent air movement through the canopy, non-uniform leaf temperatures and surface roughness (Grace, 1974). The resistance to heat

loss calculated from equation (4.1) was halved to account for easier transfer through the turbulent boundary layer (Schuepp, 1993).

Transpiration drives the latent heat loss of plants and is influenced by the humidity of the local environment. The water content of air was measured relative to fully saturated air rather than an absolute measurement. An empirical equation describing the partial pressure of water vapour in air is (Jones, 2013)

$$e_{max} = 0.6108 exp \frac{17.27 T_a}{(T_a + 237.3)} * 10^3, \tag{4.2}$$

where:

$e_{max}$ is the saturation vapour pressure [Pa], and

$T_a$ is the ambient temperature [℃].

Vapour pressure deficit is the absolute difference between water vapour pressure in ambient air from the maximum and was calculated from saturation pressure and relative humidity, the ratio of current vapour pressure to the maximum at saturation. Linearization of the vapour pressure curve allows for estimation of the saturation pressure at the temperature of the surface where evaporation occurs (Jones, 2013). This creates another explicit dependency on the leaf-air temperature difference. The diffusion of water depends on the driving pressure difference between saturated air near the leaf surface, assumed to have the same temperature as the leaf, to ambient air. The slope of the linearized curve is

$$s = \frac{4098(0.6180 exp(17.27 T_a/(T_a + 237.3)))}{(T_a + 237.3)^2} * 10^3, \tag{4.3}$$

where:

$s$ is the rate of change of the saturation vapour pressure with temperature [Pa·K$^{-1}$], and

$T_a$ is the ambient temperature [℃].

Sky temperature is acquired from the Brunt equation, based on ambient temperature and relative humidity, calibrated for all-day clear sky conditions and validated for the contiguous

United States (Li et al., 2017). The Brunt equation calculates a sky emissivity to modify the ambient temperature, resulting in

$$T_{sky} = \epsilon_{sky}^{1/4} T_a, \tag{4.4}$$

and

$$\epsilon_{sky} = 0.618 + 0.056\sqrt{e_{max} * RH}, \tag{4.5}$$

where:

$\epsilon_{sky}$ is the effective sky emissivity,

$RH$ is the relative humidity, and

$e_{max}$ is the saturation pressure at ambient conditions [hPa].

Assuming no biochemical energy activity from plant growth processes such as photosynthesis, the radiation absorbed is balanced by sensible and latent heat loss. A net-zero energy balance can be rearranged to solve for the difference between the leaf and ambient temperature (Jones, 2013),

$$T_{leaf} - T_a = \frac{r_{HR}(r_{aW} + r_{\ell W})\gamma G_{ni}}{\rho_a c_p[\gamma(r_{aW} + r_{\ell W}) + sr_{HR}]} - \frac{r_{HR} VPD}{[\gamma(r_{aW} + r_{\ell W}) + sr_{HR}]}, \tag{4.6}$$

where:

$r_{HR}$ is the combined parallel resistance to convective and radiative heat transfer [s·m$^{-1}$],

$\gamma$ is the psychrometric constant relating the partial pressure of water in air to temperature [Pa·K$^{-1}$],

$\rho_a$ is the density of air [kg·m$^{-3}$],

$c_p$ is the specific heat of air [J·kg$^{-1}$·K$^{-1}$], and

$VPD$ is the air vapour pressure deficit [Pa].

Rearranging to isolate the stomatal component of the energy balance nets

$$g_{\ell W}^{-1} = r_{\ell W} = \frac{r_{HR}\rho_a c_p(VPD + s(T_{leaf} - T_a))}{\gamma(r_{HR}G_{ni} - \rho_a c_p(T_{leaf} - T_a))} - r_{aW}, \tag{4.7}$$

where:

$g_{\ell W}$ is the stomatal conductance [m·s$^{-1}$].

This is a theoretical energy balance that has been investigated in field studies (Leinonen et al., 2006) and the interaction between terms has been modelled to determine the behaviour of the equation as terms change (Maes and Steppe, 2012). The specific heat of air was assumed constant at 1010 J·kg$^{-1}$·K$^{-1}$. The psychometric constant and density of air were obtained from linear interpretation of lookup tables based on ambient air temperature (Jones, 2013).

With temperature data acquired continuously, the energy balance can be expanded to a non-steady state analysis considering the rate of change of leaf temperature as a physical sink/source of energy as in

$$g_{\ell W}^{-1} = r_{\ell W} = \frac{r_{HR}\rho_a c_p(VPD + s(T_{leaf} - T_a))}{\gamma(r_{HR}G_{ni} - \rho_a c_p(T_{leaf} - T_a) - r_{HR}\rho_\ell c_{p\ell}\ell^* \frac{\Delta T}{\Delta t})} - r_{aW}, \tag{4.8}$$

where:

$\rho_\ell$ is the density of the leaf [kg·m$^{-3}$],

$c_{p\ell}$ is the specific heat of the leaf [J·kg$^{-1}$·K$^{-1}$],

$\ell^*$ is the volume to area ratio of the leaf (leaf thickness) [m], and

$\frac{\Delta T}{\Delta t}$ is the rate of change of leaf surface temperature [K·s$^{-1}$].

Leaf thermal properties are based on water values, assumed because leaf tissue is 80-90% water. Specific heat of the leaf was assumed to be 3600 J·kg$^{-1}$·K$^{-1}$ (Jayalakshmy and Philip, 2010) and density was assumed as 760 kg·m$^{-3}$ (Jones, 2013). The wheat leaf thickness was assumed to be 0.5 mm.

## 4.4 Data

Weather and thermocouple data acquired every minute between August 12th and August 17th were saved to the datalogger. The two pyranometers were verified to be in agreement when the photosynthetically active radiation measurement was converted to incident radiation in SI units. Thermal images were captured and saved to an onboard SD card every minute over the same period, except for a brief interruption around noon on August 16th. The scene in each thermal image contained full wheat plants, including all leaves with thermocouples attached, several spots of bare ground, and a PVC container below the canopy that housed thermocouple connections. All images were acquired with emissivity set to one and saved as radiometric 14-bit depth TIFF files with each pixel value representing the apparent temperature. Of the original twelve thermocouples that were attached to the wheat leaves, only two maintained contact with a leaf over the entire measurement period. All other thermocouple readings were discarded and not investigated further.

## 4.5 Analysis

Each thermal image captured from the field was processed using the Python package scikit-image (van der Walt et al., 2014) to extract temperatures for use in the energy balance model. The .tiff images were loaded into memory and individually processed. Segmentation of thermal images started with the application of a black top-hat morphological transform which returns an image with high values of intensity where objects smaller than a specified element size exist with an intensity lower than the immediate surroundings in the thermal image. The selection element used in this implementation was a 13x13 pixel square. The resultant image from the top hat transform had a bimodal histogram of intensity values and Otsu's method of thresholding (Otsu, 1979) was applied to the intermediate image to separate the leaf pixels from the background elements. This mask was morphologically opened to clean up rough edges then morphologically eroded to remove mixed pixels which could contain temperature information about the leaf and background objects due to the low resolution of the sensor (Jones and Sirault, 2014). Small sections of the background were erroneously

**Table 4.1:** Summary table of analysis steps listing parameters evaluated and produced in sequential order. Any parameter with * is estimated.

| Step | Required | Produced |
|---|---|---|
| 1 | $T_a$ | $s, e_{max}, \rho_a, c_p, r_R, \gamma$ |
| 2 | $T_a, RH$ | $VPD, \epsilon_{sky}, T_{sky}$ |
| 3 | $u, d^*$ | $r_{aH}, r_{aW}$ |
| 4 | $T_{sky}, T_\ell, T^*_{bg}, G_s, T_a, \alpha^*_{leaf}, R^*_{ground}$ | $G_{ni}$ |
| 5 | $r_R, r_{aH}$ | $r_{HR}$ |
| 6 | $all$ | $g_{\ell W}$ |

classified as foreground because they had lower temperatures than their surroundings and were removed by filtering out small objects in the mask. The visual steps of the image segmentation process can be viewed in figure 4.4.

The areas outlined with bright white above the false colour thermal image in figure 4.5 are pixels kept for analysis from automatic image processing for a sample image. Masks created from this operation included only leaves but did not encompass all leaves in the image. Unwanted items such as stems, heads of wheat, soil, and dead plant matter at ground level were all excluded. The mean temperatures extracted from the masked thermal images was shown to demonstrate the trends from automated segmentation and extraction. With leaf temperature data in hand, the leaf energy balance was investigated with two cases: a steady-state case that assumes that all radiant energy taken in at any instant is balanced by sensible and latent heat loss (4.7), and an unsteady-state case that includes physical energy storage based on the thermal mass and change of temperature of the leaf (4.8). Metabolic storage and energy dynamics of photosynthesis, respiration and fluorescence were not considered in either model. An overview of parameters needed in each analysis step is included in table 4.1.

## 4.6 Results

Temperatures acquired from contact and non-contact methods are shown in figure 4.6 to demonstrate the range and trends of leaf temperature alongside the incident sunlight. This

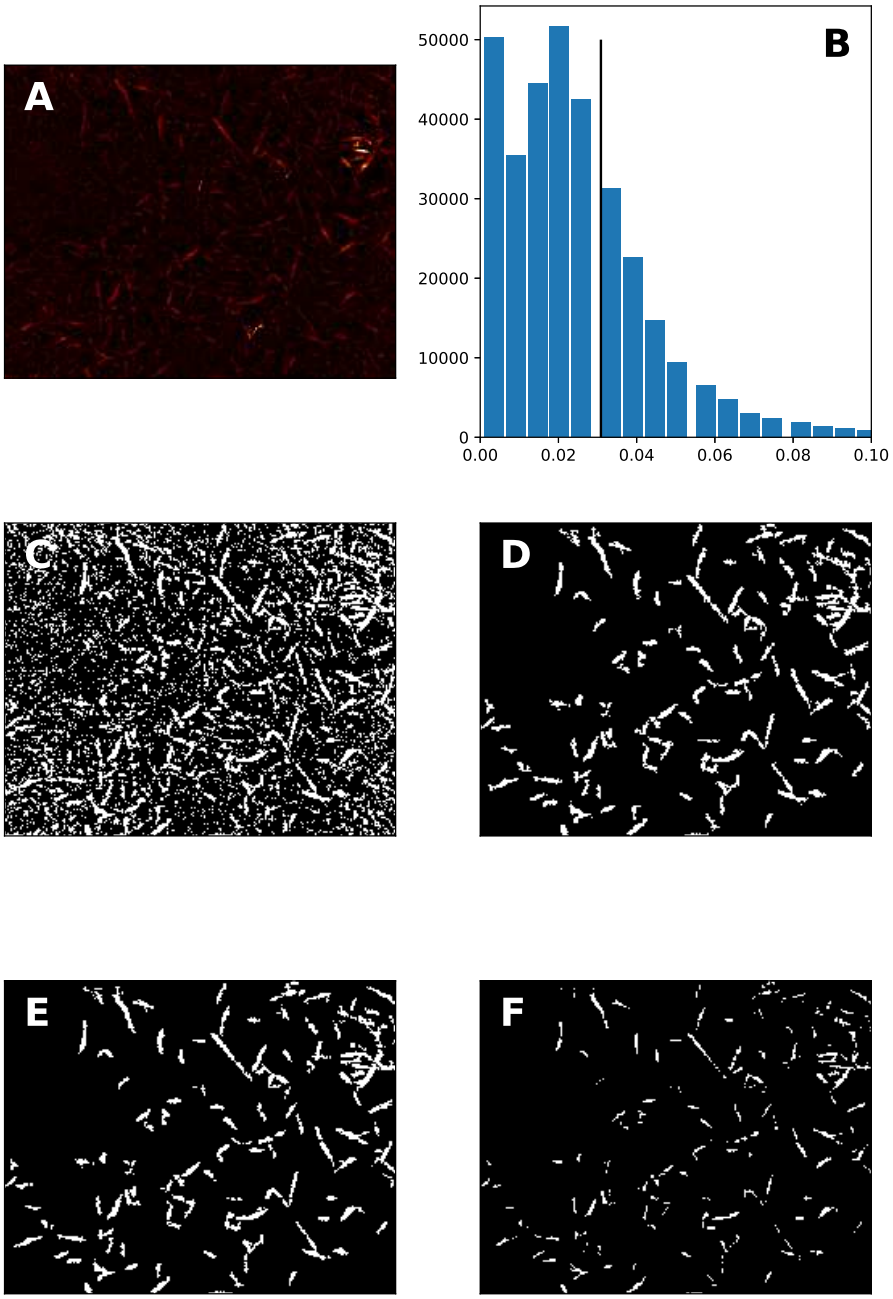


**Figure 4.4:** The steps of segmentation. A) The image returned by black top hat morphological operator. B) The histogram of A) with Otsu's threshold at 0.31. C) Output of thresholding. D) Output after removing small objects. E) Output after morphological opening. F) Output after morphological erosion.

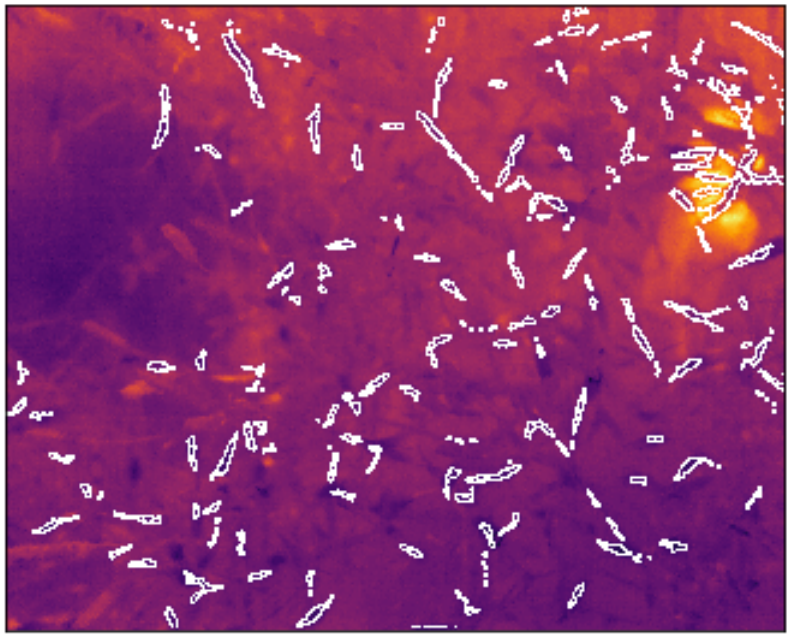

**Figure 4.5:** The results of automated segmentation of wheat leaves. Areas outlined in white are pixels representative of leaf tissue. The warm indistinct object is a PVC container that held thermocouple junctions.

figure demonstrates how difficult it could be to go into the field blind and compare temperature acquired at different times as minute to minute variation is enormous. While the temperatures from camera data were an average of all leaf pixels, thermocouples measured a single point on a single leaf each. The thermal images could not be segmented automatically to isolate the leaves with thermocouples as the sensors and clips were too small to be distinguished in the images. Temperatures obtained from the thermal camera responded strongly to shifts in sunlight conditions such as the dip near 14:15, and the similar change in thermocouple temperatures lends credence to the response being indicative of leaf behaviour. As temperature reported from both measurement methods had significant minute to minute variation, it appears non-contact measurements and image processing were not introducing that variation. The smaller change in thermocouple temperatures was due in part to their poor contact with the leaves. Thermocouples were not thermally insulated, and they reported a temperature somewhere between leaf surface and ambient. For this reason, contact temperature data were discarded and not investigated further. The leaf temperature variation of each day as shown in figure 4.7 was a result of a constantly shifting energy balance. Passive

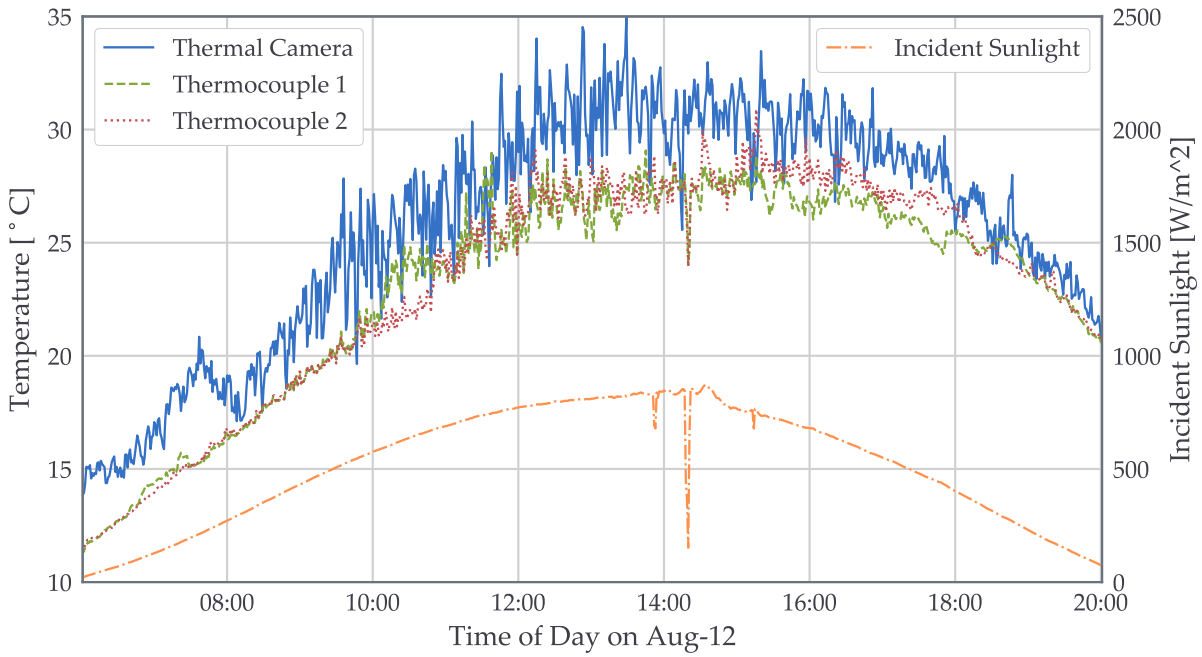


**Figure 4.6:** Leaf temperature acquired from non-contact and contact methods across one day in the field plotted alongside the incident sunlight strength.

heat loss from the leaf is governed by the difference between leaf and ambient temperatures, and that difference was also highly varied, but rarely exceeded 6℃ except near the hottest parts of the day as shown in figure 4.8. A sensitivity study showing the effect of some of the assumptions on the value of stomatal conductance is shown in figure 4.9. To produce these figures, a nominal case was calculated and shown with a dot and in nine other cases, one variable was set at 100 points between the values on the x-axis while other variables were held at their nominal value. The largest contributors to stomatal conductance change were the amount of absorbed sunlight, the leaf temperature, and the relative humidity. The effect of wind speed on stomatal conductance is drastically reduced after the boundary layer over the leaf is assumed turbulent.

Because the time constant of stomatal opening and closing in response to light is in the region of a few minutes (Jones, 2013), stomatal conductance values shown in all figures were smoothed with a five minute moving average to better reflect the stomatal response. August 12th, 13th, and 16th had nearly cloudless, all-day sunny conditions. The five minute moving average of leaf-air temperature difference for those three days can be viewed in figure 4.10.

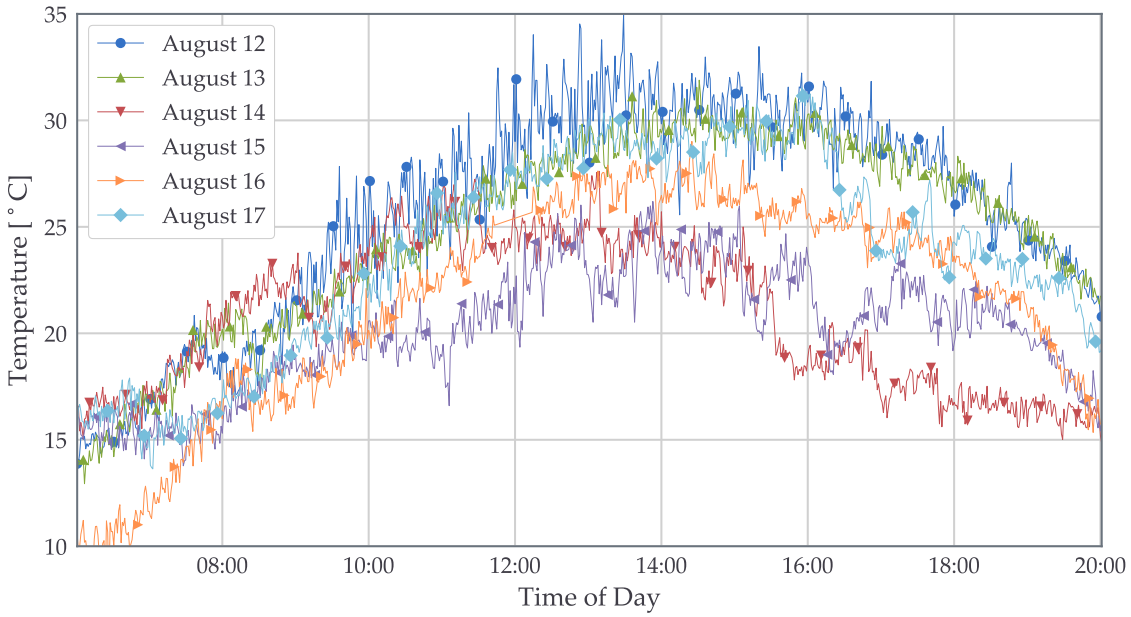


**Figure 4.7:** Mean leaf temperature from thermography across all days in the field.

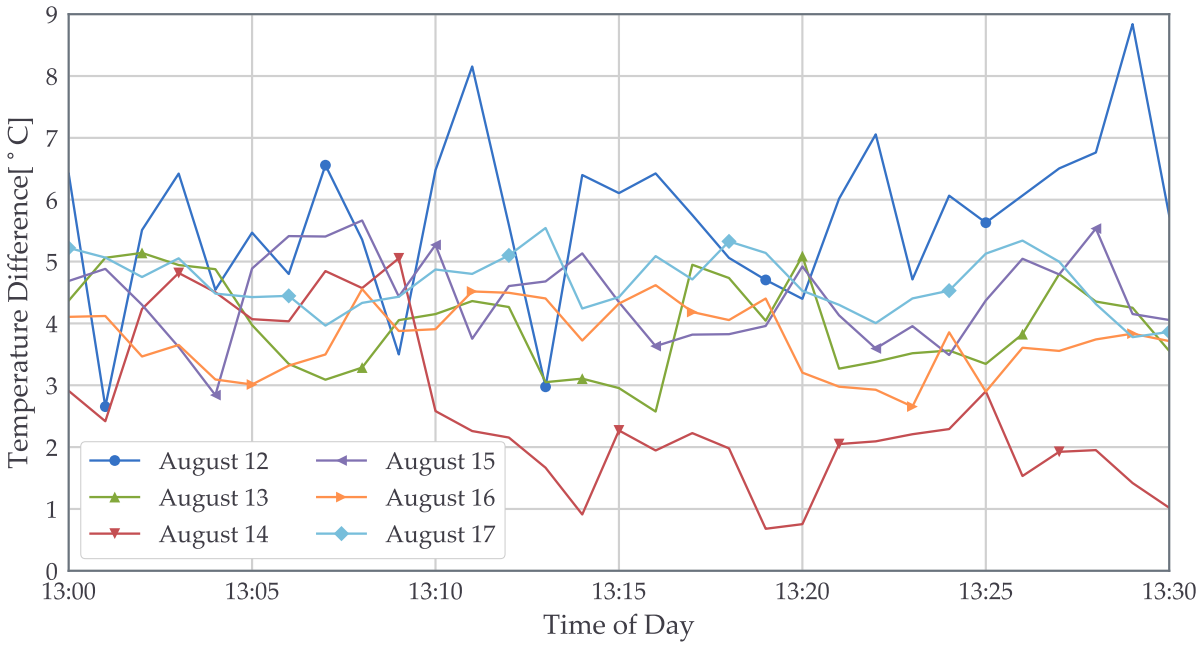


**Figure 4.8:** Trends of the difference between leaf temperature and ambient air temperature for half an hour in the afternoon for six days in the field.

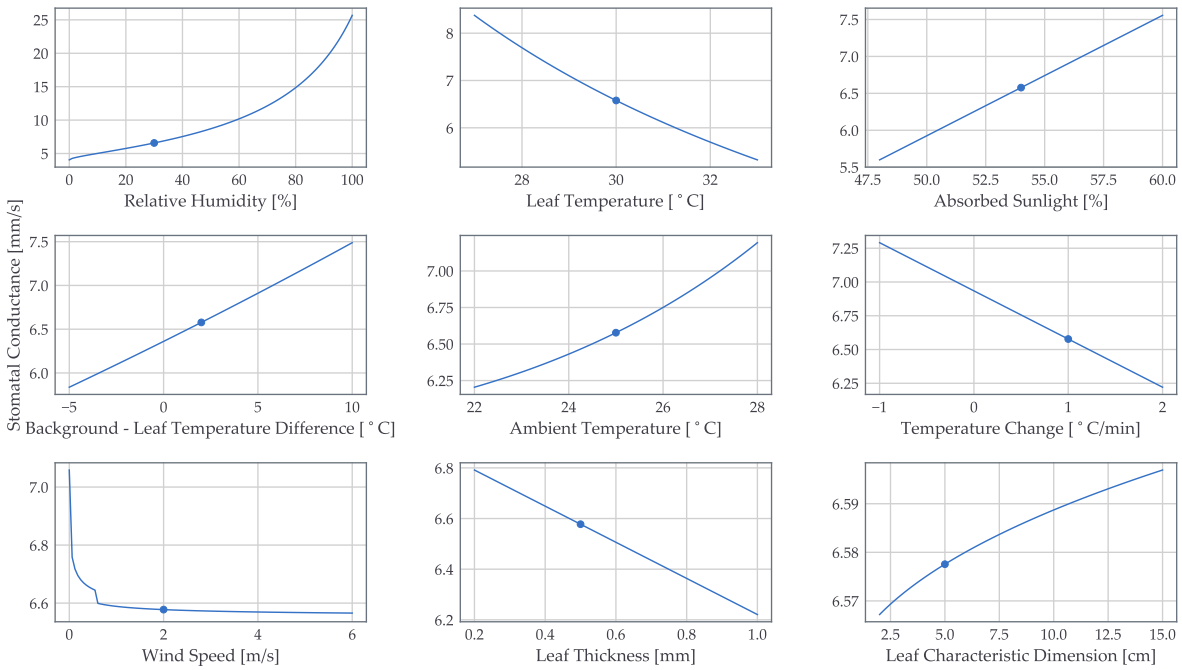


**Figure 4.9:** Sensitivity of stomatal conductance to several assumed values. Nominal values are noted by points on the curves.

Stomatal conductance calculated from equation (4.8) were very similar across those days as shown for daytime hours in figure 4.11. In all following figures showing stomatal conductance, data from August 13th were used as the reference ideal sunny day.

Daily trends of stomatal conductance calculated from equation (4.8) are shown in figure 4.12. Values near zero indicate stomatal closure and the slowing or shutdown of the transpiration process. Stomatal conductance is expected to be near zero at night as incident radiation is no longer heating the plant and there is no need for active cooling but gas exchange is still occurring for growth (Jones, 2013). Stomatal conductance dipping below zero is an error. This error could crop up because of poor characterization of the radiation balance at night with the assumption of background temperature based on leaf temperature and the use of an all-day model of clear sky temperature instead of more accurate models that separate day from night and include cloud cover corrections. The model has no heat generation at night resulting in a net energy loss, and an impossible inverse transpiration is required to satisfy the measured leaf temperature during nighttime hours. The poor performance of the energy balance model at night is likely the result of the exclusion of respiratory pro-

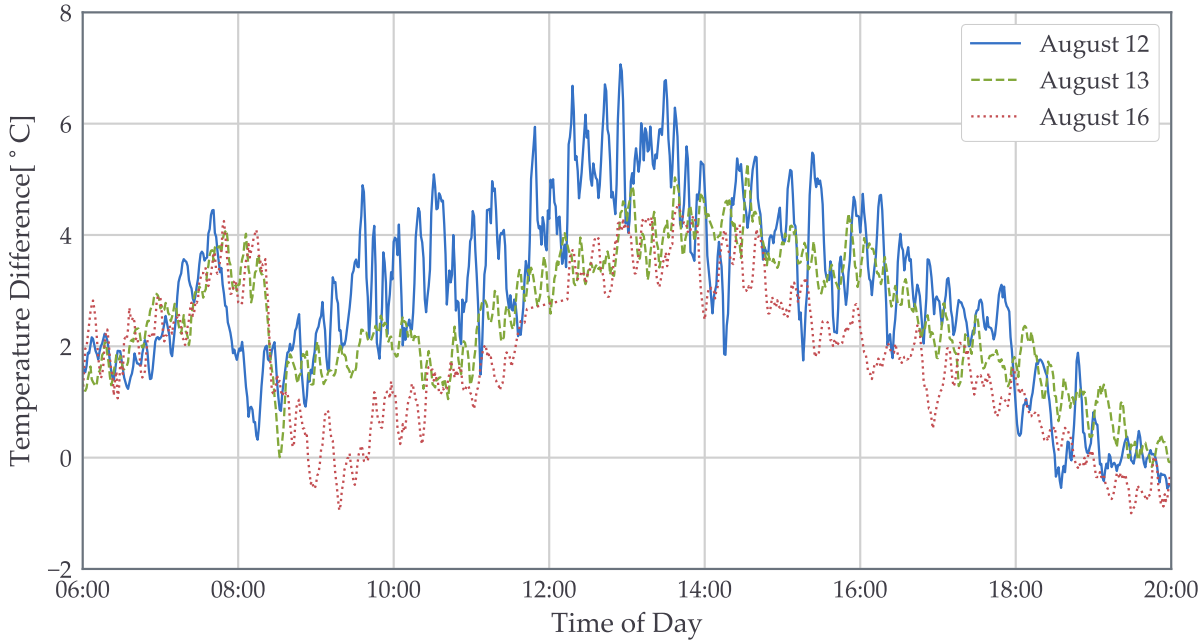


**Figure 4.10:** Leaf-air temperature difference in daytime hours for three mostly cloudless days.

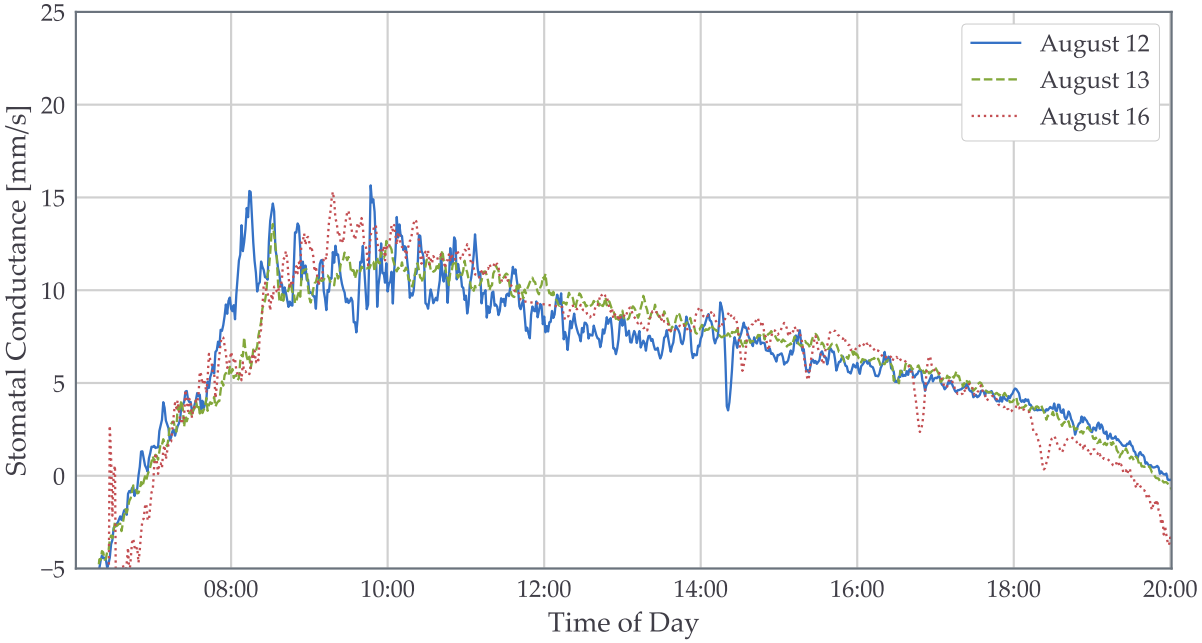


**Figure 4.11:** Daytime stomatal conductance over three mostly cloudless days.

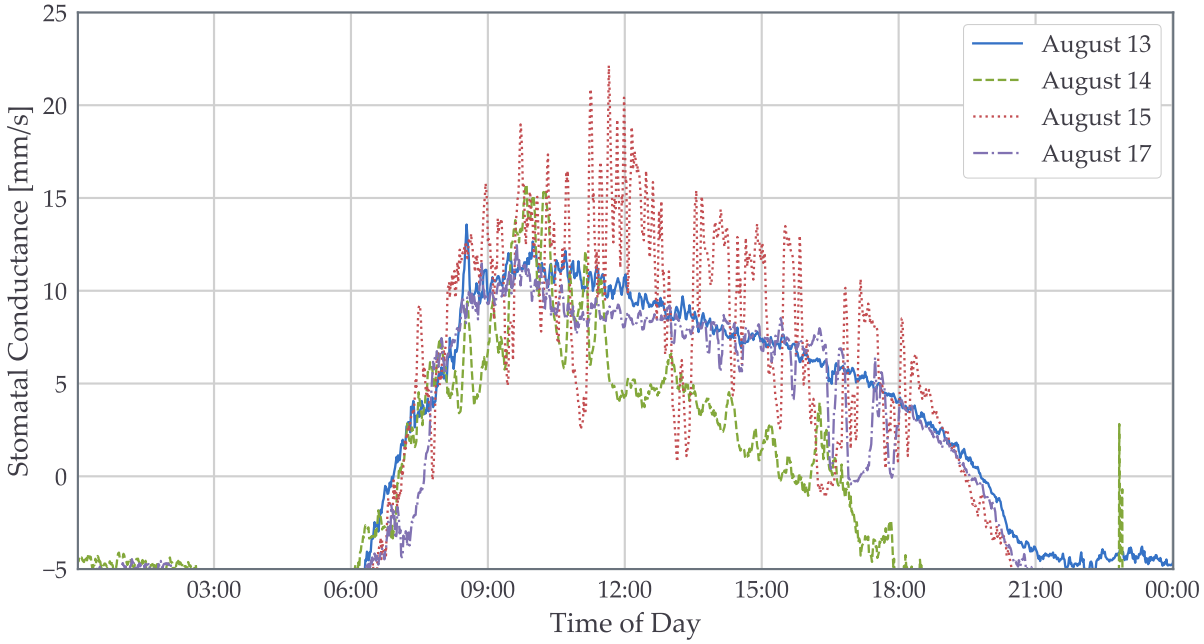


**Figure 4.12:** Stomatal conductance to satisfy the non-steady state energy balance implemented for each minute across four days with variable conditions.

cesses from the model which release stored energy to enable growth at night (Jones, 2013). Discarding observations from the night and focusing on daytime values is a better use of the energy balance model for two reasons: infield phenotyping is unlikely to occur at night, and characterization of the scene is more accurate during daytime hours under clear sky conditions.

Isolation of the daytime values of stomatal conductance modelled in the steady and non-steady state cases can be viewed in figure 4.13 and figure 4.14 respectively. Including energy storage in the model lowers stomatal conductance overall, reduces peak values, and introduces slight variance at points with low incident sunlight strength. The trends in stomatal conductance values from the baseline day of August 13th are strongly related to the amount of net isothermal radiation which can be viewed in figure 4.15. Net isothermal radiation is shown for the same daytime period, with a dip below zero near the beginning and end of the day as sunlight strength diminishes and the direction of net radiative transfer reverses. Clouds rolled in the afternoon of the 14th and with less solar loading, stomatal conductance lowered as there is less requirement for evaporative cooling to satisfy the energy balance. On

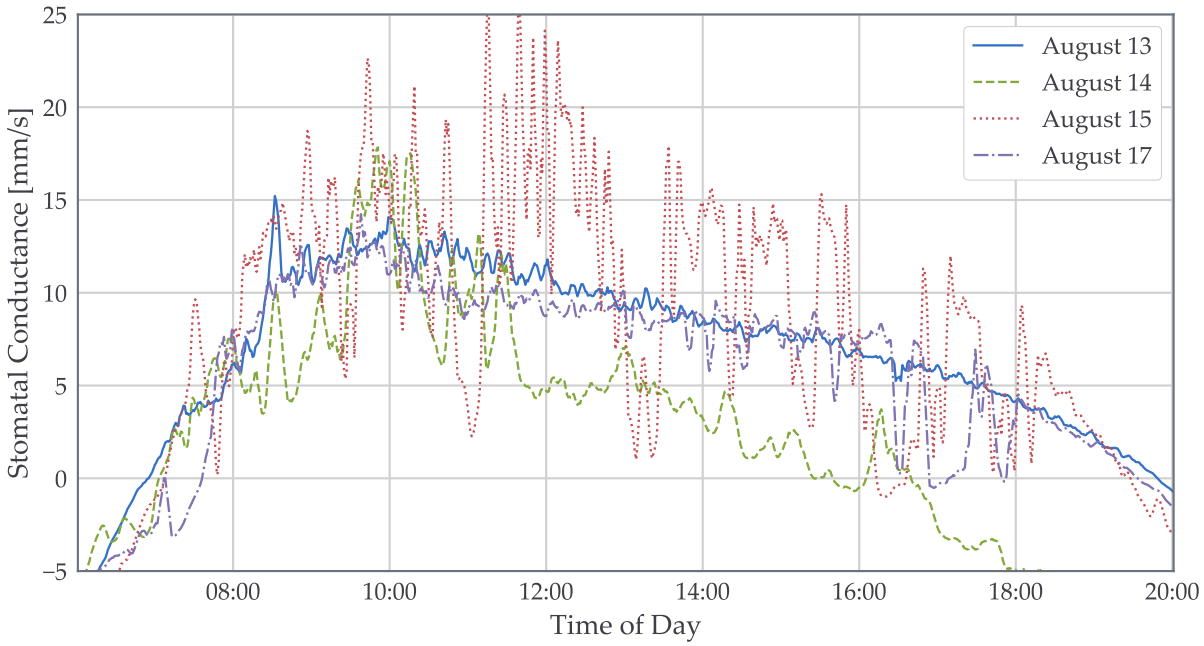


**Figure 4.13:** Stomatal conductance calculated to satisfy the steady state energy balance in daylight hours.

the afternoon of August 15th, there was considerable oscillation between sunny and cloudy periods throughout the afternoon, and deviation from the baseline radiation is reflected in stomatal conductance in both cases as viewed in figure 4.13 and figure 4.14. When direct sunlight hits the plants after being shaded on the 15th, stomatal conductance is higher than values at that time of day across the rest of the week and maintains a significant increase above the expected values clouds cover the sun again. Similarly, after clouds cover the sun the stomatal conductance drops below the trendline observed in sunny conditions. August 17th saw clouds roll in at about 17:00 and persist for about half an hour, reflected in stomatal conductance lowering then returning to a baseline shared with August 13th with no overshoot as net radiation also returns to the expected trend at that time.

A closer look at the dynamic response on August 14th is shown in figure 4.16. As sunlight fades, stomatal conductance drops quickly afterwards as the calculation relies heavily on the value of net isothermal radiation. Leaf temperature slowly drops even with lower stomatal conductance. Stomatal conductance does not rise when leaf temperature drops.

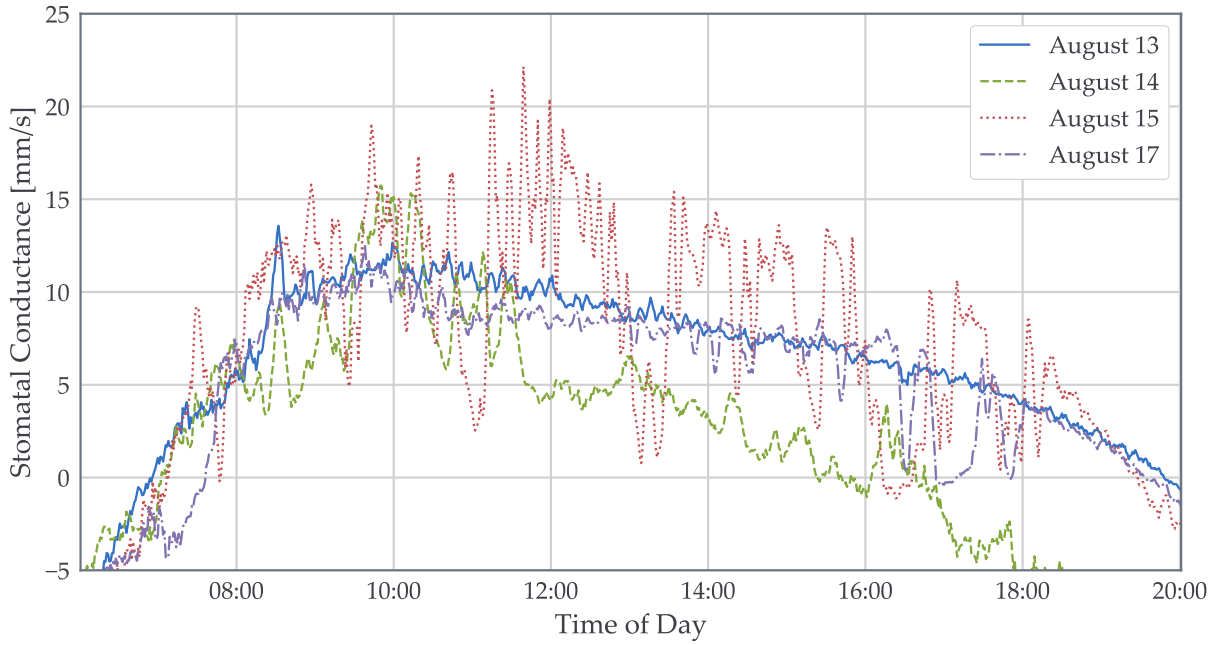


**Figure 4.14:** Stomatal conductance calculated to satisfy the non-steady state energy balance in daytime hours.

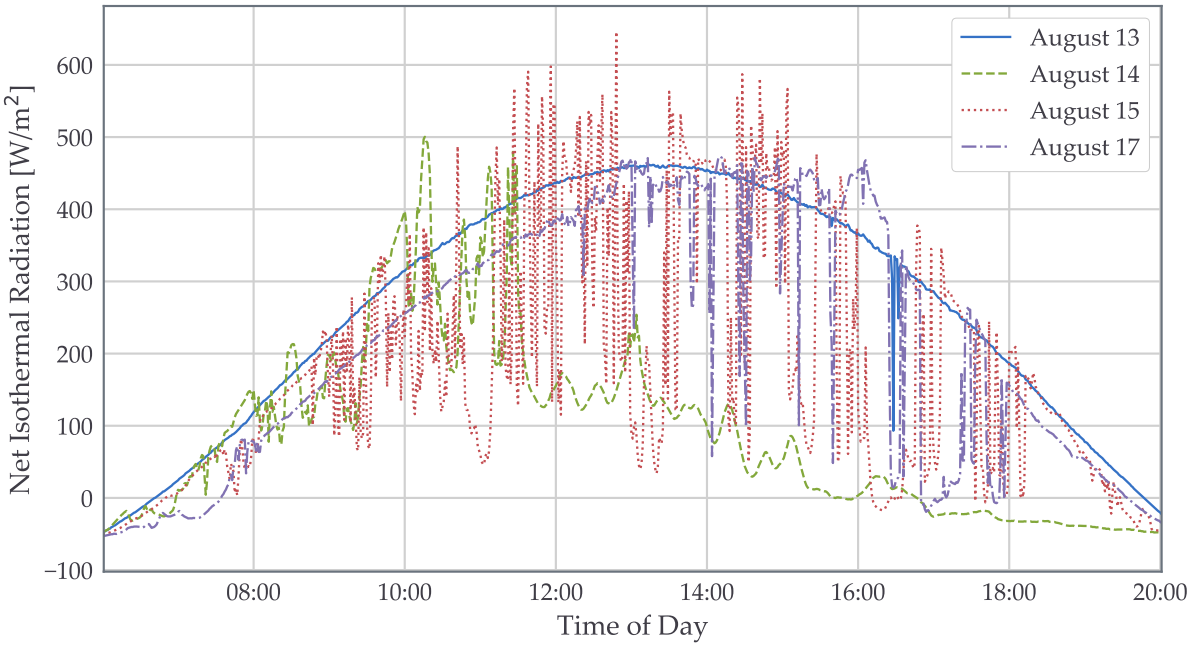


**Figure 4.15:** Net isothermal radiation incident to the leaves, modelled with consideration of the behaviour of short and long wavelength radiation in the field.

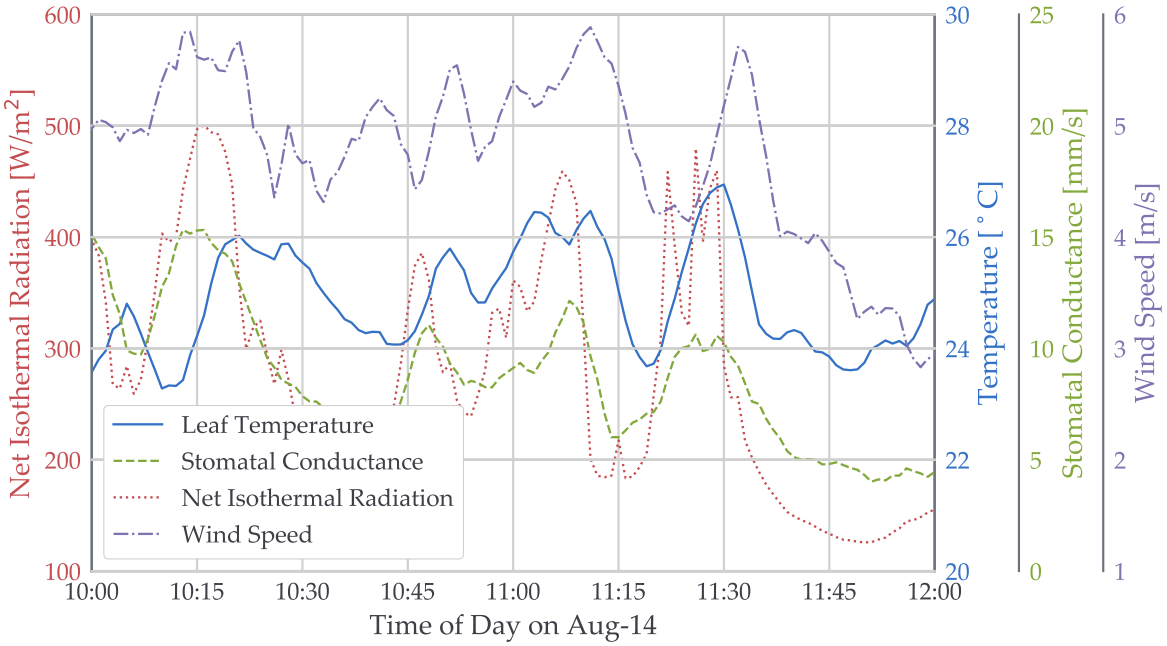


**Figure 4.16:** Net isothermal radiation and the response of leaf temperature and stomatal conductance.

## 4.7 Discussion

This study investigated methods to capture temperature of leaves over a long unsupervised period of time. Contact measurements were difficult to acquire with thermocouples held with thin clips. The clips had to be light to avoid mechanical stress on the leaf, but they were easily shaken off by leaves moving in the wind. The thermal camera required only a USB power source in field, whereas the thermocouples and all weather data sensors needed a datalogger to support recording. Automated processing enabled the efficient extraction of field crop leaf temperatures from every thermal image acquired. The initial hypothesis of enabling comparisons of temperature acquired at different times did not materialize. Excessive variation across small timespans in both contact and non-contact data stymies temperature comparisons. High-frequency variance is not a consequence of image processing as contact measurements were a solid indication that leaf temperatures shift constantly. Minute to minute variations in leaf temperature were observed in both the thermal camera and thermocouple data, particularly at points with high solar irradiance.

Weather data in this case were from an very local source that was set up for this study. Assumptions of similar conditions at the location of the weather station and the plants would have to keep in mind the sensitivity of the model to changes in sunlight strength or wind speed. Wind speed is likely to be the most confounding as it is hyper-local and leaves can experience different speeds based on their position within the canopy. The assumption here is that turbulent air moving through the canopy induce a turbulent boundary layer over the leaf at a very low Reynolds number. Many values of critical Reynolds numbers have been reported in the past (Schuepp, 1993), and the assumption of a low critical Reynolds number makes the effect of wind speed on stomatal conductance very slight after turbulence is achieved at fairly low wind speeds. Other model assumptions that can be discarded are the linearization of the water saturation curve and the concept of net isothermal radiation. The usage of these elements allows for this energy balance model to be described as a function of the difference of leaf and ambient temperatures, but they are not strictly necessary. The saturation pressure at the temperature of the leaf can be calculated directly and net radiation can be substituted for net isothermal radiation. Changing net isothermal radiation,$R_{ni}$, to net radiation, $R_n$, would also require removal of radiative resistance, $r_R$, by replacing $r_{HR}$ with $r_{aH}$.

The most important parameters to investigate to ensure accuracy of the model are all related to the calculation of net radiation. A spectral sensor evaluating the reflection of sunlight bands could assist in determining more precisely the absorbance of light on a per-leaf basis. The other large consideration is how to characterize the background temperatures and the sky temperatures. Background temperatures were using an assumed value based on leaf temperature while the sky temperatures were acquired from an empirical model. Both are large contributors to the radiation balance and need to be specified accurately to achieve correct values of stomatal conductance as demonstrated by figure 4.9. Parameters introduced by the non-steady state analysis such as leaf thickness or rate of temperature change do not have a significant effect on stomatal conductance. Characteristic dimension does not have much of an impact on stomatal conductance as the critical Reynolds value is so low that the boundary layer does not significantly develop before it becomes fully turbulent.

The combination of temperature and weather data in an energy balance model uncovers

what plant behaviour must be to satisfy the temperature response. The stomatal conductance expected in plants varies considerably over the day and is expected to vary along the plant lifespan as crops progress from using energy solely for vegetative growth and begin to invest resources into reproduction. The value of stomatal conductance is a notable phenotype for crop development that describes water usage behaviour and both the dynamic response and maximum values are a function of the genotype (Munns et al., 2010). Reference values suggest that the maximum stomatal conductance for grasses should be roughly between two and eight millimetres per second (Jones, 2013). The magnitude of stomatal conductance reported here for late-season wheat is higher than expected. Stomatal conductance models may have too much sensitivity to sunlight energy intake which results in higher than expected values in the day, lower than possible in the night and very large drops when shaded. Biochemical processes such as photosynthesis and respiration that involve chemical energy usage and collection were ignored. The impact of photosynthesis on the energy balance would be to lower the amount of incident energy converted to heat, which lessens the required cooling and would have the model predict a lower stomatal conductance. The exact magnitude and dynamics of the reduction of stomatal conductance due to photosynthesis was not investigated.

## 4.8 Conclusion

High-resolution thermal images providing insight into the energy handling behaviour for cultivar development. Thermal images were automatically processed with morphological methods to extract mean leaf temperature from each image of a sparse wheat canopy. The raw temperature of leaves extracted from thermal images at different times are not suited for comparisons to assess stress due to extreme variance in the signal. Stomatal conductance modelled in part from leaf temperature nearly overlap in a diurnal cycle. Plant behaviour can be expected to be very consistent day-to-day but it should be stressed that no work has been done to influence the stomatal conductance. Further work would include development of the model to include more energy related processes and verify the dynamics of stomatal conductance modelled over short contiguous spans. Stomatal conductance modelled here was based on data acquired every minute for a week, which is a significant investment of

time. Plant breeding efforts may not be able to justify the cost of dedicating many sensors to continuously monitor only a small portion of the field each. However, information about phenotypic development that stomatal conductance modelling uncovers can expedite breeding programs. Further efforts with phenotypic modelling may assist plant scientists in discovering genetic markers that indicate a particular cultivar behaviour which can be tracked through generations.

# Chapter 5

# Comparing Energy Balance Models with Unique Approaches to Environmental Characterization

## 5.1 Introduction

A plant balances energy uptake and cooling by regulating mass and gas transfer between the plant and environment by adjusting stomatal opening on the leaf surfaces (Jones, 2013). The energy state of the plant is influenced by the transpiration process which sheds water from a plant through stomata to provide active cooling (Munns et al., 2010). Plant water usage is an essential factor of plant growth and a lack of water available to a plant induces an abiotic stress state where transpiration is impaired and biomass generation is stifled. Transpiration is reduced and less water exits the leaf as stomatal opening and conductance decreases (Costa et al., 2013). Leaf tissue temperature is a result of the energy balance and is directly related to the transpiration rate. Drought stress can be considered with quantifiable scales that indirectly chart the water usage of a plant based on leaf temperature in relation to temperatures of operator selected references such as ambient air or leaves with maximal or minimal transpiration for the given conditions (Jackson et al., 1981, Maes et al., 2014, Möller et al., 2006).

Leaf temperature is clouded by significant short-term variance as most field crops are small, quick-to-respond organisms (Aubrecht et al., 2016, Chaves et al., 2002). Leaf temperature is the end result of all the interactions in the field and combining thermal data with weather data can model the active plant response to the given situation. Energy balance

models that calculate stomatal conductance accept leaf temperature as an observable output of plant processes and environmental conditions (Maes and Steppe, 2012). Models use two general approaches to characterizing the environment. A theoretical approach based on first principles physics and micrometeorology describes interactions between leaves and light, fluids, and heat in outdoor conditions. Empirical style models avoid mechanistic equations and use the temperature behaviour of reference surfaces as additional sources of information. Reference surfaces ideally behave in a controlled manner representative of leaf behaviour at extreme transpiration rates to create boundary conditions to impose on true leaf temperature (Maes et al., 2016, Pou et al., 2014).

This study compared stomatal conductance models that use temperature measurements of plants extracted from thermal imagery to determine stress state. Collecting large amounts of leaf temperature data is simple with a radiometric thermal camera as segmentation of leaf pixels can be automated. This study applied three energy balance equations to wheat in the vegetative portion of its lifecycle planted in containers with controlled soil water content situated outdoors. Drought stress should lower the stomatal conductance as less water is transpired when water conserving behaviours are expressed (Tardieu and Simonneau, 1998). Each energy balance model uses a different sources of data to characterize the local environment. Comparing the performance of models that calculate stomatal conductance will inform the design of data acquisition systems about which sensors and sources of environmental information must be employed to contextualize the raw temperature measurements. It is crucial that stomatal conductance calculated from the models display significant differences between well-watered and water deficient crops (Munns et al., 2010). Reliable information of energy handling can be used to assess the state of the plant to determine if stress exists as well as the magnitude of growth impairment.

## 5.2 Methods

Modelling stomatal conductance from outdoor plants requires outlining what data each modelling approach requires, how to acquire the data and the generation of appropriate targets to investigate.

### 5.2.1 Energy Balance Implementation

Energy balance models investigated were of three types: theoretical, semi-empirical, and empirical, all of which use leaf temperature as a response influenced by the local environment and indicative of plant behaviour. Each model has a unique approach of describing the environment and has its own list of assumptions and required information. These models were evaluated on their performance in calculating stomatal conductance from field observations.

#### 5.2.1.1 Method 1 - Theoretical

An entirely theoretical energy balance applied at the leaf level considers radiation interactions as well as heat and water vapour transfer through the boundary layer of air above the leaf (Maes and Steppe, 2012). The initial form of the energy balance considers radiation incident to the leaf, the sensible heat transfer, physical storage and evaporative flux as shown in:

$$G_n - C - \lambda E = S \tag{5.1}$$

where:

$G_n$ is the net radiation [W·m$^{-2}$],

$C$ is the sensible heat transfer [W·m$^{-2}$],

$\lambda$ is the latent heat of evaporation of water [J·kg$^{-1}$],

$E$ is the evaporative flux [kg·m$^{-2}$·s$^{-1}$], and

$S$ is the heat flux into physical storage[W·m$^{-2}$].

Radiation present outdoors includes thermal wavelengths emitted by all objects at normal biotic temperatures and shorter wavelengths emitted by the sun. Every interaction between the leaf and the environment must be quantified, and the energy balance derivation includes assumptions of radiation absorption coefficients, boundary layer development, and thermal characteristics. These assumptions are necessary to calculate sensible energy fluxes based on the interaction of light, heat, and air with the leaf. The only missing portion of equation (5.1)

is the latent heat loss and the last remaining parameter to satisfy the energy balance equation is the stomatal conductance. An entirely theoretical approach to the energy balance with explicit assumptions of analysis parameters is considered method one. The specific numerical assumptions necessary for the theoretical model included:

1. zero reflection of shortwave radiation from the background due to the high canopy coverage (detailed later),
2. the leaf absorbed 54% of incident shortwave light which is slightly higher than a single leaf to account for canopy trapping radiation (Jones, 2013),
3. the leaf absorbs and emits thermal radiation at the maximum rate with emissivity equal to one,
4. the temperature of the surroundings were 2℃ hotter than extracted leaf temperature,
5. leaf temperature was assigned to a theoretical rigid, horizontal leaf acted on by free field conditions,
6. the specific heat capacity of air was 1010 $J{\cdot}kg^{-1}{\cdot}K^{-1}$ (Jones, 2013),
7. leaf specific heat capacity was 3600 $J{\cdot}kg^{-1}{\cdot}K^{-1}$ (Jayalakshmy and Philip, 2010),
8. leaf density was 760 $kg{\cdot}m^{-3}$ (Jones, 2013), and
9. leaf thickness was 0.5 mm.

Assumptions that define how the energy balance is constructed and expanded are covered in chapter 4. Stomatal conductance isolated by rearranging the expanded energy balance equation is

$$g_{\ell W}^{-1}{}_{-1} = \frac{r_{HR}\rho_a c_p(VPD + s(T_{leaf} - T_a))}{\gamma(r_{HR}G_{ni} - \rho_a c_p(T_{leaf} - T_a) - r_{HR}\rho_\ell c_{p\ell}\ell^* \frac{\Delta T}{\Delta t})} - r_{aW}, \tag{5.2}$$

where:

$g_{\ell W}$ is stomatal conductance [$m{\cdot}s^{-1}$],

$r_{HR}$ is the combined parallel resistances to wind-driven convective and radiative heat transfer [s·m$^{-1}$],

$\rho_a$ is the density of air [kg·m$^{-3}$],

$c_p$ is the specific heat capacity of air [J·kg$^{-1}$·K$^{-1}$],

$VPD$ is the air vapour pressure deficit [Pa],

$s$ is the rate of change of saturation vapour pressure with temperature [Pa·K$^{-1}$],

$T_{leaf}$ is the leaf temperature [K],

$T_a$ is the ambient temperature [K],

$\gamma$ is the psychrometric constant relating the partial pressure of water in air to temperature [Pa·K$^{-1}$],

$G_{ni}$ is the incident net isothermal radiation [W·m$^{-2}$],

$\rho_\ell$ is the density of the leaf [kg·m$^{-3}$],

$c_{p\ell}$ is the specific heat capacity of the leaf [J·kg$^{-1}$·K$^{-1}$],

$\ell^*$ is the volume to area ratio of the leaf (leaf thickness) [m],

$\frac{\Delta T}{\Delta t}$ is the rate of change of leaf surface temperature [K·s$^{-1}$], and

$r_{aW}$ is the isolated boundary layer resistance to water vapour transfer [s·m$^{-1}$].

#### 5.2.1.2 Method 2 - Semi-empirical with reference surfaces

The rigid structure of the first principles theoretical approach requires explicit quantification of all energy fluxes in the field, while empirical methods substitute in-field references. The temperature of reference surfaces can indirectly represent the environmental influence on energy transfer (Leinonen et al., 2006). A dry reference with no evaporation at the surface, assuming similar optical and aerodynamic properties to a leaf, can be a proxy of incident radiation energy. The wet reference surface eliminates the need to model humidity driven

transpiration by representing a leaf with the maximum amount of evaporative cooling and otherwise similar properties (Maes et al., 2016). Orientation of the reference surfaces would affect sunlight and wind incident to the surface and care must be taken that reference surfaces experience equivalent conditions to the target. The stomatal conductance index quantifies the behaviour of the leaf relative to references in the following fashion,

$$I_g = (T_{dry} - T_{leaf})/(T_{leaf} - T_{wet}), \tag{5.3}$$

where:

$I_g$ is the stomatal conductance index,

$T_{dry}$ is the dry reference temperature [K], and

$T_{wet}$ is the wet reference temperature [K].

With the acquisition of dry, wet, and leaf temperatures, stomatal conductance can be calculated from what remains of the energy balance equation (Guilioni et al., 2008). The introduction of reference temperatures makes this method a half theoretical and half empirical approach termed here method two. Stomatal conductance calculated from method two is in the form

$$g_{\ell W\_2}^{-1} = (r_{aW} + 2r_{HR}VPD/\gamma)I_g^{-1}. \tag{5.4}$$

#### 5.2.1.3 Method 3 - Empirical

The third method discards the theoretical derivation to exploit the relation of stomatal conductance to the stomatal conductance index by modelling stomatal conductance as a function of the leaf, ambient air, and reference surface temperatures only (Maes et al., 2016). Stomatal conductance from method three is

$$g_{\ell W\_3} = (a_0 + a_1 T_a)I_g + (b_0 + b_1 T_a)I_g^2, \tag{5.5}$$

where $a_0$, $a_1$, $b_0$, and $b_1$ are constants developed from fitting the equation to measured stomatal conductance. The equation was fit using a non-linear least squares regression to a

handful of datapoints similar to the paper that introduced the empirical method (Maes et al., 2016). Manual collection of stomatal conductance is not an expedient process and long-term repeated collection is a significant undertaking to enable method three.

### 5.2.2 Target Plants

To create appropriate wheat plants to test the validity of the stomatal conductance models, samples with controlled water content were created. Ten plastic containers with a depth of 38 cm and an open area of 38 by 43 centimetres were filled with approximately 60 litres of Sunshine Mix #4 soilless growth medium (Sun Gro Horticulture, Agawam, MA) and sown with wheat (*Triticum aestivum* L.). Five of the containers contained the Stettler wheat cultivar and five contained the Superb wheat cultivar. These varieties were selected based on their expected different response to water deficit. Stettler has shown better performance under drought stress than Superb with higher harvest index and water-use efficiency (Willick et al., 2017). All containers held 40 plants, with five centimetres between each plant in a square spacing pattern.

Plants were seeded in the greenhouse on May 4th 2018. The lighting in the greenhouse was on for a 14 hour photoperiod and the lights output approximately 300 $\mu mol \cdot m^{-2} \cdot s^{-1}$ of photosynthetically active radiation at the level of the canopy. The temperature setpoint in the greenhouse cycled between 24℃ during the day and 18℃ at night. A fan kept a large amount of air flowing over the containers. Daily watering kept the soil near the outlined water conditions and 20-20-20 liquid fertilizer with 800 ppm nitrogen was applied every two to three days. In addition, 30-40 pieces of dry 14-14-14 Osmocote 100-day slow release fertilizer were added to each container to supply nutrients. The volumetric water content of soil in the containers was maintained at 30% by volume for two weeks to facilitate growth. After two weeks, two containers of each variety were allowed to naturally dry, one to 20% and one to 10% volumetric water content to induce drought stress at two levels. All containers are watered daily to maintain, for each variety, three containers at or above 30%, one at 20% and one at 10% volumetric water content as measured by CS655 time-domain reflectivity probes (Campbell Scientific, Logan, UT) and verified by weighing containers. Four weeks after sowing, the containers were moved outdoors and subjected to in-field conditions. Once outdoors,

watering was restricted to two of the well-watered containers and all other treatments were left to dry without any watering. Implementing tiers of water deficit and restricting watering created four unique representations of water status for both varieties: continuously well-watered (WWc), well-watered (WW), mild deficit (MD) and severe deficit (SD) which are summarized in table 5.1. One of the continuously well-watered treatments is kept to represent a control for water deficit. The other WWc treatment was kept as a spare. WWc was compared to WW to assess the development of drought stress in the WW treatment because they started at similar conditions and differences should arise only because of the natural drying.

### 5.2.3 Outdoor Data Collection

A FLIR Vue Pro R thermal camera (FLIR Systems, Nashua, NH) with a spatial resolution of 640x512 pixels observed the eight containers of wheat from nadir. The reported measurement accuracy of the FLIR Vue Pro R was ±5℃ with a sensitivity of 0.04℃. Weather data were acquired by sensors attached to the frame that held the thermal camera. Ambient temperature and relative humidity were measured with a Campbell Scientific HC2S3-L probe (Campbell Scientific) with standard error of ±0.1℃ for temperature and an error of ±0.8% for relative humidity. Wind speed was measured with a R.M. Young 05103-10 mechanical wind sensor (R.M. Young, Traverse City, MI) with a standard error of ±0.3m·s$^{-1}$. Incident solar radiation power was measured with a Kipp and Zonen SP Lite2 pyranometer (Kipp and Zonen, The Netherlands) installed horizontally with the sensor facing straight up. The error

**Table 5.1:** Summary table for drought treatments of wheat in containers. The nominal water content and watering schedule applied when containers were moved outdoors is noted.

| Treatment | Initial Water Content | Daily Watering |
|---|---|---|
| WWc | 30% | 2 litres for 60 litres of soil |
| WW | 30% | none |
| MD | 20% | none |
| SD | 10% | none |

of the pyranometer was ±5% of the incident power at high angles of incidence and considerably less as the sun moves away from the horizon. The pyranometer, ambient temperature sensor, and wind speed sensor were installed on a horizontal bar on the frame approximately 3m above the ground. The thermal camera was contained within a white bucket to avoid solar heating of the sensor array within the camera. All sensors connected to a cabinet which contains power supplies and a Campbell Scientific CR1000 datalogger (Campbell Scientific).

Reference surfaces required for empirical methods were established when moving the plants outside (Leinonen and Jones, 2004, Jones, 1999). A dry leaf reference was not created in field as suggested creation of a reference is to cover stomatal surfaces with petroleum jelly to block transpiration, but that method is not suited for continuous monitoring (Maes et al., 2016). An equation to calculate the dry leaf temperature from net isothermal radiation was used to calculate the expected dry reference temperature (Jones, 1999). The equation relies on calculation of net isothermal radiation and requires iteration as a new leaf temperature will influence the net radiation.

$$T_{dry} - T_a = \frac{r_{HR} G_{ni}}{\rho_a c_p} \tag{5.6}$$

The wet reference temperature was the measured value of temperature of a wetted artificial leaf. The false leaf was constructed from thin green cotton cloth stretched over a wire frame to emulate the size and shape of a wheat leaf. The false leaf was set into the spare control container of Stettler wheat so the wet reference would experience similar air movement as a natural leaf in the canopy. A reservoir of water was connected to the cloth so that the wet reference cloth was able to wick water to stay wetted. The water container was covered in aluminum foil to prevent algae growth and avoid sunlight heating. Thermocouples sewn into the cloth provided the wet reference temperature. The wet leaf setup can be viewed in figure 5.1. If the temperature of the references were not exactly indicative of a real leaf accuracy of methods two and three would be affected. As long as the response of the reference was stable it would allow comparisons between empirical methods. Weather and wet reference thermocouple data were acquired every minute, synchronized with the images captured by the thermal camera.

**Figure 5.1:** Wet reference in the spare tub of Stettler wheat circled in red. The water container and ribbon leading to the leaf are visible on the right.

## 5.3 Data

### 5.3.1 Growing Conditions and Observations

Visible signs of nutrient deficiencies were observed in the plants and biotic stress impacted all containers due to an infestation of thrips, small insects that fed on leaves, noticed on May 27th. On May 29th an application of half a litre of Kontos insecticide at a concentration of 0.5 millilitre per litre as well as a biological treatment of cucumeris were applied to each of the containers to exterminate thrips early in their life cycle (Banik, 2018). The water status of containers was logged every fifteen minutes, but those measurements were lost except for a handful of manually recorded points. The water status of some treatments of Stettler wheat are shown in figure 5.2.

On the afternoon of June 2nd 2018, the containers were moved out of the greenhouse and set underneath the thermal camera setup to capture images as in figure 5.3. A light rain of fewer than two millimetres fell on the plants the morning of June 4th, but otherwise,

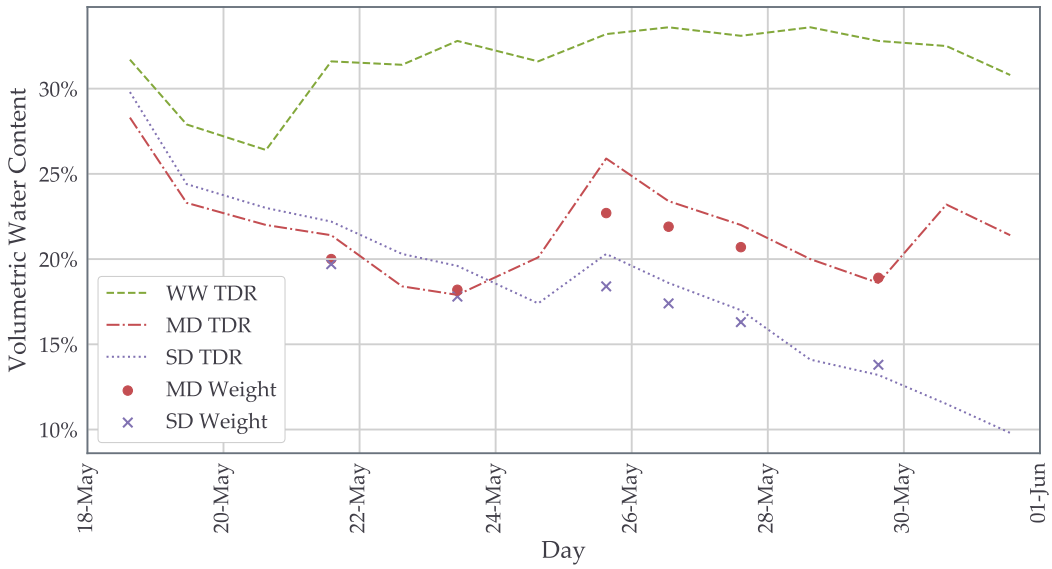


**Figure 5.2:** Greenhouse water status for WW, MD and SD treatments of Stettler wheat containers. The trendlines were constructed from point data from CS655 time domain reflectivity (TDR) probes while weight based measurements are shown as individual points.

conditions were mostly sunny. Weather and wet reference thermocouple data was captured by the datalogger every minute of the days of June 3rd to June 8th. Some periods in that span had no images acquired, likely due to issues with power delivery to the camera. Power issues are also believed to impact camera self-calibration as small continuous sets of images had horizontal bars of unexpected temperatures across the image until another automatic re-calibration eliminated the bars. All thermal images were automatically segmented to isolate regions of leaf tissue. Each leaf region highlighted by segmentation was associated with the container that holds the plant based on the centroid location of the region. A mean value of leaf temperature for each variety and treatment was extracted automatically from each thermal image and used to model corresponding values of stomatal conductance.

Equation (5.6) did not predict useful values of a dry leaf temperature. From data not shown, the calculated dry leaf temperature was roughly 30℃ above the ambient temperature during the daytime. From previous experience observing wheat canopy temperature in chapter 4, it was noted that the leaf-air temperature difference did not exceed 10℃, and the dry leaf temperature was assumed to be 10℃ higher than the ambient air temperature

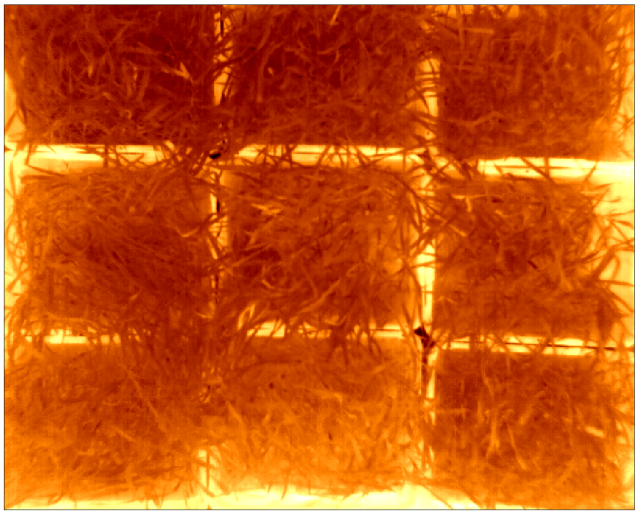

**Figure 5.3:** Sample thermal image showing the wheat containers. From left to right, top to bottom: Stettler WWc, WW, MD, SD, Superb WWc, WW, MD, SD, and Stettler spare.

to represent a leaf with impaired transpiration. Thermocouple recordings of the wet reference temperature were available for the entire data acquisition period, enabling the use of reference-based attempts at modelling stomatal conductance. At points of high VPD, the wet reference dried faster than could be replenished by the passively fed system. The water container had to be filled up every day so that water could transfer along the cloth to the reference surface more easily. Porometer measurements of stomatal conductance were attempted, but the steady-state porometer used had an undetected internal blockage and could not achieve steady conditions. Manual retrieval of stomatal conductance was abandoned and there was no measured baseline values available to compare against modelled values.

## 5.4 Analysis

Without baseline manually collected stomatal conductance there was no way to assess absolute accuracy and analysis proceeded without any ground truth stomatal conductance to compare each model against. Therefore, analysis was limited to contrasting different models applied to the same target, and comparing a single model across different water deficit treatments. The empirical equation (5.5) was fit to a subset of stomatal conductance calculated from equation (5.4), the half-empirical model, as they are both based on stomatal conduc-

tance index. Five values from each of the six days were selected and the equation coefficients were fit to thirty samples of stomatal conductance calculated by method two. Datapoints were taken at 10:00, 12:00, 14:00, 16:00 and 18:00 each day. The fitted coefficients were used to calculate stomatal conductance using the weather data acquired every minute.

T-tests were used to compare variance within groups to the variance between groups to establish if groups were statistically distinct. The contiguous time-series stomatal conductance data calculated from method one and leaf-air temperature difference data were split into groups to be used in t-tests. T-tests were applied to groups that represent the same time period. T-tests were run between WWc and WW treatments of the same variety to assess when these samples diverge given they should have started at similar conditions. In this implementation, groups were constructed of 30 samples, representing 30 minutes. As an example, the stomatal conductance values for Stettler WWc treatment and Stettler WW treatment between 11:00 and 11:30 formed the two groups and t-tests assessed if those two groups were statistically distinct considering the difference within each group and the difference between the groups. The null hypothesis stated groups would have no significant difference and the null hypothesis was rejected if the p-value of the t-test was lower than 0.05. Reporting a cumulative sum of tests that rejected the null hypotheses showcased when differences between contiguous sets of data representing WWc and WW treatments developed. The divergence between WWc and WW groups in stomatal conductance was compared to divergence based on the leaf-ambient temperature difference.

## 5.5 Results

Stomatal conductance was calculated every minute, except for any case where leaf temperature was missing due to image segmentation failing to highlight regions of leaves. The cases without leaf temperature were assigned a NaN value of stomatal conductance. Stomatal conductance presented in figures is a ten-minute rolling average that ignores NaN values, to create smoother trendlines and highlight distinctions. This averaging better represents the behaviour of stomatal response as opening and closing occurs over several minutes (Jones, 2013). The leaf temperatures and net isothermal radiation for June 3rd and June 8th are

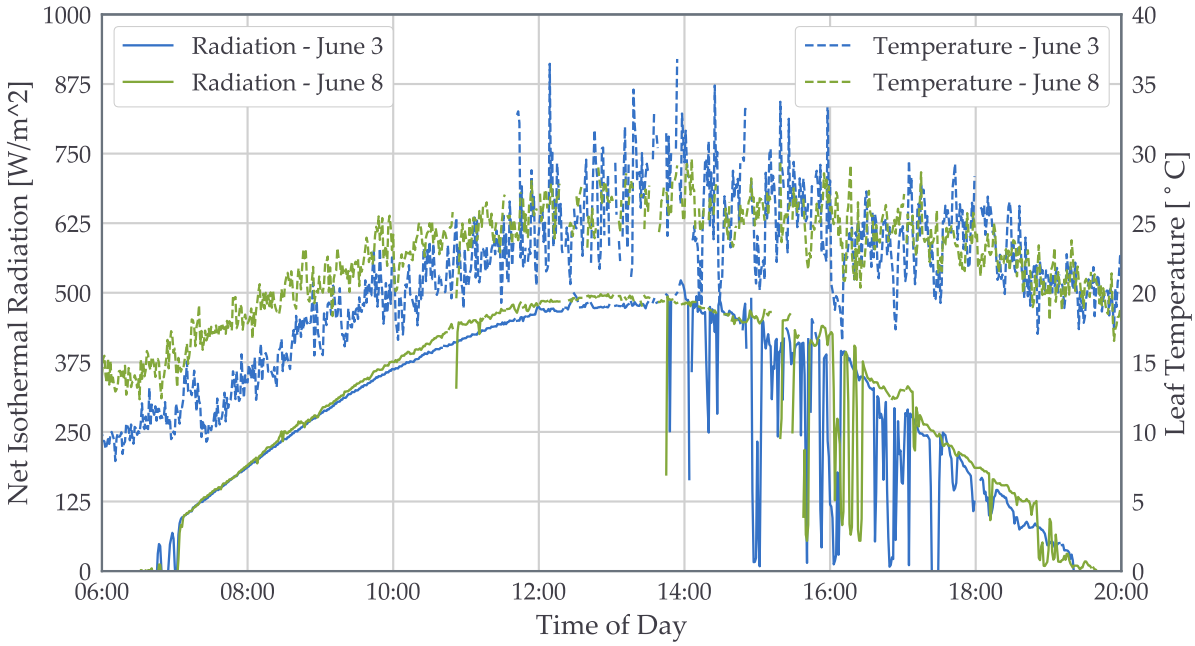


**Figure 5.4:** Calculated net isothermal radiation and measured leaf temperature of the control treatment of Stettler on the first and last day of outdoor data acquisition.

shown in figure 5.4 to showcase the trends of the common measured parameter of all stomatal conductance models as well as the incoming energy. June 3rd and June 8th both had fairly sunny conditions all day until about 15:00. Net isothermal radiation is shown alongside any figures displaying stomatal conductance trendlines for the first and last full days of data acquisition: June 3rd and June 8th. Stomatal conductance from the theoretical model is shown in figure 5.5 for all treatments of Stettler and in figure 5.6 for all treatments of Superb on June 8th. In both varieties on June 8th, there was a slight difference between WWc and MD treatments compared to a substantial difference between WWc and SD treatments.

Stomatal conductance calculated by all methods for the WWc treatment of Stettler on June 8th are shown in figure 5.7. Method two has a peak in the morning, similar to method one but then stomatal conductance drops to very low values for the rest of the day. Method three completely overlaps method two, even though a very small subset of data was used to fit the equation. Stomatal conductance trends from method two are relatively flat, but a distinction still exists between WWc and SD similarly to what is viewed for method one (not shown). Stomatal conductance from method one is very high compared to method two

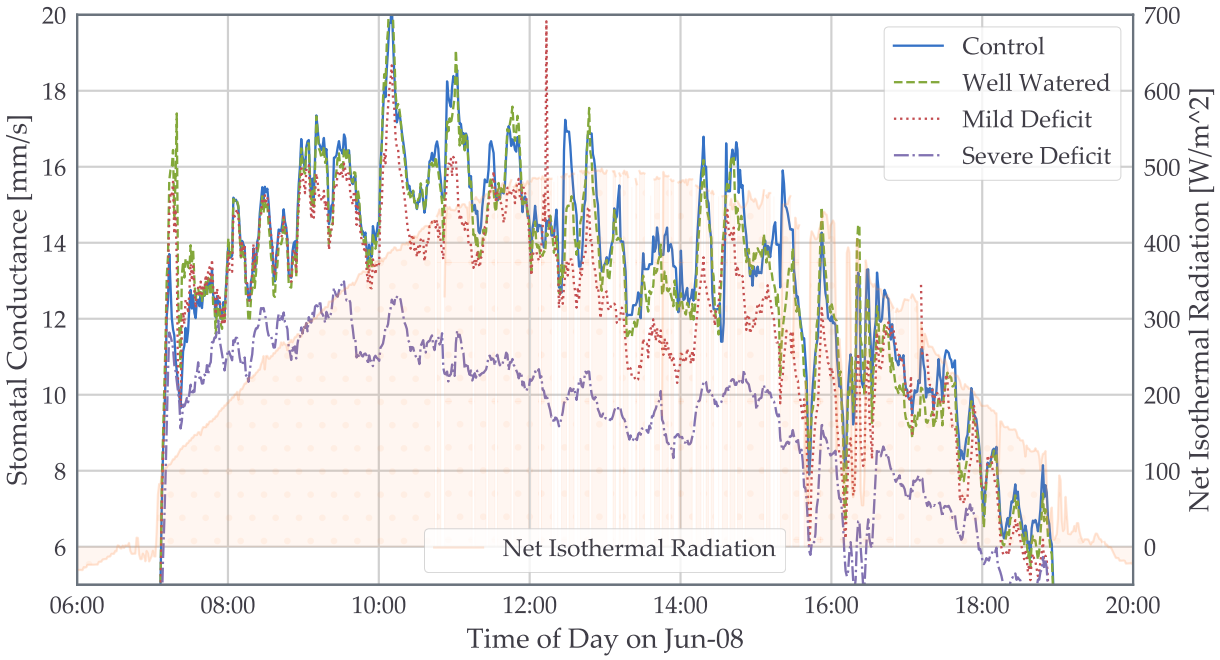


**Figure 5.5:** Stomatal conductance for all treatments of Stettler as calculated from the first principles model. Net isothermal radiation is shown with the filled area under the curve.

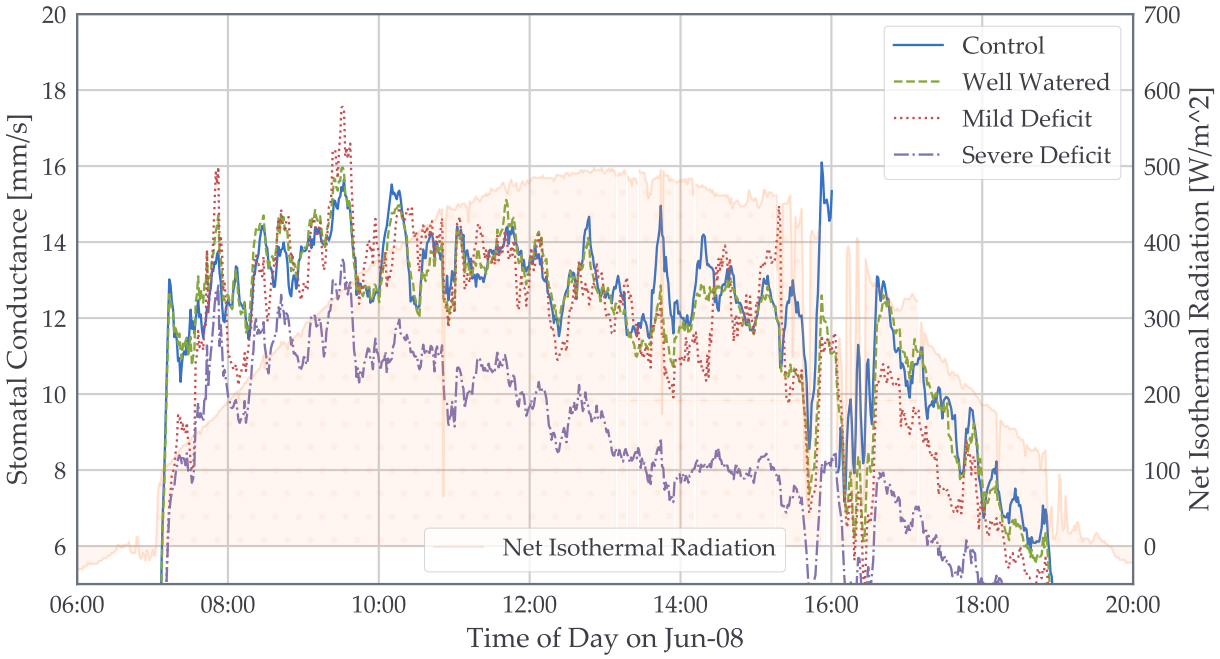


**Figure 5.6:** Stomatal conductance for all treatments of Superb as calculated from the first principles model. Net isothermal radiation is shown with the filled area under the curve.

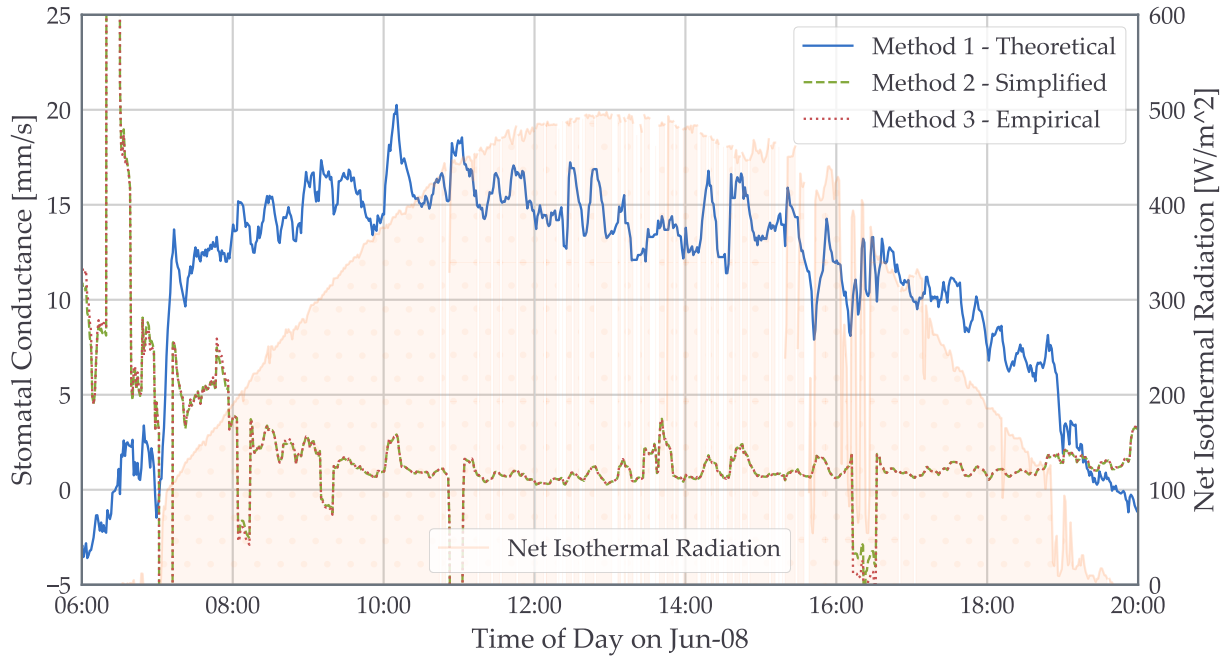


**Figure 5.7:** Stomatal conductance calculated from all three methods for control treatment of Stettler. Methods 2 and 3 overlap entirely except for a small period of time after 16:00. Net isothermal radiation is shown with the filled area under the curve.

and three which are quite low. The accuracy of methods could not be calculated directly, but references suggest that the maximum stomatal conductance for cultivated grasses could be between two to eight millimetres per second, which is a very broad range that did not investigate diurnal variation (Jones, 2013). Method three overlapped method two almost completely in all eight of the target containers, which verifies that the derivation of the empirical equation is valid. Negative values of stomatal conductance index strongly affected method two and three. Negative values in the index occurred when the wet reference temperature rose above leaf temperature when the reference dried out. Both method two and three result in negative values of stomatal conductance near 11:00 and 16:15 in figure 5.7.

Despite the spiky behaviour of stomatal conductance in method one, there were consistent differences between WWc and SD treatments on the first day of data acquisition, as shown in figure 5.8 and figure 5.9 for Stettler and Superb, respectively. These trendlines of stomatal conductance were expected to be far apart and Stettler data does show a significant difference in the morning with distinction fading later in the day, while Superb data shows slightly more difference between treatments during the morning before the difference fades. Trendlines in

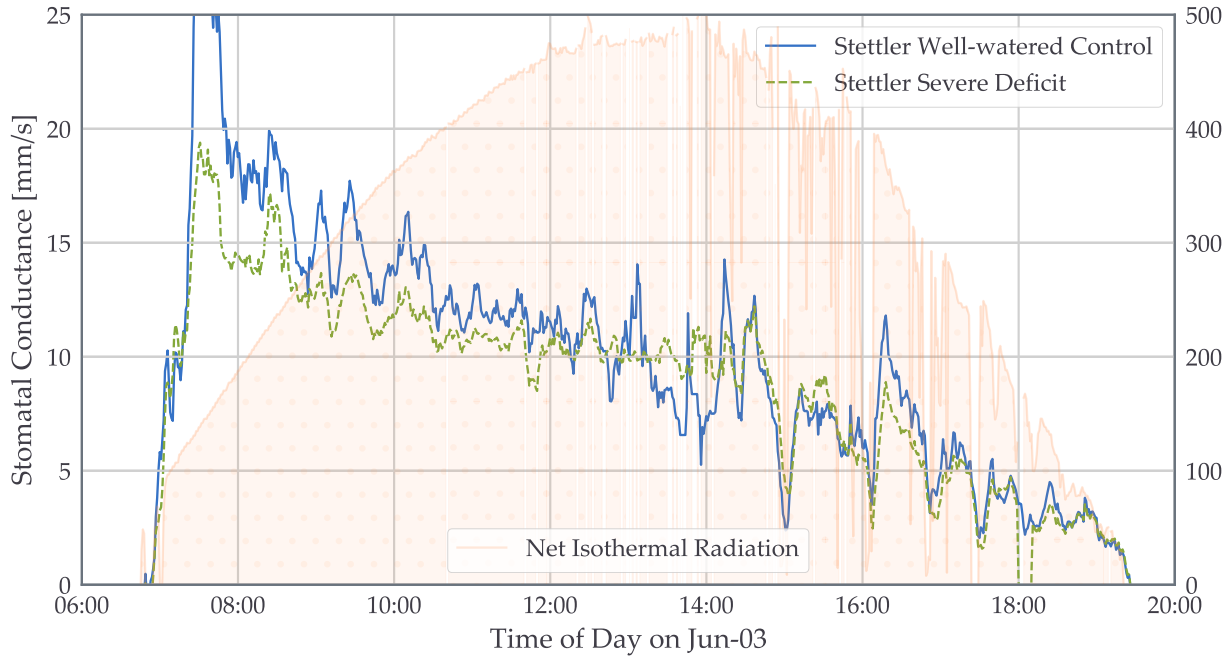


**Figure 5.8:** Stomatal conductance modelled from first principles for control and severe water deficit treatments of Stettler on the first day of data acquisition. Net isothermal radiation is shown with the filled area under the curve.

stomatal conductance have more specificity in identifying imposed deficit than the traditional method of leaf-air temperature difference, in which the expected relation between WWc and SD treatments of Stettler inverted in the afternoon as shown in figure 5.10.

The observable onset of stress over time denoted by the cumulative sum of significantly different WW and WWc groups in Stettler and Superb is shown in figure 5.11. In both varieties, the leaf-air temperature diverged more often and faster than stomatal conductance. A difference in stomatal conductance takes a long time to develop as WW and WWc stomatal conductance nearly overlap after several days of soil drying as shown in figure 5.5. Superb had more distinction between treatments, reinforced in figure 5.6 which has slightly more departure between WWc and WW than similar data for Stettler. Superb had significant differences in both stomatal conductance and leaf-air temperature difference between WW and WWc treatments spike mid-day on July 6th and 7th while the only significant jump for Stettler is early in the morning of July 6th. A representation of the groupings and how they are compared is shown in figure 5.12. The 90% confidence interval surrounds the mean value of each half hour grouping of stomatal conductance and the grey overlap shows where the

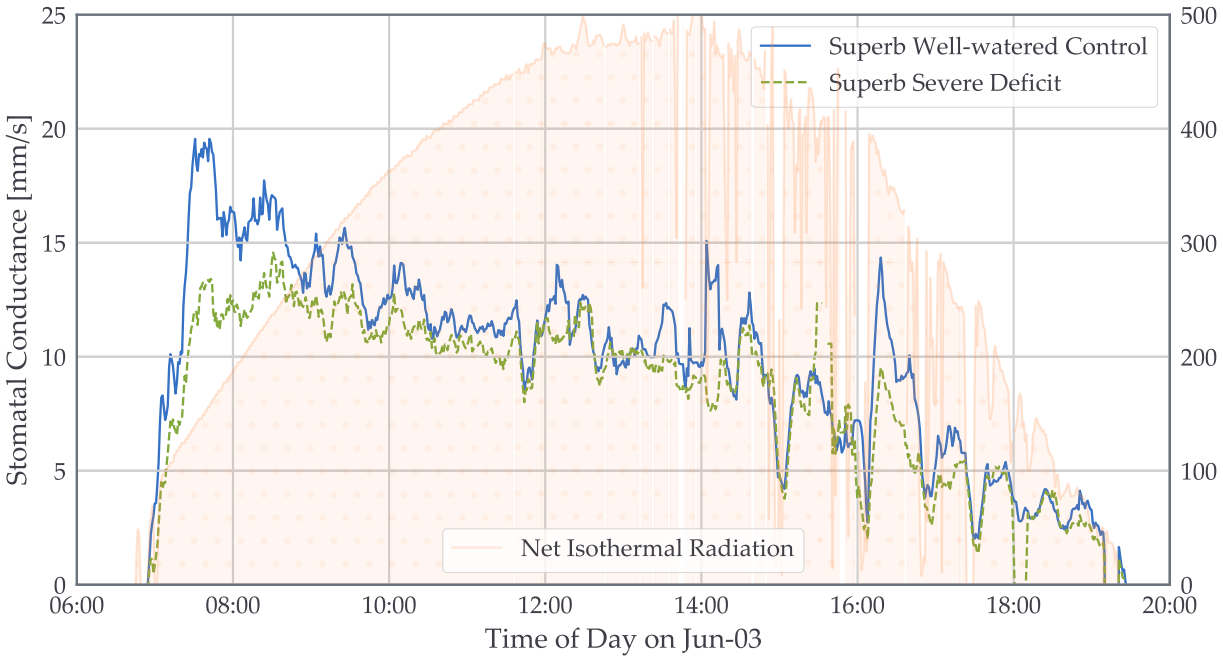


**Figure 5.9:** Stomatal conductance modelled from first principles for control and severe water deficit treatments of Superb on the first day of data acquisition. Net isothermal radiation is shown with the filled area under the curve.

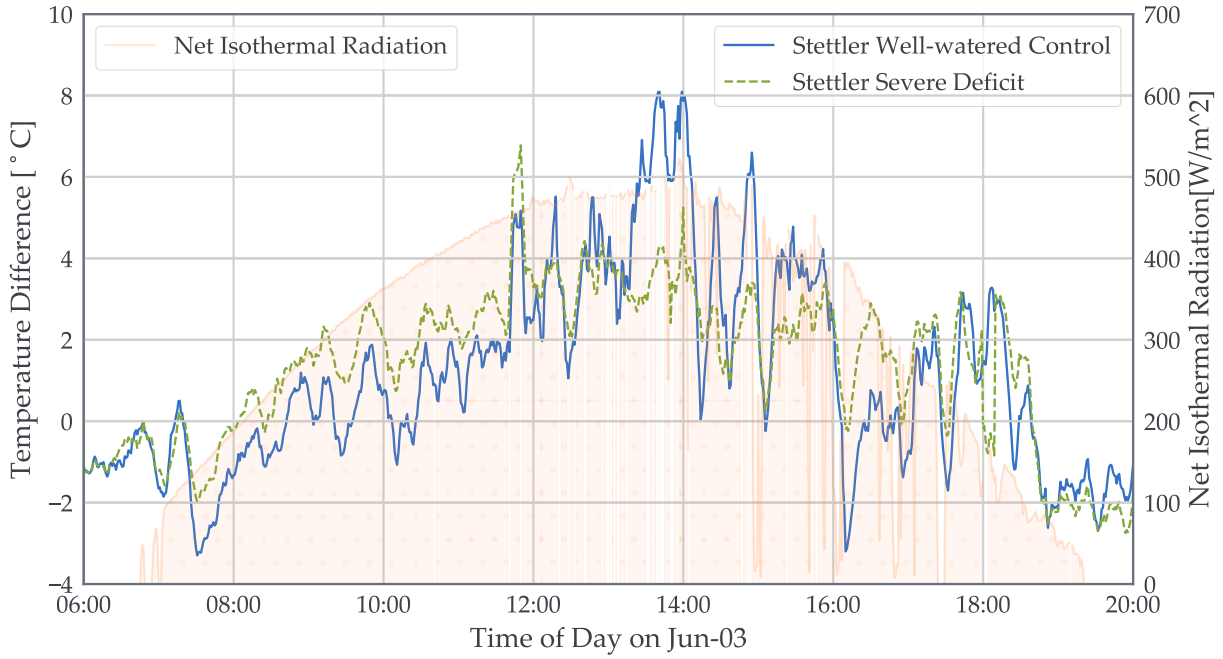


**Figure 5.10:** Leaf-air temperature difference for control and severe water deficit treatments of Stettler on the first day of data acquisition. Net isothermal radiation is shown with the filled area under the curve.

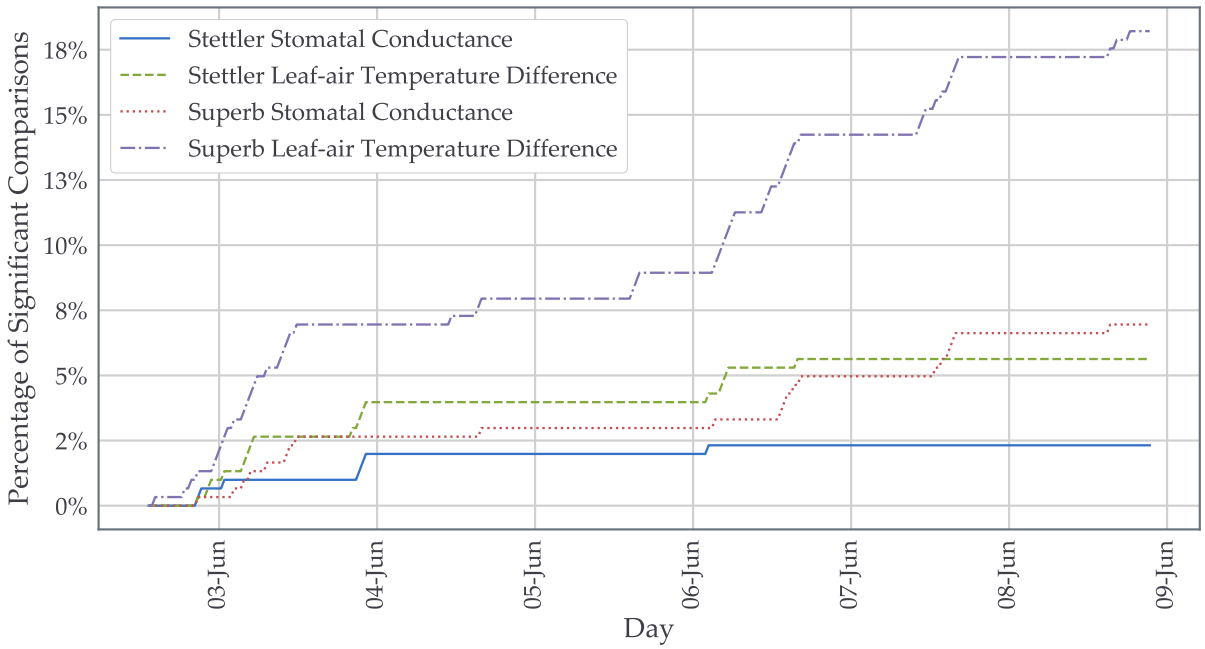


**Figure 5.11:** Cumulative sum of significant t-tests ($p<0.05$). 30 minute subsets of control data were compared to their corresponding measure in the well-watered treatment over the same time period.

t-test rejected separation at a p-value of 0.05.

## 5.6 Discussion

Qualitative assessment of cultivar behaviour in this study was achieved by comparing stomatal conductance response between treatments of the same variety in the same image under the same conditions. The cultivar tolerance to drought stress was assessed under the assumption that lower water availability will lead to greater impairment of transpiration in drought-sensitive varieties. Due to the limited nature of this study, no strict conclusions of cultivar behaviour can be made here but it appears that Stettler was impacted less by the growth medium drying over a week. Stomatal conductance and leaf-air temperature difference modelled from WWc and WW treatments are very similar for a full week under drying conditions. Further work of conclusively assessing plant drought tolerance would require further replications with tighter control of water status. The leaf-air temperature difference was determined to be a more sensitive indicator of drought than stomatal conductance which

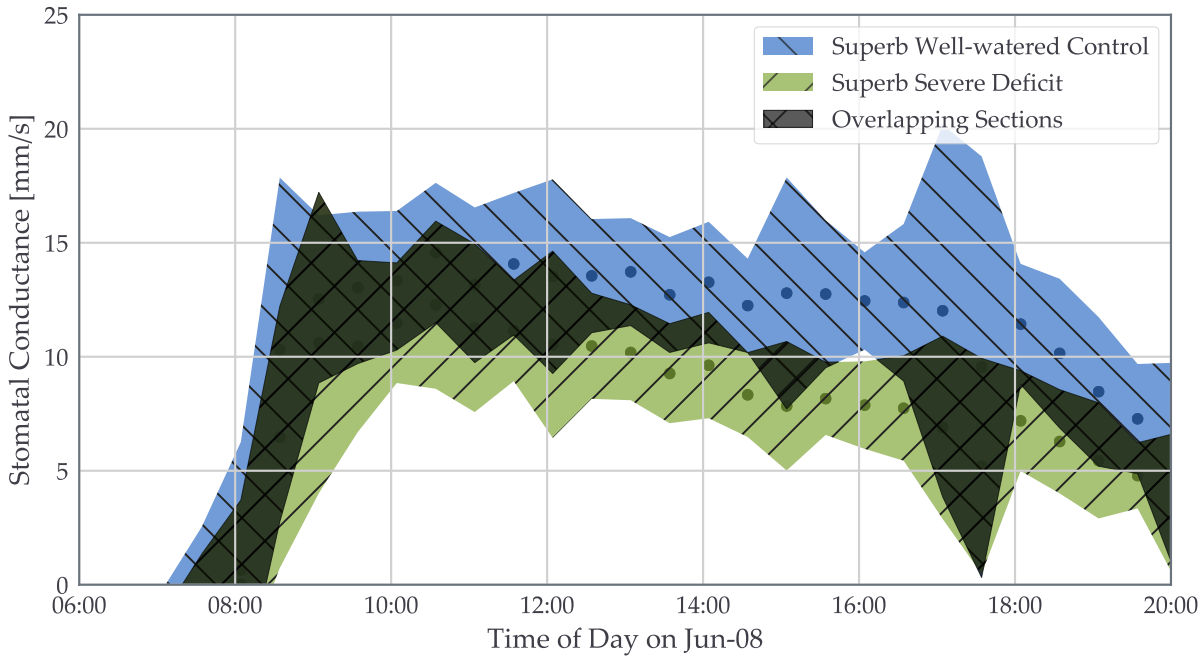


**Figure 5.12:** Superb WWc and SD stomatal conductance grouped into thirty minute samples, noted by the dots. The 90% confidence interval is filled in with overlaps between the two samples filled with a dark grey.

does not develop large consistent changes in behaviour until soil water is severely depleted.

The description of stomatal conductance used throughout this study may not strictly match the actual stomatal opening. The parameter of stomatal conductance was calculated solely on the energy balance. It is a description of water usage required to satisfy the temperature response. If water content in the plant is very low, it may be that stomata are open but water is not lost effectively. In that case, the calculated value of stomatal conductance is lower than could be calculated by analysis of the gas exchange. If stomata remain open, growth processes that rely on gas exchange may not be hampered despite reduction of transpiration.

Empirical methods relax the amount of assumptions made in analysis by referencing surfaces that ideally have stable behaviour and interact with the environment similarly to actual leaves. The wet reference used here did report a value less than leaf temperature while the surface remained wet but in periods where the reference dried out it did not have a lower temperatures than the leaves, making methods two or three unusable at those times. Stettler wheat under severe water deficit had leaf temperatures roughly 8℃ higher

than ambient and Superb had leaf-air temperature difference peak at 10℃, suggesting that the dry leaf temperature of 10℃ above ambient was appropriate to represent wheat with impaired transpiration. The implementation of reference surfaces here did not work perfectly, but there is the possibility to use reference based methods in small studies provided careful attention is paid to the upkeep of a wet reference. The approach of method three of fitting an empirical stomatal conductance model to measured values is a difficult prospect as well. A tremendous amount of work would be necessary to validate model fits across days and in different environments using train/test splits and comparing to manually collected data. A well thought out evaluation scheme might make this method viable without needing to fit the model to manually collected data each time it is used but that would be a tremendous undertaking to create the standard.

Data collection was kept to the minimum that would enable a theoretical based approach. As such, method one carries a lot of errors in the current implementation due to the myriad of assumptions made, but the analysis is entirely transparent and repeatable. Data from more field sensors can be used to validate sections of analysis and associated parameters, such as the radiation interactions based on reflectance, rather than adjust an overall index to fit the data. The way forward when modelling stomatal conductance with theoretical methods is far more clear than empirical methods.

## 5.7 Conclusion

The theoretical method of calculating stomatal conductance results in clear trends of stomatal conductance based on the water content and has been shown to respond in the expected way to drought treatments. Empirical methods that rely on wet and dry reference surfaces to calculate stomatal conductance should be avoided for the sake of repeatable and traceable analysis. Implementing reference surfaces introduces many practical complications as the analysis relies on assumptions implemented when the reference is created and established in field. The requirements to using the empirical models are ambiguous and will depend significantly on the experimental set-up. The theoretical energy balance model explicitly describes the assumptions required and are applied during analysis, not during acquisition.

The first principles model accuracy can be improved by adjusting parameters or including more energy interactions and it is recommended to do so. Analysis implemented in an automated processing pipeline will provide more insight to stress development, recovery and impact on yield. The traceable and repeatable methods are invaluable in plant studies that rely heavily on replications and standardization.

Stress response was evaluated by observing stomatal conductance modelled from data gathered in the field without an operator present. Analysis of stomatal behaviour as implemented here requires continuous data to group samples for t-tests and observe smoothed trends which are consistent under sunny, cloudless conditions. Further work is required to determine how to assess stomatal conductance quickly and confidently to minimize the time required to uncover stress state of crops in the field. T-tests using grouped samples were the first attempt at automatic stress assessment and found differences between stressed and unstressed wheat develop initially in the early afternoon, as shown on June 8th in the difference between MD and WWc. Consistent stomatal conductance difference is easily visible in the morning of June 3rd between SD and WWc. Stomatal conductance difference expands across the entire day in extreme drought as shown by SD vs WWc on June 8th.

# Chapter 6

# Conclusions Related to Phenotyping

## 6.1 Hypotheses

Hypotheses were evaluated on their merits individually, away from the overarching goal of phenotyping. Hypotheses were covered in order they were introduced. Hypothesis one was covered in chapter 3. Hypotheses two, three, and four were addressed in chapter 4. The last two hypotheses were investigated in chapter 5.

### 6.1.1 Hypothesis 1 - Directionality of Long-wave Infrared Radiation Reflection and Scattering from Leaves

The physical basis of non-contact temperature measurement relies on separating radiation based on the surface emissivity. The initial hypothesis stated that leaf emissivity would be above 0.96 in for all view angles. High emissivity bolsters radiative heat loss which effectively discards energy incident to the plant that is not collected. It was shown here that emissivity is high for crop leaves at all angles above the leaf upper surfaces, and reflection of thermal infrared radiation from a leaf surface is not significantly specular. Radiometric corrections can be applied at any time after acquisition to separate the emitted radiation from the total radiation outbound from a surface. The difference between surface and apparent temperature of leaves is small as the surface temperature dominates the total outward radiation. The value of reflected temperature contributes very little to the overall and no specular behaviour should arise in leaves.

### 6.1.2 Hypothesis 2 - Leaf Temperature Extraction

Approaches to thermal image processing throughout this document included examples of tedious and difficult to replicate manual methods employed in the lab experiment as well as automated methods employed in the field experiments. The hypothesis stated there would exist an automated method of segmenting images that could be applied to thermal images of crops in the field. Automated image processing based on morphological methods successfully segmented thermal images of wheat canopies in outdoor conditions at all times of day and all sun conditions into leaf regions with traceable and repeatable methods. The automated approach used here works excellently on sparse canopies where each leaf is distinct over a hot background. With a fuller canopy, it was challenging to isolate leaves using the value of temperature within regions relative to their surroundings. The algorithm proposed here is not perfect, but it is simple, based on methods that are implementable with images of any scale or orientation and make no assumption of what leaf temperature should be.

### 6.1.3 Hypothesis 3 - Leaf Temperature Stability

Leaf temperature is varied over small periods of time, verified at the leaf level by contact and non-contact sensors. The variation observed was not due to thermal camera inaccuracy or constant re-calibration. The hypothesis stated that leaf temperature varies significantly over small time periods because small, thin leaves do not have enough thermal mass to buffer short term effects of changing sunlight conditions or wind. As determined in the field, the latent heat loss based on stomatal conductance values was fairly stable across the day, so passive heat loss processes that scale up as leaf temperature increases lead to oscillations in temperature. Variation in leaf temperature was stronger under full sunlight conditions because of the greater fluxes involved with maintaining the energy balance. Active regulation of plant temperature through transpiration was relatively slow to respond and was not sensitive to minor jumps in leaf temperature.

### 6.1.4 Hypothesis 4 - Phenotype Evaluation

Models incorporating environmental conditions and plant interactions open the door to greater understanding of the resultant phenotype. The hypothesis stated that a stable description of plant behaviour in creating the temperature response could be extracted from an energy balance model. The environmental influence on the plant energy was quantified in an energy balance model and the behaviour required to satisfy the temperature measurement revealed sensitivity to the environment. Regular plant processes are interrupted in the presence of stress, and the degree of cultivar specific sensitivity is incredibly important for for crop screening and cultivar development. Stomatal conductance is a measure of how readily water can be lost through the stomatal openings on a leaf to satisfy the energy balance. The stomatal conductance trendline was distinct from trends of net isothermal radiation or leaf temperature and the behaviour is consistent across days. The day-to-day consistency of the stomatal conductance proves inclusion of weather data in the analysis of the plant response creates a robust parameter to study in phenotyping applications.

### 6.1.5 Hypothesis 5 - Energy Based Modeling Approaches

Water shortage is an abiotic stress marked by impaired transpiration resulting in a change in temperature due to a loss of latent cooling. Theoretical models of energy balance performed as expected during daytime hours with less water availability resulting in lowered stomatal conductance. The hypothesis was that stress would affect the plant response and result in a consistent all-day offset of plant behaviour from the unstressed case. This hypothesis was fulfilled in part as stomatal conductance values were significantly different across the full day between well-watered and cultivars of wheat under severe water deficit. The hypothesis holds in extreme stress conditions, but effective stress determination has to consider how stomatal conductance changes as stress develops. Differences emerged between control and naturally drying treatments early and often during sunny midday periods, and leaf-air temperature difference was more divergent, particularly in the case of the drought-susceptible Superb wheat variety. Time of day is crucial to consider when assessing stress because the influence of water deficit on stomatal conductance depends on the time of day. The dynamics of

energy handling would also be influenced by photosynthesis, fluorescence, and respiration processes that were not incorporated into the models. More complete models that include more interactions of the plant physiology may change the time-dependency of the results.

### 6.1.6 Hypothesis 6 - Quantifying Environmental Influence

The hypothesis was that energy balance implementations required quantifiable data from several sensors. Empirical methods replaced environmental data with temperatures of reference surfaces. Stomatal conductance calculated from the entirely empirical method and the half empirical methods follow distinct trends that are very different than stomatal conductance trends from the theoretical method. All methods showed distinctions between water deficit treatments as expected under sunny conditions. Overlap of wet reference and leaf temperature during periods of high evaporative demand, which would be the best time to use these methods to scout for stress, lead to instability in the stomatal conductance index which ruined the calculation of stomatal conductance. Without significant promise in methods that use references, they should be set aside, freeing up data collection from the constraint of purpose-built reference surfaces. The theoretical model is traceable and repeatable, which is very difficult to achieve with wet or dry reference surfaces. Standardized and consistent phenotypic data is invaluable for plant scientists who rely on trials with many replicates across different environments to validate any conclusions drawn regarding plant behaviour at a genetic level.

## 6.2 Goals

After validation of the hypotheses, the discussion must shift into the phenotyping sphere. The goals relate directly to the prospect of using this work to further phenotyping research and development.

### 6.2.1 Practical Concerns

The practical concerns raised in the introduction relate specifically to the operation of a thermal camera in a field. Considerations included how to set up the instrument, how to acquire data effectively and how to apply corrections. These three elements are intertwined, and there is no universal best method to gather data. The work presented here raises two significant points to consider: how will images be processed, and what reference elements can exist in the field. Automatic image processing to isolate leaves should be rooted in morphological methods as leaves in thermal images are distinguishable from other plant material and have typical shapes, although leaf angle within the canopy will affect its shape in the image. The morphological black top hat transform applied to thermal images in this work identified and isolated sparse canopy leaves but the performance was not as good with full canopies. Setting the threshold applied to the results of morphological operations to include more items in the foreground mask may highlight more leaf tissue but the regions will coalesce together in heavier canopies where leaf borders cannot be distinguished. Leaf temperature data obtained from a segmented thermal image can be corrected to reduce error. Bias is the primary concern in thermal camera accuracy and is generally avoided with camera self-calibration by closing off the sensor to outside influences briefly when not capturing images. Calibrating the images by adjusting the temperatures derived from the images to match a more precisely measured reference temperature of a surface in the image would aid in absolute accuracy (Gómez-Candón et al., 2016). Radiometric corrections can be implemented to calculate surface temperature based on the value of apparent temperature coupled with emissivity and reflected temperature, but that would be only a minor accuracy gain as leaf emissivity is very high.

### 6.2.2 Theoretical Concerns

Leaf temperature and stress are related but it is not a simple, consistent relation. Monitoring temperature response of plants was a surface level view of the complicated system of energy transfer and plant growth. This work has shown that implementing an energy balance which identified the contributions of the environment on a point measurement of temperature can

model what the plant behaviour must be in order to satisfy the observation. This work touched on how to quantify the plant behaviour and if changes in plant behaviour signal can signify stress. Grass crops such as wheat have well-known drought tolerance and stomatal conductance in wheat was not severely affected for several days under soil drying conditions (Tardieu and Simonneau, 1998). Comparisons between known unstressed and slowly drying plants has shown that drought response is stronger in Superb wheat compared to Stettler as Superb experiences faster change in stomatal conductance and leaf temperature when water is scarce. The first changes induced in stomatal conductance of wheat due to water scarcity were not overall offsets from a baseline, but instead short-term lowering to conserve water in the warmest parts of the day which leads to an increased temperature. The stress signal is then dependent on the time of day and the local conditions, with hot dry afternoons the strongest contributors to drought stress and the most likely times to observe a plant response (Berni et al., 2009b).

### 6.2.3 Approaches to Phenotyping

Several approaches to energy balance implementation were explored to determine the modelling requirements and results. Small studies have favoured empirical methods to detect stresses in sample populations in controlled conditions (Maes et al., 2014). As field phenotyping data collection expands, theoretical based models should be adopted as the standard approach. Theoretical models are expandable, traceable and use standardized data with explicit assumptions when necessary. Other models may have their uses in small-scale studies, but they will be difficult to replicate. Repeatable theoretical methods can be used in a two-step process to validate its usage in the field when investigating stress. The first step is to investigate the behaviour of the model and establish the conditions that allow the model to distinguish between states. In this study, the state to be examined was soil water status and the continuous values of stomatal conductance over a week in field were related to the soil water conditions. The second step is to use that validated behaviour and apply the model to assess the water status of plants in the field. Stress sensing data collection would likely have short continuous spans of data available as any mobile data collection platform would quickly pass over an entire field in order to assess it entirely. With confidence in the results

from the long-term study, a comparison between an expected value and the field value can be used to determine the stress state.

### 6.2.4 Future Work in Energy Balance Models

Through the assessment of goals outlined at the beginning, it is apparent that research efforts can build on the work presented here to better the field of phenotyping. The goals will have to be refined in any further research efforts, and there are a myriad of ways that research could proceed. Future work has been identified in areas of effective use of thermal images, stomatal conductance model accuracy, connecting stress development and stress handling to yield, as well as strategies to incorporate more data sources to increase precision and accuracy in phenotyping. Many of these avenues seek to more effectively use the spatial information within thermal imagery. There is no theoretical barrier to applying energy balance modelling at the individual leaf level, and most of the future work is identifying and overcoming the practical barriers to individual leaf models.

#### 6.2.4.1 Thermal Imagery Segmentation

Thermal images have been segmented to specifically isolate leaf tissue, but further work could utilize the spatial data more effectively. Registering thermal images with other images that represent wavelengths such as RGB or mid-wave infrared would improve segmentation. There is potential for more in-depth examination of spatial information in plant response and determining leaf-by-leaf or plant-by-plant response instead of an average of all leaf tissue in a region. Registration could allow for features from all images to be used in isolating leaf tissue, and a generated mask could be applied to all images. If the mask was generated based on edge detection, it would be possible to separate leaves in both heavy and sparse canopies. An energy balance could be applied to a single leaf in this case, with each leaf supplied with specific parameters such as net isothermal radiation based on shading and leaf orientation. Current methods apply a leaf temperature as the response of an ideal horizontal leaf at the top of the canopy experiencing direct sunlight and free-field conditions for wind speed.

Localized effects of biotic stress can be viewed with better segmentation allowing individual leaf temperature distributions to be viewed (Baranowski et al., 2015). Contrasting the

temperature of the stress-affected area to the rest of the leaf or the rest of the canopy signals the stress location and magnitude (Maes et al., 2014). The confluence of abiotic and biotic stresses spawns an abundance of primarily negative interactions between them (Suzuki et al., 2014).

#### 6.2.4.2 Stomatal Conductance Model Accuracy

The theoretical energy balance model implemented here has apparent issues with too little energy accrued at night, and too much energy accrued in the daytime. Verification of short-term dynamics in stomatal conductance by comparing with manually collected data would be difficult if not impossible as the measurement method is slow. Manual measurements could assess if modelled values of stomatal conductance for stressed and unstressed plants are close to expected and if modelled values diverge at the same time as measured values. In the pursuit of more accurate models, any assumed parameter in the energy balance implementation should be investigated to see if other instruments included within a full phenotyping application could provide a measured value. Metabolic and photochemical processes which impact plant energy handling are entirely ignored in this application but could be folded into the first-principles theoretical models of stomatal conductance in the pursuit of comprehensive energy analysis. Photosynthesis converts incoming energy to chemical energy and not considering that activity creates a model where all incident energy is converted to thermal energy. Stomatal conductance is inaccurately scaled very high because of the increased requirement for cooling to satisfy the temperature response observed. This effect is more prominent with data in chapter 5 from young plants that are still growing in the vegetative state as compared to data from plants near the end of their reproductive phase in chapter 4.

#### 6.2.4.3 Stress Development and Yield

Observation of phenotypic response to imposed water deficit over time could lead to more understanding about the development of plant stress and recovery from a stressed state. To explore around-the-clock dynamics, better characterization of the environment during sunlight transition and night time periods is necessary. The continuous and long-term monitoring of stomatal conductance here has uncovered some information about stress development in

crops. There was no connection made between yield impact and stomatal conductance here, but further studies could attempt to relate model behaviour with yield or other characteristics such as the ratio of root and shoot biomass. Effective stress assessment would capitalize on the understanding of how the modelled values of stomatal conductance dynamically respond to stress and how greatly yield is impacted. Data collection for stress assessment could then be adjusted for sensitivity or specificity by adjusting the time of data collection and/or repetitions. In the cultivars of wheat explored here, midday is the earliest point of small changes in stomatal conductance, while consistently lowered stomatal conductance occurs in the morning after soil water content was significantly lowered.

#### 6.2.4.4 Data Fusion

The integration of thermal images with other data gathering systems has the potential to address all of the previous concerns of image processing, accurate analysis and effective estimation of yield loss. One of the most intriguing options is to include spectral sensing alongside thermography which can investigate parameters estimated or ignored in this work. Spectral sensing could determine more precisely the amount of sunlight energy rejected by a leaf by observing reflections of visible wavelengths. In addition to improving energy balance modelling, spectral information can be used to predict stress development by investigating photochemical processes stimulated by sunlight. Phenotyping projects can investigate stress development more precisely and more confidently when employing several distinct approaches.

# References


Alchanatis, V., Cohen, Y., Cohen, S., Moller, M., Sprinstin, M., Meron, M., Tsipris, J., Saranga, Y., and Sela, E. (2009). Evaluation of different approaches for estimating and mapping crop water status in cotton with thermal imaging. *Precision Agriculture*, 11(1):27–41.

Araus, J. L. and Cairns, J. E. (2014). Field high-throughput phenotyping: the new crop breeding frontier. *Trends in Plant Science*, 19(1):52–61.

Aubrecht, D. M., Helliker, B. R., Goulden, M. L., Roberts, D. A., Still, C. J., and Richardson, A. D. (2016). Continuous, long-term, high-frequency thermal imaging of vegetation: Uncertainties and recommended best practices. *Agricultural and Forest Meteorology*, 228-229:315–326.

Banik, P. (2018). Personal Communication.

Baranowski, P., Jedryczka, M., Mazurek, W., Babula-Skowronska, D., Siedliska, A., and Kaczmarek, J. (2015). Hyperspectral and thermal imaging of oilseed rape (Brassica Napus) response to fungal species of the genus alternaria. *PLOS ONE*, 10(3):e0122913.

Berni, J., Zarco-Tejada, P., Sepulcre-Cantó, G., Fereres, E., and Villalobos, F. (2009a). Mapping canopy conductance and CWSI in olive orchards using high resolution thermal remote sensing imagery. *Remote Sensing of Environment*, 113(11):2380–2388.

Berni, J., Zarco-Tejada, P., Suarez, L., and Fereres, E. (2009b). Thermal and narrowband multispectral remote sensing for vegetation monitoring from an unmanned aerial vehicle. *IEEE Transactions on Geoscience and Remote Sensing*, 47(3):722–738.

Blum, A., Mayer, J., and Gozlan, G. (1982). Infrared thermal sensing of plant canopies as a screening technique for dehydration avoidance in wheat. *Field Crops Research*, 5(C):137–146.

Brewster, M. Q. (1992). *Thermal Radiative Transfer and Properties*. John Wiley & Sons.

Carter, G. A., Cibula, W. G., and Miller, R. L. (1996). Narrow-band reflectance imagery compared with thermal imagery for early detection of plant stress. *Journal of Plant Physiology*, 148(5):515–522.

Chapman, S. C., Chakraborty, S., Dreccer, M. F., and Howden, S. M. (2012). Plant adaptation to climate change—opportunities and priorities in breeding. *Crop and Pasture Science*, 63(3):251–268.

Chaves, M. M., Pereira, J. S., Maroco, J., Rodrigues, M. L., Ricardo, C. P. P., Osório, M. L., Carvalho, I., Faria, T., and Pinheiro, C. (2002). How plants cope with water stress in the field? photosynthesis and growth. *Annals of Botany*, 89(7):907–916.

Coburn, C. A., Gaalen, E. V., Peddle, D. R., and Flanagan, L. B. (2010). Anisotropic reflectance effects on spectral indices for estimating ecophysiological parameters using a portable goniometer system. *Canadian Journal of Remote Sensing*, 36(November 2017):S355–S364.

Costa, J. M., Grant, O. M., and Chaves, M. M. (2013). Thermography to explore plant–environment interactions. *Journal of Experimental Botany*, 64(13):3937–3949.

Ćwiek-Kupczyńska, H., Altmann, T., Arend, D., Arnaud, E., Chen, D., Cornut, G., Fiorani, F., Frohmberg, W., Junker, A., Klukas, C., Lange, M., Mazurek, C., Nafissi, A., Neveu, P., Oeveren, J., Pommier, C., Poorter, H., Rocca-Serra, P., Sansone, S. A., Scholz, U., Schriek, M., Seren, Ü., Usadel, B., Weise, S., Kersey, P., and Krajewski, P. (2016). Measures for interoperability of phenotypic data: Minimum information requirements and formatting. *Plant Methods*, 12(1):1–18.

da Luz, B. R. and Crowley, J. K. (2007). Spectral reflectance and emissivity features of broad leaf plants: Prospects for remote sensing in the thermal infrared (8.0–14.0 $\mu$m). *Remote Sensing of Environment*, 109(4):393–405.

Ellenson, J. L. and Amundson, R. G. (1982). Delayed Light Imaging for the Early Detection of Plant Stress. *Science*, 215(4536):1104–1106.

Esmaeili, A., Poustini, K., Ahmadi, H., and Abbasi, A. (2016). Use of IR thermography in screening wheat (Triticum aestivum L.) cultivars for salt tolerance. *Archives of Agronomy and Soil Science*, 63(2):161–170.

Fahlgren, N., Gehan, M. A., and Baxter, I. (2015). Lights, camera, action: High-throughput plant phenotyping is ready for a close-up. *Current Opinion in Plant Biology*, 24:93–99.

Faye, E., Dangles, O., and Pincebourde, S. (2016). Distance makes the difference in thermography for ecological studies. *Journal of Thermal Biology*, 56:1–9.

Fiorani, F. and Schurr, U. (2013). Future scenarios for plant phenotyping. *Annual Review of Plant Biology*, 64(1):267–291.

Furbank, R. T., Quick, W. P., and Sirault, X. R. (2015). Improving photosynthesis and yield potential in cereal crops by targeted genetic manipulation: prospects, progress and challenges. *Field Crops Research*, 182:19–29.

Gale, J., Manes, A., and Poljakoff-Mayber, A. (1970). A rapidly equilibrating thermocouple contact thermometer for measurement of leaf-surface temperatures. *Ecology*, 51(3):521–525.

Gates, D. M. (1970). Physical and physiological properties of plants. *Remote Sensing with Special Reference to Agriculture and Forestry: with special reference to agriculture and forestry*, page 224.

Gates, D. M., Keegan, H. J., Schleter, J. C., and Weidner, V. R. (1965). Spectral properties of plants. *Applied Optics*, 4(1):11.

Gates, D. M. and Tantraporn, W. (1952). The reflectivity of deciduous trees and herbaceous plants in the infrared to 25 microns. *Science*, 115(2997):613–616.

Gerhards, M., Rock, G., Schlerf, M., and Udelhoven, T. (2016). Water stress detection in potato plants using leaf temperature, emissivity, and reflectance. *International Journal of Applied Earth Observation and Geoinformation*, 53:27–39.

Gómez-Candón, D., Virlet, N., Labbé, S., Jolivot, A., and Regnard, J.-L. (2016). Field phenotyping of water stress at tree scale by UAV-sensed imagery: new insights for thermal acquisition and calibration. *Precision Agriculture*, 17(6):786–800.

Gonzalez-Dugo, V., Zarco-Tejada, P., Nicolás, E., Nortes, P. A., Alarcón, J. J., Intrigliolo, D. S., and Fereres, E. (2013). Using high resolution UAV thermal imagery to assess the variability in the water status of five fruit tree species within a commercial orchard. *Precision Agriculture*, 14(6):660–678.

Grace, J. (1974). The effect of wind on grasses. *Journal of Experimental Botany*, 25(3):542–551.

Guilioni, L., Jones, H., Leinonen, I., and Lhomme, J. (2008). On the relationships between stomatal resistance and leaf temperatures in thermography. *Agricultural and Forest Meteorology*, 148(11):1908–1912.

Hackl, H., Baresel, J. P., Mistele, B., Hu, Y., and Schmidhalter, U. (2012). A comparison of plant temperatures as measured by thermal imaging and infrared thermometry. *Journal of Agronomy and Crop Science*, 198(6):415–429.

Halcro, K. A. and Noble, S. D. (2018). The prospect of thermal imaging to estimate stomatal conductance through energy balance modelling. In *2018 Detroit, Michigan July 29 - August 1, 2018*, number 1800271. American Society of Agricultural and Biological Engineers.

Hatfield, J., Vauclin, M., Vieira, S., and Bernard, R. (1984). Surface temperature variability patterns within irrigated fields. *Agricultural Water Management*, 8(4):429–437.

Hedlund, H. and Johansson, P. (2000). Heat capacity of birch determined by calorimetry: implications for the state of water in plants. *Thermochimica Acta*, 349(1-2):79–88.

Hirayama, T. and Shinozaki, K. (2010). Research on plant abiotic stress responses in the post-genome era: past, present and future. *The Plant Journal*, 61(6):1041–1052.

Humplík, J. F., Lazár, D., Husičková, A., and Spíchal, L. (2015). Automated phenotyping of plant shoots using imaging methods for analysis of plant stress responses – a review. *Plant Methods*, 11(1):29.

Ihuoma, S. O. and Madramootoo, C. A. (2017). Recent advances in crop water stress detection. *Computers and Electronics in Agriculture*, 141:267–275.

Jackson, R. D. (1986). Remote sensing of biotic and abiotic plant stress. *Annual Review of Phytopathology*, 24(1):265–287.

Jackson, R. D., Idso, S. B., Reginato, R. J., and Pinter, P. J. (1981). Canopy temperature as a crop water stress indicator. *Water Resources Research*, 17(4):1133–1138.

Jayalakshmy, M. S. and Philip, J. (2010). Thermophysical properties of plant leaves and their influence on the environment temperature. *International Journal of Thermophysics*, 31(11-12):2295–2304.

Jones, H. G. (1999). Use of infrared thermometry for estimation of stomatal conductance as a possible aid to irrigation scheduling. *Agricultural and Forest Meteorology*, 95(3):139–149.

Jones, H. G. (2013). *Plants and microclimate: A quantitative approach to environmental plant physiology*. Cambridge University Press.

Jones, H. G., Serraj, R., Loveys, B. R., Xiong, L., Wheaton, A., and Price, A. H. (2009). Thermal infrared imaging of crop canopies for the remote diagnosis and quantification of plant responses to water stress in the field. *Functional Plant Biology*, 36(11):978–989.

Jones, H. G. and Sirault, X. (2014). Scaling of thermal images at different spatial resolution: The mixed pixel problem. *Agronomy*, 4(3):380–396.

Khanal, S., Fulton, J., and Shearer, S. (2017). An overview of current and potential applications of thermal remote sensing in precision agriculture. *Computers and Electronics in Agriculture*, 139:22–32.

Kim, Y., Still, C. J., Hanson, C. V., Kwon, H., Greer, B. T., and Law, B. E. (2016). Canopy skin temperature variations in relation to climate, soil temperature, and carbon flux at a ponderosa pine forest in central oregon. *Agricultural and Forest Meteorology*, 226-227:161–173.

Korb, A. R., Salisbury, J. W., and D'Aria, D. M. (1999). Thermal-infrared remote sensing and Kirchhoff's law 2. Field measurements. *Journal of Geophysical Research: Solid Earth*, 104(B7):15339–15350.

Leigh, A., Close, J. D., Ball, M. C., Siebke, K., and Nicotra, A. B. (2006). Leaf cooling curves: measuring leaf temperature in sunlight. *Functional Plant Biology*, 33(5):515–519.

Leinonen, I., Grant, O. M., Tagliavia, C. P., Chaves, M. M., and Jones, H. G. (2006). Estimating stomatal conductance with thermal imagery. *Plant, Cell and Environment*, 29(8):1508–1518.

Leinonen, I. and Jones, H. G. (2004). Combining thermal and visible imagery for estimating canopy temperature and identifying plant stress. *Journal of Experimental Botany*, 55(401):1423–1431.

Li, M., Jiang, Y., and Coimbra, C. F. (2017). On the determination of atmospheric longwave irradiance under all-sky conditions. *Solar Energy*, 144:40–48.

López, A., Molina-Aiz, F., Valera, D., and Peña, A. (2012). Determining the emissivity of the leaves of nine horticultural crops by means of infrared thermography. *Scientia Horticulturae*, 137:49–58.

Maes, W. H., Baert, A., Huete, A. R., Minchin, P. E., Snelgar, W. P., and Steppe, K. (2016). A new wet reference target method for continuous infrared thermography of vegetations. *Agricultural and Forest Meteorology*, 226-227:119–131.

Maes, W. H., Minchin, P. E. H., Snelgar, W. P., and Steppe, K. (2014). Early detection of Psa infection in kiwifruit by means of infrared thermography at leaf and orchard scale. *Functional Plant Biology*, 41(12):1207–1220.

Maes, W. H. and Steppe, K. (2012). Estimating evapotranspiration and drought stress with ground-based thermal remote sensing in agriculture: A review. *Journal of Experimental Botany*, 63(13):4671–4712.

Mahan, J. R. and Yeater, K. M. (2008). Agricultural applications of a low-cost infrared thermometer. *Computers and Electronics in Agriculture*, 64(2):262–267.

McAdam, S. A. and Brodribb, T. J. (2015). The evolution of mechanisms driving the stomatal response to vapor pressure deficit. *Plant Physiology*, 167(3):833–843.

McCarthy, C. L., Hancock, N. H., and Raine, S. R. (2010). Applied machine vision of plants: A review with implications for field deployment in automated farming operations. *Intelligent Service Robotics*, 3(4):209–217.

Möller, M., Alchanatis, V., Cohen, Y., Meron, M., Tsipris, J., Naor, A., Ostrovsky, V., Sprintsin, M., and Cohen, S. (2006). Use of thermal and visible imagery for estimating crop water status of irrigated grapevine. *Journal of Experimental Botany*, 58(4):827–838.

Munns, R., James, R. A., Sirault, X. R. R., Furbank, R. T., and Jones, H. G. (2010). New phenotyping methods for screening wheat and barley for beneficial responses to water deficit. *Journal of Experimental Botany*, 61(13):3499–3507.

Ortega-Farías, S., Ortega-Salazar, S., Poblete, T., Kilic, A., Allen, R., Poblete-Echeverría, C., Ahumada-Orellana, L., Zuñiga, M., and Sepúlveda, D. (2016). Estimation of energy balance components over a drip-irrigated olive orchard using thermal and multispectral cameras placed on a helicopter-based unmanned aerial vehicle (UAV). *Remote Sensing*, 8(8):638.

Otsu, N. (1979). A threshold selection method from gray-level histograms. *IEEE Transactions on Systems, Man, and Cybernetics*, 9(1):62–66.

Pou, A., Diago, M. P., Medrano, H., Baluja, J., and Tardaguila, J. (2014). Validation of thermal indices for water status identification in grapevine. *Agricultural Water Management*, 134:60–72.

Prashar, A. and Jones, H. (2014). Infra-red thermography as a high-throughput tool for field phenotyping. *Agronomy*, 4(3):397–417.

Prashar, A., Yildiz, J., McNicol, J. W., Bryan, G. J., and Jones, H. G. (2013). Infra-red thermography for high throughput field phenotyping in Solanum tuberosum. *PLoS ONE*, 8(6):e65816.

Prytz, G., Futsaether, C. M., and Johnsson, A. (2003). Thermography studies of the spatial and temporal variability in stomatal conductance of Avena leaves during stable and oscillatory transpiration. *New Phytologist*, 158(2):249–258.

Qiu, G. Y., Omasa, K., and Sase, S. (2009). An infrared-based coefficient to screen plant environmental stress: concept, test and applications. *Functional Plant Biology*, 36(11):990.

Reda, I., Konings, J., and Xie, Y. (2015). A method to measure the broadband longwave irradiance in the terrestrial direct solar beam. *Journal of Atmospheric and Solar-Terrestrial Physics*, 129:23–29.

Reynolds, M., Singh, R., Ibrahim, A., Ageeb, O., Larqué-Saavedra, A., and Quick, J. (1998). Evaluating physiological traits to complement empirical selection for wheat in warm environments. *Euphytica*, 100(1/3):85–94.

Rossini, M., Fava, F., Cogliati, S., Meroni, M., Marchesi, A., Panigada, C., Giardino, C., Busetto, L., Migliavacca, M., Amaducci, S., and Colombo, R. (2013). Assessing canopy PRI from airborne imagery to map water stress in maize. *ISPRS Journal of Photogrammetry and Remote Sensing*, 86:168–177.

Salisbury, J. W., Wald, A., and D'Aria, D. M. (1994). Thermal-infrared remote sensing and Kirchhoff's law 1. Laboratory measurements. *Journal of Geophysical Research: Solid Earth*, 99(B6):11897–11911.

Schaepman-Strub, G., Schaepman, M., Painter, T., Dangel, S., and Martonchik, J. (2006). Reflectance quantities in optical remote sensing—definitions and case studies. *Remote Sensing of Environment*, 103(1):27–42.

Schuepp, P. H. (1993). Tansley Review No. 59. Leaf boundary layers. *The New Phytologist*, 125(3):477–507.

Sirault, X. R. R., James, R. A., and Furbank, R. T. (2009). A new screening method for osmotic component of salinity tolerance in cereals using infrared thermography. *Functional Plant Biology*, 36(11):970.

Snyder, W. and Wan, Z. (1998). BRDF models to predict spectral reflectance and emissivity in the thermal infrared. *IEEE Transactions on Geoscience and Remote Sensing*, 36(1):214–225.

Struthers, R., Ivanova, A., Tits, L., Swennen, R., and Coppin, P. (2015). Thermal infrared imaging of the temporal variability in stomatal conductance for fruit trees. *International Journal of Applied Earth Observation and Geoinformation*, 39:9–17.

Suzuki, N., Rivero, R. M., Shulaev, V., Blumwald, E., and Mittler, R. (2014). Abiotic and biotic stress combinations. *New Phytologist*, 203(1):32–43.

Tardieu, F., Cabrera-Bosquet, L., Pridmore, T., and Bennett, M. (2017). Plant phenomics, from sensors to knowledge. *Current Biology*, 27(15):R770–R783.

Tardieu, F. and Simonneau, T. (1998). Variability among species of stomatal control under fluctuating soil water status and evaporative demand: Modelling isohydric and anisohydric behaviours. *Journal of Experimental Botany*, 49(Special):419–432.

Urban, J., Ingwers, M., McGuire, M. A., and Teskey, R. O. (2017). Stomatal conductance increases with rising temperature. *Plant Signaling & Behavior*, 12(8):e1356534.

Vadez, V., Kholova, J., Medina, S., Kakkera, A., and Anderberg, H. (2014). Transpiration efficiency: New insights into an old story. *Journal of Experimental Botany*, 65(21):6141–6153.

van der Walt, S., Schönberger, J. L., Nunez-Iglesias, J., Boulogne, F., Warner, J. D., Yager, N., Gouillart, E., and Yu, T. (2014). scikit-image: image processing in python. *PeerJ*, 2:e453.

Wang, Z., Coburn, C. A., Ren, X., and Teillet, P. M. (2014). Effect of surface roughness, wavelength, illumination, and viewing zenith angles on soil surface BRDF using an imaging BRDF approach. *International Journal of Remote Sensing*, 35(19):6894–6913.

White, J. W., Andrade-Sanchez, P., Gore, M. A., Bronson, K. F., Coffelt, T. A., Conley, M. M., Feldmann, K. A., French, A. N., Heun, J. T., Hunsaker, D. J., Jenks, M. A., Kimball, B. A., Roth, R. L., Strand, R. J., Thorp, K. R., Wall, G. W., and Wang, G. (2012). Field-based phenomics for plant genetics research. *Field Crops Research*, 133:101–112.

Willick, I. R., Lahlali, R., Vijayan, P., Muir, D., Karunakaran, C., and Tanino, K. K. (2017). Wheat flag leaf epicuticular wax morphology and composition in response to moderate drought stress are revealed by SEM, FTIR-ATR and synchrotron x-ray spectroscopy. *Physiologia Plantarum*, 162(3):316–332.

Zarco-Tejada, P., González-Dugo, V., and Berni, J. (2012). Fluorescence, temperature and narrow-band indices acquired from a UAV platform for water stress detection using a micro-hyperspectral imager and a thermal camera. *Remote Sensing of Environment*, 117:322–337.

Zhang, R. (2005). On the applicability of Kirchoff's law and the principle of heat balance in thermal infrared remote sensing: a non-isothermal system. *Science in China Series D*, 48(1):53.